DISSERTATION

CHARACTERIZATION OF MODES AND KINETICS OF MUTATION ACCUMULATION IN *SACCHAROMYCES CEREVISIAE* THROUGH THE ANALYSIS OF DEFINED CELLULAR LINEAGES

Submitted by

Joseph Stewart

Graduate Degree Program in Cell and Molecular Biology

In partial fulfillment of the requirements

For the Degree of Doctor of Philosophy

Colorado State University

Fort Collins, Colorado

Summer 2024

Doctoral Committee:

Advisor: Juan Lucas Argueso

Julie Moreno
Daniel Regan
Claudia Wiese

ABSTRACT

CHARACTERIZATION OF MODES AND KINETICS OF MUTATION ACCUMULATION IN *SACCHAROMYCES CEREVISIAE* THROUGH THE ANALYSIS OF DEFINED CELLULAR LINEAGES

In the field of evolution, gradualism is the process of incremental adaptation supported by a slow and random accumulation of mutations that, over time, lead to genetic diversification and fitness gains. Although this Darwinian model is well supported and widely accepted, it cannot always explain the rapid changes seen in some instances such as tumors with extremely high and complex mutation loads. Recent reports in various organisms, including from our group using Saccharomyces cerevisiae, provide evidence for an additional mode of rapid and non-independent accumulation of chromosomal rearrangements. We have used a yeast model to follow the accumulation of structural genomic rearrangements such as loss of heterozygosity (LOH). We found that while chances of a single LOH event happening are very low, two or more LOH tracts co-occurred at rates 25- to 200-fold higher than expected if these events were independent of each other; therefore, the conventional process of slow and independent accumulation of mutations are not sufficient to account for every change in the genome. In the present study, we focused on temporal kinetics of bursts of LOH accumulation in yeast. We developed a hybrid diploid yeast experimental strain that enables identification of LOH event both through counter-selection and visual screening for colony color. This hybrid strain, made from the S288c and SK1 genetic backgrounds,

possesses ~55,000 heterozygous SNPs distributed throughout the genome and allows for ease of tracking LOH events through sequencing. The screening approach was used in combination with microcultures (one cell grown for 5 or 6 divisions) in phylogenetic analyses that unambiguously revealed 18 cases where multiple LOH events co-occurred in the same cell division cycle. Collectively, these studies offer support for punctuated bursts of mutation accumulation caused by systemic genomic instability (SGI). Additionally, we have investigated a potential mechanism that influences SGI, namely global noise in gene expression.

ACKNOWLEDGEMENTS

I was able to complete my degree as a student in the Cell and Molecular Biology program with the help of many individuals.

To my advisor Lucas Argueso – You have been an excellent mentor and friend these past 5 years. All of my accomplishments could not have been possible without your inspiration and guidance. I thank you for your countless hours spent teaching me the right ways of being a scientist and how to be an effective leader in the lab setting. I will miss working in your lab.

To my committee members: Julie Moreno, Dan Regan, and Claudia Wiese – Thank you for the countless years of support as you watched me grow as a scientist. Each of you played a major role in my graduate career, either as a rotation mentor or a professor for a class. I will never forget the kindness and excitement shown by each of you in our meetings.

To my factory employees: Camryn Schmelzer and Mackenzie Wienke – Both of you were integral to the development and completion of this project. I will always remember how much fun we were able to make science and the countless lunches spent together in-between experiments. The amount of work and impact we were able to generate was only possible through both of your help.

To the rest of the Argueso lab: Lydia Heasley, Ruthie Watson, Joy Love, and Melody Hayman – Thank you for the additional support that you offered during my time in lab. Our lab was able to have such a collaborative and positive environment due to all the

work and attitude each of you brought. I know going forward I will never have a lab as special as this again.

To my parents: Rob and Kristi – It is hard to put into words the amount of support and impact both of you have played in my life. There were many times in my life where I was told “no,” but when it came to my aspirations and what I wanted to do with my life, that was never the case. Thank you for allowing me to grow and accepting me always for who I am.

To the rest of my family and friends – There are too many to name, but each of you have also supported me beyond what is required. Thank you to all who listened to me when I things to say and offered advice when I needed it the most. I will never forget any face past or present that played a helping role in who I have become today.

TABLE OF CONTENTS

CHAPTER 1 - INTRODUCTION

Gradualism and Punctuated Equilibrium

In the field of evolution, gradualism is the process of incremental adaptation supported by a slow and random accumulation of mutations that over time lead to genetic diversification and fitness gains (Figure 1A). This process is also often referred to as the Darwinian model, paying respect to Charles Darwin's original observations he published (Darwin 1859). This model is strongly supported by abundant evidence and has been widely adopted by evolutionary biologists and paleontologists to describe changes seen in the fossil record (Rose et al. 1986; Bell 2009). In recent years, advances in genomic technologies have corroborated the gradual accumulation of genome-wide mutations seen in experimental models (Lynch et al. 2008; Lynch 2010; Loeillet et al. 2020; Wei et al. 2022), as well as in the cancer context (Nowell 1976; Podlaha et al. 2012; Seferbekova et al. 2023). However, roughly 100 years after Darwin published "On the Origin of Species," Eldredge and Gould proposed an additional explanation that aimed to address gaps in fossil records. They proposed the idea of "punctuated equilibrium" where short periods of large morphological change could supplement gradualism (Eldredge and Gould 1972). Punctuated equilibrium in the molecular context refers to short, transient periods of instability where multiple mutations can arise at very quickly (a few cell cycles) before returning to a period of stability again (Figure 1C). Additionally, the mutator phenotype is another mutation accumulation mode that has been well characterized and is important in the cancer context (Loeb 2011; Natali and Rancati 2019). This model shows that one destabilizing

mutation, specifically in key genome maintenance genes, can lead to a permanent increase in mutation rate causing a rapid and progressive accumulation of many mutations like those seen in tumors (Figure 1B). However, this model again does not fit examples where stability returns and the drastic changes in mutation rate are only transient. Numerous more studies have come out that provided experimental support of punctuated equilibrium (Newman et al. 1985; Gould and Eldredge 1993; Casanova and Konkel 2020). These studies range from biology focused questions, but also extend to diverse disciplines such as to sociological and technology-based ideas, with punctuated changes, sometimes also referred to as saltations, being both large and small (Mokyr 1990; Bentley 2022). In molecular biology, punctuated equilibrium can be used to address the recent observations where gradual intermediates between cell populations are lacking, as well as supplementing rapid large genomic changes where gradualism on its own is not a sufficient explanation (Dennis and Eichler 2016; Jangam et al. 2017; Van Etten and Bhattacharya 2020). However, there is yet to be studies where punctuated equilibrium has been captured and characterized over a short time period, with a resolution of very few cell divisions. In the present study, we use a purpose designed experimental system to track the accumulation patterns of a structural genomic variation class known as loss of heterozygosity (LOH), and with it we were able to unambiguously detect punctuated equilibrium, or mutation bursts, and to show that this process is responsible for a substantial proportion of multiple LOH accumulation events.

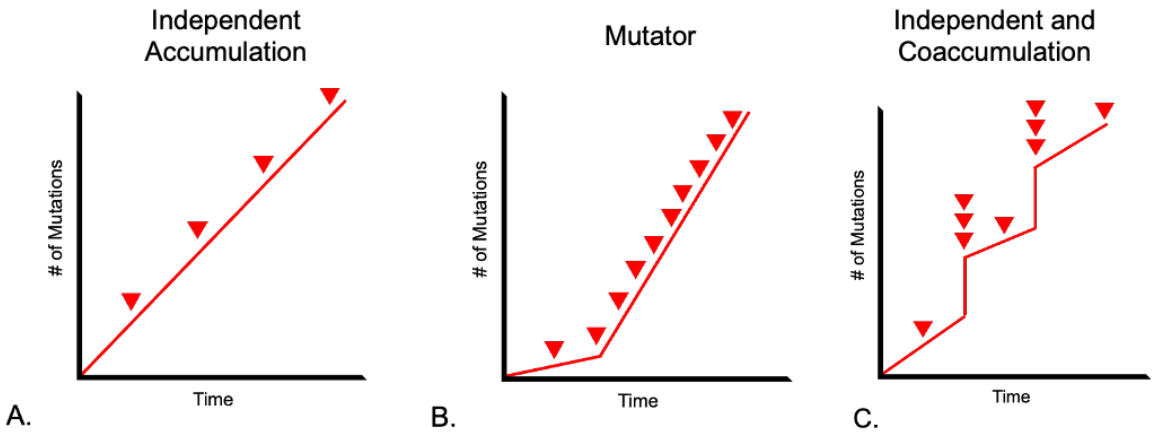

Figure 1. A. Gradualism (independent accumulation) is described as the slow, random, and independent accumulation of mutations over a long time period. **B.** Mutator phenotypes are seen when one destabilizing mutation permanently raises the mutation rate and never returns to stability. **C.** Punctuated bursts (independent and coaccumulation) are described as periods of rapid instability where multiple mutations are acquired together, then return to a period of stability. Red arrows denote mutational events. Adapted from Heasley *et al.* 2021 Current Genetics.

Loss of Heterozygosity

Loss of heterozygosity (LOH) is described as a mutation, typically a structural chromosomal change as an outcome of DNA damage, where one of the two alleles originally present at a heterozygous locus is lost (Zhang and Sjöblom 2021; Smukowski Heil 2023). There are two main categories of LOH, copy-neutral LOH (CN-LOH) and copy-loss LOH (CL-LOH). CN-LOH results in the preservation of two copies of the locus, but one of the alleles is lost, while the remaining allele becomes duplicated. In the typical diploid genome context, CN-LOH is manifested as a heterozygous position mutating to become homozygous for one of the two original alleles. Mechanistically, CN-LOH is the product of homologous recombination between the two homologous chromosomes in mitotic or somatic cells with a diploid genome. Homologous recombination involves the genetic recombination between similar or the same DNA sequences from two different molecules, where a double stranded break in one of them is repaired using the second as a template (Symington et al. 2014; Jinks-Robertson and Petes 2021). Upon a double stranded break, both broken ends of the duplex DNA are resected by an exonuclease activity in the 5’ to 3’ direction, thus generating single stranded regions with a free 3’ end. One of these 3’ overhangs participates in a homology search where it invades the double stranded DNA of a homologous sequence template (in the case of CN-LOH, on the homologous chromosome) forming a displacement loop that is now primed for extension DNA synthesis using the invaded sequence as a template. The other end of the break may also be captured and use the now displaced sequence as a template for replication. Following a short round of replication, the sequences are ligated together forming Holiday junctions. Depending on

the resolution of these junctions, a cross over can occur (Figure 2C) that can eventually lead to a CN-LOH after chromosome segregation. If the second end is not immediately captured, following synthesis the newly replicated strand is displaced and re-anneals back to the other half of the broken DNA molecule. Synthesis may then occur to fill in the single stranded DNA on the other strand (Figure 2E). This process is known as synthesis dependent strand annealing (SDSA) and can lead to a gene conversion, another CN-LOH (Figure 2G). Finally, if one side of the broken DNA fails to engage in repair and is lost completely (typically the telomere-proximal side), extension DNA synthesis of the centromere-proximal broken DNA can continue as the displacement loop migrates down the to the end of the chromosome where replication is eventually terminated at the telomere. This process is known as break-induced replication (BIR) and can also result in a CN-LOH. LOH derived from either the mitotic crossover or BIR (Figure 2F) pathways typically will result in terminal LOH tracts, where heterozygosity is lost from a region in the vicinity of precursor DSB all the way to telomere. These terminal tracts can be very long, as long as a whole chromosome arm. On the other hand, CN-LOH derived from the SDSA pathway (Figure 2G) or through a non-crossover (i.e., gene conversion) resolution of Holiday junctions are manifested in the form of interstitial tracts where heterozygosity is lost locally in within a Kb of the precursor DSB.

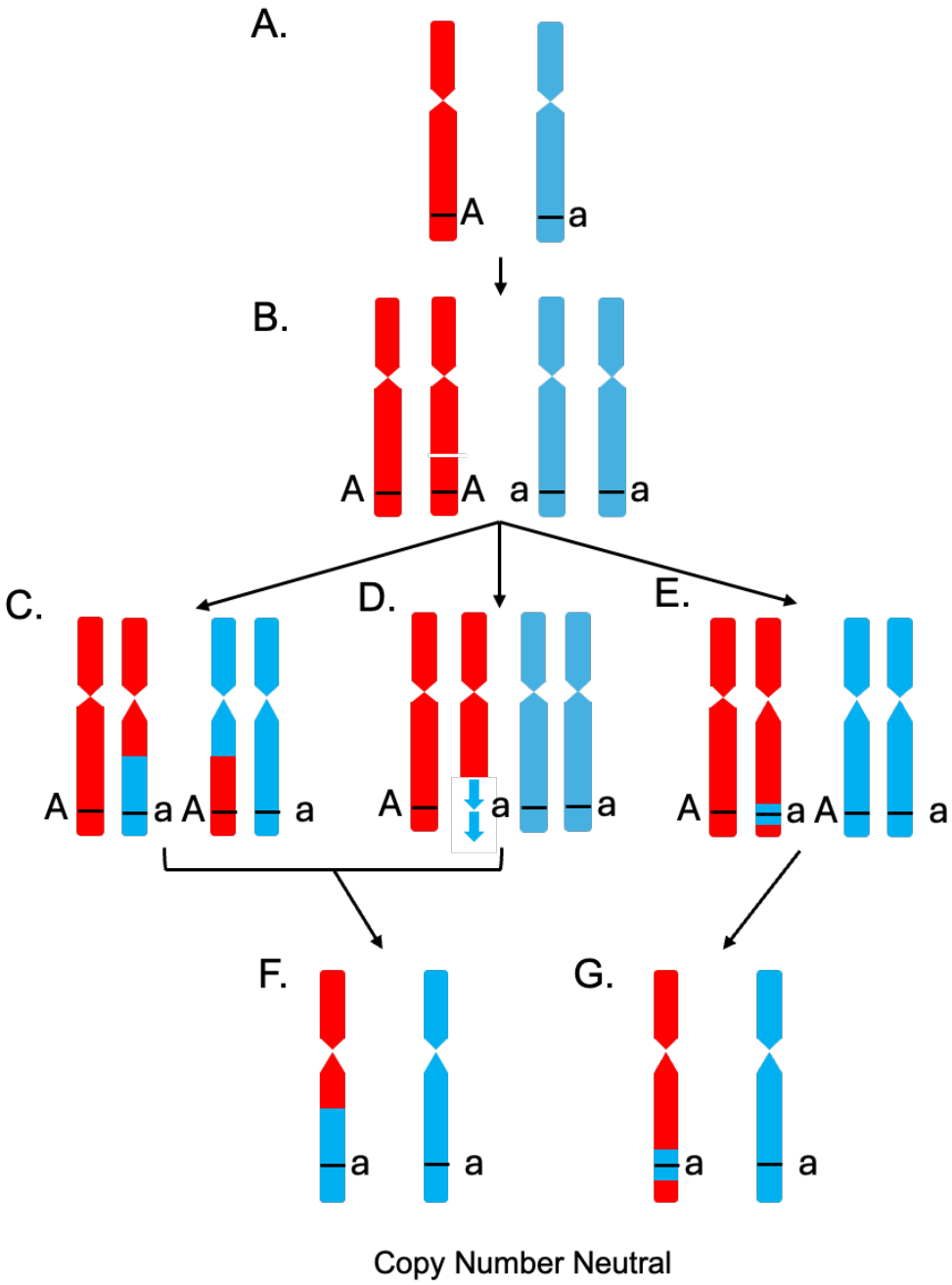

Figure 2. Copy neutral loss of heterozygosity overview. **A.** A pair of homologous chromosomes that are heterozygous for allele A/a. **B.** Double-strand break at the "A" loci on the red chromosome following DNA replication. **C.** Cross over is initiated with the other homologue through homologous recombination or **D.** loss of the other broken end allows for the initiation of replication using the other homologue as a template. **E.** Repair of the break by synthesis dependent strand annealing. **F., G**. Resolution of the DSB resulting in various types of LOH. Copy neutral LOH can result by **F.** a reciprocal crossover or BIR or a **G.** gene conversion resulting in the homozygous a/a genotype.

CL-LOH results in the loss of one allele through such mechanisms as a deletion (Figure 3C) or whole chromosome loss (Figure 3D), without duplication of the second allele. Regardless of copy number neutrality or loss, mitotic LOH is always an irreversible form of mutation, because the unique single nucleotide polymorphisms (SNPs) associated will be lost allele cannot be recovered without the fusion of two meiotic gametes. This particular feature makes LOH extremely useful mutation class for tracking mutation accumulation through phylogenies. In other words, LOH is a unidirectional mutation type. Once an LOH tract has formed, the corresponding region can never go back to its original heterozygous state as long as mitotic propagation continues.

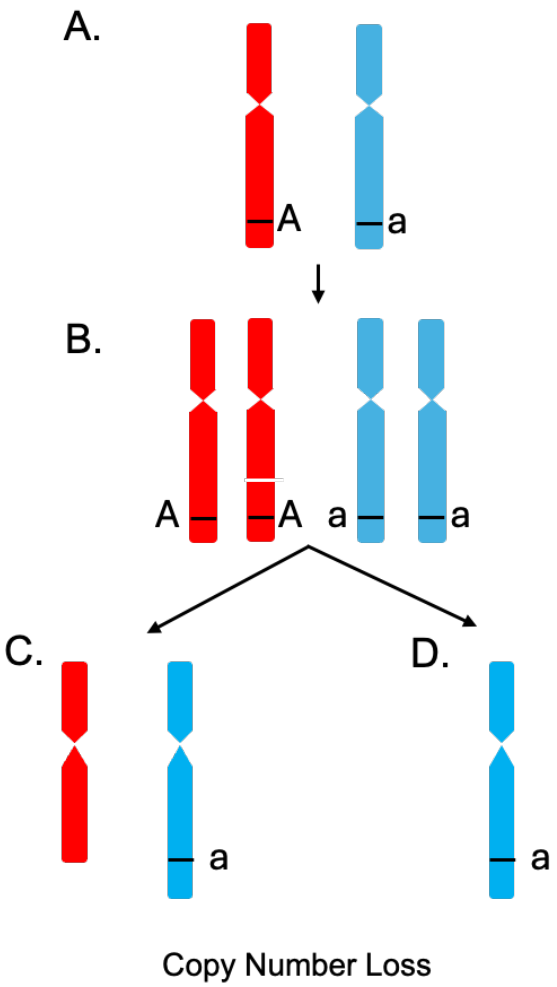

Figure 3. Copy-loss **l**oss of heterozygosity overview. **A.** A pair of homologous chromosomes that are heterozygous for allele A/a. **B.** Double-strand break at the "A" loci on the red chromosome following DNA replication. Through a variety of mechanisms, **C.** a deletion of the "A" allele or **D.** whole chromosome loss can lead to copy-loss loss of heterozygosity.

LOH is associated with a number of genetic diseases, such as cancer (Ryland et al. 2015; Nichols et al. 2020; Hwang et al. 2021). Retinoblastoma is a classic example of LOH-induced cancer, as LOH spanning the *Rb*1 gene can lead to the loss of the functional allele of this tumor suppressor gene allowing for tumorigenesis to begin (Zhu et al. 1992). Other examples exist of LOH playing a role in somatic mosaicism in humans outside the cancer context. Ichthyosis with confetti (IWC) is a rare skin disease where affected patients possess erythroderma (a severe skin irritation, literally meaning “red skin”), and are also prone to bacterial infections and growth defects. Through various studies, researchers have identified the cause of this disease is a dominant mutation in the human *KRT10* gene. Affected IWC patients are heterozygous, so the mutant dominant triggers the red skin phenotype. However, throughout the surface of their bodies, hundreds of small patches of normal, healthy skin are clearly visible. These patches, or confetti, are areas of skin where the cells have undergone LOH spanning the *KRT10* locus, causing the loss of the mutant allele and duplication of the WT allele. This structural, chromosome level mutation effectively removes the disease, and once mutant cells are free of the disease allele, they outgrow their diseased neighbors and expand to form visible healthy confetti islands (Choate et al. 2010; Nomura 2020). Each of these patches are independent LOH events and are spread across the body. The highly visual nature of the ICW phenotype highlights how high of a rate interhomolog mitotic recombination leading to CN-LOH is in humans, orders of magnitude higher than point mutations on a per locus basis. As seen in Figure 2, even though the DNA lesion that triggers LOH events is small and localize, its impact can span thousands of Kb, even an entire chromosome arm and all genes in it. In contrast, other mutations such as

nucleotide substitution mutations only span a few base pairs, and at most impact the function of a single gene. Along with its irreversibility, the large range of genotypic and phenotypic impact associated with LOH makes it possible for a study like ours to be conducted. Uncovering the underlying mechanisms of LOH formation, and in particular the processed that can lead to multiple LOH events occurring rapidly in diploid genomes can offer key insights into potential consequences for genome evolution and human health.

LOH in Yeast

There are several studies that investigated genome wide LOH in *S. cerevisiae* that highlight both the utility of baker's yeast as a model system as well as LOH as a mutation class (Rosen et al. 2013; Chumki et al. 2016; Dutta et al. 2021; Stewart et al. 2021; Dutta et al. 2022). One such study was done in 2020 by Sui *et al*. In their mutation accumulation assays, they subcultured 93 hybrid diploid yeast strains around 100 times each, followed by extensive deep coverage whole genome DNA sequencing (WGS). Nearly half of the ~2500 events they observed were CN-LOH events (Argueso and Alani 2020; Sui et al. 2020). This high frequency that was detectable in yeast further validated our decision to use LOH as our mutation to track in this study. Furthermore, it highlights yeast as a model system for high resolution analysis of these events.

Transient Mutator States

The idea of a population of cells undergoing a brief period of instability or hypermutable subpopulations is not new. There have been multiple studies in a variety of microbes, including *E. coli*, *S. cerevisiae*, and *C. albicans*, that highlight that under selection or stress, cells can enter into a state of high mutation rate that is not heritable

by future generations (Ninio 1991; Torkelson et al. 1997; Rosenberg et al. 1998; Bull et al. 2000; van Dijk et al. 2015; Woo et al. 2018; Pribis et al. 2019; Zhai et al. 2023). These have since been termed transient mutator states and have been hypothesized to provide variation during the stationary phase of bacteria as well as a potential link to how multiple somatic mutations can arise simultaneously and lead to cancer in multicellular organisms. These early works support the idea of mutational bursts, where something like stress from antibiotic exposure and selection could cause rapid changes that returns to stability when that stress is no longer present. These studies however do not distinguish between increased mutations rates as the result of punctuated bursts or gradualistic accumulation.

Punctuated Equilibrium in Cancer

There have been several studies looking into the role of punctuated equilibrium in the context of cancer. Evidence of bursts has been seen in a variety of cancer types including melanoma, colorectal, and breast cancer (Cross et al. 2016; Gao et al. 2016; Sievers et al. 2017; Field et al. 2018). Of note, in a recent paper by Leighton *et al* in 2023, they reconstructed lineages of triple negative breast cancers through their powerful single-cell DNA sequencing technology. They analyzed five patient tumor biopsy samples and recreated lineages based off WGS of ~5000 cells each. Remarkably, of the 5 biopsies, two of them exhibited cell populations that contained “no gradual intermediates,” suggesting that these populations could have arisen from a mechanism like punctuated equilibrium (Leighton et al. 2023), where multiple mutations formed simultaneously during an early, but brief genome instability episode, which was then followed but long period where cells were able to stably propagate the coincidently

acquired mutations to achieve tumor expansion. Although these data are exciting in their support of punctuated mutation accumulation, there are important limitations to its conclusions. A normal tumor contains billions of cells, where in the study they could only analyze roughly 5,000. This is unquestionable a very large number by current single-cell WGS technology standards, but nonetheless represents only a minute fraction of the tumor. It is still possible that gradual intermediates did exist in other cells that made up the tumors that were not sampled. It is because of this reason that retrospective studies like this one are not capable of offering direct and unambiguous demonstrations that coincidental mutations are the only possible option for these types of highly mutated cell populations to arise.

Previous Investigations of punctuated mutation accumulation in yeast

Two 2020 studies by our own group suggested the existence of a transient mutator state in heterozygous *S. cerevisiae* diploids. The first study by Sampaio et al reported on the presence of multiple unselected structural variation events (predominantly CN-LOH, but also CNV and aneuploidy) when selecting for a single mutation event. This study was prompted by the observation that one specific yeast clone which had been isolated from a phenotypic screen for an LOH tract spanning the *ACE2* locus on chromosome XII (Chr12), also contained seven additional independent unselected structural chromosomal changes dispersed elsewhere in its genome (Rodrigues-Prause et al. 2018; Sampaio et al. 2020). This was an extremely high frequency of mutation coincidence that was difficult to reconcile through the conventional gradualistic model. In follow-up experiments, the same heterozygous parent was used to isolate additional 28 colonies that were phenotypically screened for

the presence of a primary *ACE2* Chr12 LOH tract, and 28 matched control colonies without any selection. Whole genome sequencing analysis showed that more of the primary screened clones had unselected secondary LOH tracts, and they also had an overall higher number of unselected tracts per clone compared to controls. Quantitative LOH mutation assays in three different strain backgrounds using the counter selectable markers *CAN1* and *URA3* found that that coincident double LOH at these different loci happened at rates up to 66-fold above the level expected from the gradualistic model. Finally, using a hybrid strain background, they also isolated and analyzed clones that were either unselected controls, or had selection for either single LOH, or were selected for double LOH of the two markers. Using WGS, they showed that none of the unselected controls had any LOH tracts anywhere in their genomes. In contrast, clones derived from single and double selection clones contained multiple additional unselected structural variation events throughout their genomes. They attributed this observation to a punctuated equilibrium-like phenomenon, rather than gradualism, and coined the term systemic genomic instability (SGI) to describe short episodes of intense vulnerability to mutation accumulation genome-wide. This systemic instability was also postulated to be transient, meaning that once the mutational bursting occurred, cells were able to resume normal accuracy of DNA repair and genome maintenance.

The second study took a slightly different approach and utilized chromosome loss as the mutational class for selection, rather than mitotic recombination leading to LOH. In Heasley *et al* 2020, colonies were selected for loss of Chr5, and subsequently phenotypically screened for loss of the *ACE2* allele on Chr12, which could have arisen from either CN-LOH homologous recombination or from whole Chr12 loss. Of the 52

colonies analyzed, 79% possessed additional chromosome loss rather compared to 21% HR (Heasley et al. 2020). In contrast, in the absence of primary selection for Chr5 loss, CN-LOH through HR is the predominant mode of Chr12 LOH which CL-LOH due to Chr12 loss is extremely rare (Rodrigues-Prause et al. 2018). This clear shift in the mutational spectrum of Chr12 LOH from HR to chromosome loss also revealed an important feature of SGI where the coincident unselected mutations have a strong tendency to match the mutation class of the primary selected mutation. Specifically, selection for chromosome loss in Heasley at al was strongly associated with unselected chromosome gains and losses (aneuploidy), whereas selection for CN-LOH through mitotic HR in Sampaio et al was associated with unselected CN-LOH. This mutational spectrum coordination between selected and unselected mutation events suggested a systemic failure of specific genome maintenance pathways in small cell subpopulations, for example, transient failure of the chromosome segregation machinery or mitotic checkpoints leading to several chromosomes being mis-segregated at the same time.

Additionally, Heasley *et al* also conducted single and double mutation rate assays using counter-selection for chromosome loss. When compared to the calculated expected rate (the multiplicative rate of the individual chromosome losses based off independence; see expanded explanation below in Results), the observed double rates of chromosome loss ranged from ~600 to ~3800-fold higher. This excess in double mutations corroborated our previous study to highlight that the assumption of independence for mutation occurrence is not sufficient to account for the multiple mutations detected in these clones, and that coincidental bursts of mutations caused by

SGI may be a substantial mode of mutation accumulation that contributed to these observations.

Together, the studies by Sampaio et al and Heasley et al highlight that independence is not only mode contributing to overall mutation accumulation and that SGI-induced bursts are an attractive additional explanation. However, one shared shortcoming of both these studies, similarly to the tumor biopsy single cell WGS work described above, is that they only offer a retrospective view of overall mutation accumulation process in the clones analyzed. Specifically, the way the experiments were designed, they were unable to directly and unambiguously discern between multiple mutations happening independently in succession versus multiple mutations truly coinciding in a very short time frame of just one or two cell cycles. In the present study, we used a novel experimental approach specifically designed to overcome this barrier. Through the genomic analysis of small and defined yeast cell lineages we were able to directly capture and identify instances of coincidental mutational events at high temporal resolution.

Possible Mechanisms of Systemic Genomic Instability

We and others have hypothesized a number of reasons as to why a punctuated burst could occur. As mentioned previously (Torkelson et al. 1997), transient mutator states were hypothesized to arise from stress. In terms of aneuploidy, Heasely et al hypothesized that impairment of several cellular processes surrounding DNA repair or mitotic spindle assembly, maintenance or checkpoint could lead to a coordinated and systemic failure that affects multiple chromosomes at once. In terms of LOH, we have hypothesized that cellular replicative ageing as well the inherent heterogeneity in gene

expression could also lead to SGI. We describe SGI as a transient coordinated failure of one or a set of pathways that would cause global instability that has the potential to lead to a transient mutator state. Of our list of potential contributors to SGI, stochastic perturbations in gene expression have become a recent focus. More specifically, changes in global gene expression (GGE) noise has become an attractive hypothesis as to a process that could lead to SGI and thus a mutation burst. Noise in GGE can be described as the natural variation in gene expression seen between cells in an otherwise genetically identical cell population (Raser and O'Shea 2005; Vallania et al. 2014). In the context of bursts, a rare cell in the population may have lower expression of a key DNA repair gene compared the average cell in that population. This same outlier cell can then easily return to the typical or average expression level of this key gene at a later time or in the next cell cycle. During this time of abnormally low (or perhaps high) expression, this cell may be phenotypically defective in DNA repair and vulnerable to acquiring multiple mutations. This cell may become DNA repair proficient again in the following cell cycle and no longer be vulnerable to bursts, propagating its many newly acquired mutations stably without continuing to display a high mutation rate. For example, around 60 genes in *S. cerevisiae* have been previously identified to play important roles in suppressing the accumulation of LOH (Andersen et al. 2008) (*i.e.*, when they are knocked out the LOH rate goes up). One such gene is *DPB3*, a DNA polymerase II (epsilon) subunit critically important for maintaining the overall fidelity of DNA replication (Araki et al. 1991; Aksenova et al. 2010). While the average cell expresses this gene at the appropriate level and at the appropriate time in the cell cycle, because of stochastic noise in the context of a large population, it is likely there

will be a small number of cells in that population that may under-express, over-express, or mistime the expression of *DPB3*. In those rare cells, during the cell cycle when this gene is not appropriately transcribed for any reason, they could experience a loss of fidelity or processivity of DNA synthesis, in which case the entire genome is systemically vulnerable to LOH at the same time. This gene expression noise effect alone could in principle be enough to cause an increased amount of LOH during this particular cell cycle, but importantly, as soon as typical gene expression resumes, the genome instability consequence would pass, and stability would resume indefinitely. Therefore, GGE noise provides a plausible mechanistic source that satisfies the key features of SGI: (1) Genome-wide coincident mutation accumulation, (2) the coordinated mutational spectrum shared by thee coincidently acquired mutations (depending on which DNA repair pathway failed transiently), and (3) resumption of normal/basal mutation rates after the transient burst episode passes.

As mentioned throughout the Introduction, there are still a number of gaps in our knowledge concerning punctuated equilibrium or mutation bursts. The present study advances this field by directly and unambiguously demonstrating the existence of coincidental mutations that are not formed by the conventional gradualistic accumulation model, and by quantifying the relative proportion of multiple mutations formed through independent (gradualistic) versus coincident (punctuated) accumulation modes. Finally, our work also presents an initial exploration GGE noise as a potential contributor to SGI.

CHAPTER 2 – RESULTS

Experimental Rationale and Parental Strain Features

The study by Sampaio *et al* 2020 reported that when selecting for clones carrying a single LOH tract at a specific marked locus, secondary unselected LOH events elsewhere in the genome were detected at a ~30-fold higher frequency than should be expected based on gradualistic and independent formation of these two mutation events. This result supported the existence of an additional mutation accumulation process, Systemic Genomic Instability (SGI), that can give rise to multiple mutations at different loci over a short period of time, in contrast to the conventional gradualist model of independent and slow accumulation. Although the results presented in Sampaio et al. study suggested the occurrence of LOH bursts, this assertion was made by indirect inference, because those experiments were not designed to directly differentiate between double LOH-carrying clones that formed through punctuated versus gradual accumulation. Therefore, in the present study, we sought to develop an improved experimental approach capable of capturing these LOH events at a high timing resolution, thus resolving their relative temporal order of formation. The novel yeast system employed here overcomes two important limitations of the previous work. Through our phylogenetic lineage analysis system, we were able to (1) directly and unambiguously identify yeast clones where multiple LOH tracts must necessarily have formed at the same time; and (2) estimate the relative contributions of punctuated and gradual mutation accumulation modes to the overall formation of clones carrying multiple LOH tracts. In addition, we used this experimental approach to conduct an

initial investigation of a mechanism that might contribute to the occurrence of punctuated bursts, specifically, global noise in gene expression (GGE noise).

In order to study individual and coincident LOH formation at two separate loci in the *S. cerevisiae* genome, we identified two long chromosome arms where LOH had been shown to accumulate at high frequency (Sui et al. 2020). These regions, the right arms of chromosomes XIII and XV (Chr13 and Chr15, respectively), do not necessarily experience more DSB lesions or interhomolog mitotic recombination than other regions of the genome of a per kilobase basis. Instead, their long arm lengths (655 Kb from *CEN13* to *TEL13R* and 755 Kb from *CEN15* to *TEL15R*) mean that HR that initiates anywhere within those large regions and is subsequently resolved as a mitotic crossover, leads to the formation of a long terminal CN-LOH tract that extends from the vicinity of the recombination initiation site to the telomere (Figure 2).

In order to detect LOH in those regions, both individually and coincidently, and both through survival selection and visual screening, we created dual-function LOH reporter cassettes (Figure 4A). These cassettes each contained a counter-selectable maker coupled with a colony color marker gene involved in the adenine biosynthesis pathway. In addition, we used a hybrid diploid parental strain background, consisting of a cross between the S288c haploid reference background, and the diverged SK1 haploid background. While these haploids are both *S. cerevisiae*, they contain around 50,000 single nucleotide polymorphisms (SNPs) evenly dispersed across their genomes. Therefore, the hybrid diploid formed by crossing them has a richly heterozygous genome (roughly 4 HetSNPs per Kb) that allowed for high resolution detection of LOH events through whole genome sequencing (WGS) analysis.

In the genome of the SK1 parent haploid strain, we integrated one copy of the *CAN1-ADE1* dual reporter at a telomere-proximal position on the right arm of Chr13, and one copy of the *$_{kl}$URA3-ADE2* dual reporter near *TEL15R* (detailed construction and positioning in METHODS). Subsequent crossing to the S288c parent produced a hybrid diploid hemizygous for the dual-function reporter insertions and heterozygous for the ~50,000 genome-wide HetSNPs (Figure 4A). A copy-neutral interhomolog mitotic recombination event (Fig X) somewhere on the right arm of Chr13 (Chr13R) leading to loss of the *CAN1-ADE1* dual reporter generates yeast cells that can be both selected for as colonies growing in media containing canavanine and can also be identified by visual screening as red color colonies in complete media (Figure 4B). As a useful validation feature of this dual reporter, Can^R colonies that are also red in color can be confidently inferred to be due the presence of an LOH tract spanning of the dual reported (rather than an inactivating point mutation in *CAN1*). Likewise, an LOH tract spanning the *$_{kl}$URA3-ADE2* dual reporter on Chr15R can be selected for in media containing 5-FOA, and also screened for as red colonies (Figure 4C). Finally, because the growth inhibition caused by *CAN1* and *$_{kl}$URA3* occur through different and independent metabolic pathways, clones containing simultaneous LOH tracts of both Chr13R and Chr15R can be selected for in media containing both canavanine and 5-FOA. In the diploid containing both hemizygous dual-function reporters, visual screening for red colonies can identify clones that carry LOH tracts on Chr13R, or Chr15R, or both Chr13R and Chr15R. Subsequent phenotyping of these clones on media lacking uracil or containing canavanine can differentiate which of the two dual reporters experienced LOH.

To ensure all mutation events recovered for analysis came from mitotic recombination, the experimental strains were homozygous a deletion of the *IME1* gene (*ime1Δ* / *ime1Δ* genotype), which encodes the master transcriptional regulator essential for initiation of the meiotic cycle. In the absence of *IME1*, yeast cell are completely incapable of initiating genome-wide meiotic recombination and then reverting back to mitosis, a process known as return-to-grown (RTG) that could potentially confound the interpretation of our result. In addition, we also made the experimental strains homozygous for the deletion of the *MSS11* gene (*mss11Δ/mss11Δ* genotype), encoding a transcription factor required for cell-cell adhesion in yeast. Removing MSS11 ensured that cells readily detach from each other after cell division in liquid culture, thus greatly improving liquid dilutions, and also allowing colony forming units seen in Petri dishes to be confidently attributed to being derived from a single cell (rather than 2 or more clumped cells).

Using this experimental strain setup, first we were able to use the counter-selection features to measure the rates of single LOH on Chr13R, single LOH on Chr15R, and the coincident double LOH rate at both regions, and in doing so corroborated the Sampaio et al observation of frequent double LOH that cannot be explained by gradualism alone. Next, using the visual screening feature, we were able to identify red-colony Chr13R or Chr15R LOH carrying-clones, which were analyzed by WGS to uncover the presence of unselected LOH tracts elsewhere in their genomes. By carrying-out this LOH screening plus WGS in defined small cultures, we were then able to use phylogenetic inference to positively and unambiguously identify clones where

LOH tracts must have occurred simultaneously in the same cell division cycle, and thus be attributed to an SGI, burst-like mutational event.

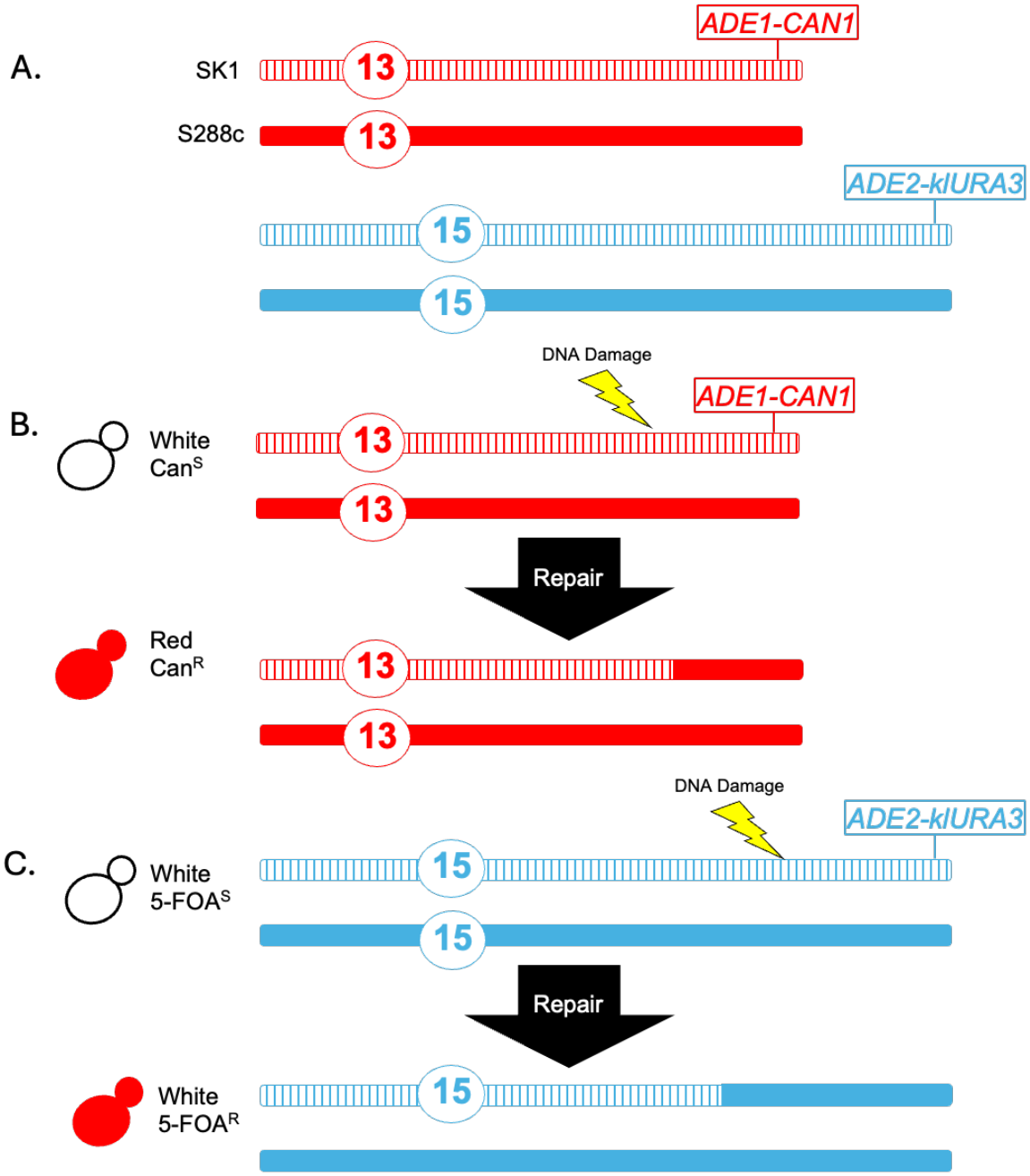

Figure 4. A. Experimental strains. Yeast chromosomes 13 and 15 that contain hemizygous makers for *ADE1-CAN1* and *ADE2-klURA3* in experimental strain. SK1 chromosomes are depicted with dashed bars while s288c chromosomes are solid. Circles depict roughly the location of the centromeres. **B, C.** Loss of heterozygosity by repair and corresponding segregation. A double stranded break of the SK1 chromosome 13 or 15 could be resolved through a variety of LOH causing events with the S288c chromosome. The resulting chromosomes lose both *ADE1* and *CAN1 or ADE2 and klURA3*, changing the colony color from white to red and gaining resistance to canavanine or 5-FOA.

Single and Double LOH Rate Measurements

To investigate the relative rates of single and double LOH events, as well as the presence of SGI, we performed mutation rate assays using our experimental strain described above. To perform this experiment, we generated 20 independent colonies utilizing our WT strain JAY3412-2. Each of these colonies were resuspended in water and plated onto four matching plate types: permissive media (YPD), and the three selective media types for Chr13R single LOH (synthetic minimal media [SC] plus canavanine), for Chr15R single LOH (SC plus 5-FOA), and for Chr13R+Chr15R double LOH (SC plus both canavanine and 5-FOA) (Figure 5A). Colony counts were gathered from these platings and we then used the maximum likelihood estimate method (MMS-MLE; (Łazowski 2023)) to calculate LOH rates for each reporter locus individually, as well as the experimental measurement of the double LOH rate. We determined that the MSS-MLE single LOH rates for Chr13R and Chr15R were 1.47×10^{-5} and 7.81×10^{-6} LOH/cell/division, respectively (Figure 5B). Under the assumptions of the gradualist model of mutation accumulation, LOH events taking place at different regions of the genome should, in principle, occur completely independently of each other. Therefore, in this case, the expected rate of coincident double LOH should be equal to the multiplicative product of the two single LOH rates, which equals 1.15×10^{-10} LOH/cell/division. However, through the quantitative rate determination experiment above, we directly measured a coincident double LOH rate of 2.73×10^{-9} LOH/cell/division, which is an almost 24-fold increase over the independence gradualistic expectation (Figure 5C). In this study and previously (Heasley et al. 2020; Sampaio et al. 2020), we have employed this ratio of experimentally observed double

mutation rate divided by the gradualistic-expected double mutation rate (assuming single mutation independence) as a key metric of SGI phenomenon. This metric is rereferred to from here on out as the SGI ratio. An SGI ratio of 1 would be indicative of fully independent mutation accumulation between the two loci. In the present study, the SGI ratio of ~24 for double LOH of Chr13R and Chr15R, corroborated and added onto the previous evidence (Sampaio et al. 2020) that double LOH events are not always independent of each other, and suggests that mutational bursts are likely contributors to the observed excess of double LOH.

Although the method of using single colonies as the starting population is ideal for relatively frequent mutation events like single LOH, it is not ideal for the measurement of very rare mutation events, such as double LOH. Because total size of the population of cells present in a single yeast colony is relatively small, it does not produce enough double LOH mutants that can be recovered and counted towards the rate calculations, thus potentially negatively affecting the accuracy of the mutation rate estimates for such rare events. On the inverse, while starting with a very large cell culture is helpful for better rate accuracy for rare events, growing a culture too large can negatively affect the accuracy of rate estimates for frequent mutation events such as single LOH. This is because each mutation event can leave many mutant descendants, particularly those events that happen early during the expansion of the culture. To accommodate both of these limitations, we also conducted our LOH rate experiments using larger liquid cultures. By combining these two experimental approaches together, we can have the strength of matched colonies with single rates and the strength of liquid cultures for double rates. Together they are able to give the most precise

estimation of the associated rates, both for frequent (single LOH) and rare (double LOH) mutation classes.

Our liquid-based cultures started with inoculating a full colony into 1 mL of rich media in a test tube and incubating the for 24 hours until saturation. These cultures were then washed and diluted before being plated onto the double selection media. After calculating the liquid-based double rate, we found it to be 3.3-fold higher compared to the same double rate calculated using the colony-based approach. Even though this new rate is slightly higher, we believe it to be a more methodologically sound estimation of the true double LOH rate. Conversely, the smaller cultures derived from the colony-based approach offer a better estimation of the single LOH rates. Thus, we compared the double LOH rate experimentally measured from liquid cultures to the expected double LOH rate calculated from colony-based cultures and obtained an alternative SGI ratio of ~79 (Figure 5C). This arguably even more robust experimental approach further strengthened the idea that double LOH events must not be entirely independent of each other, and that bursts may be happening relatively often.

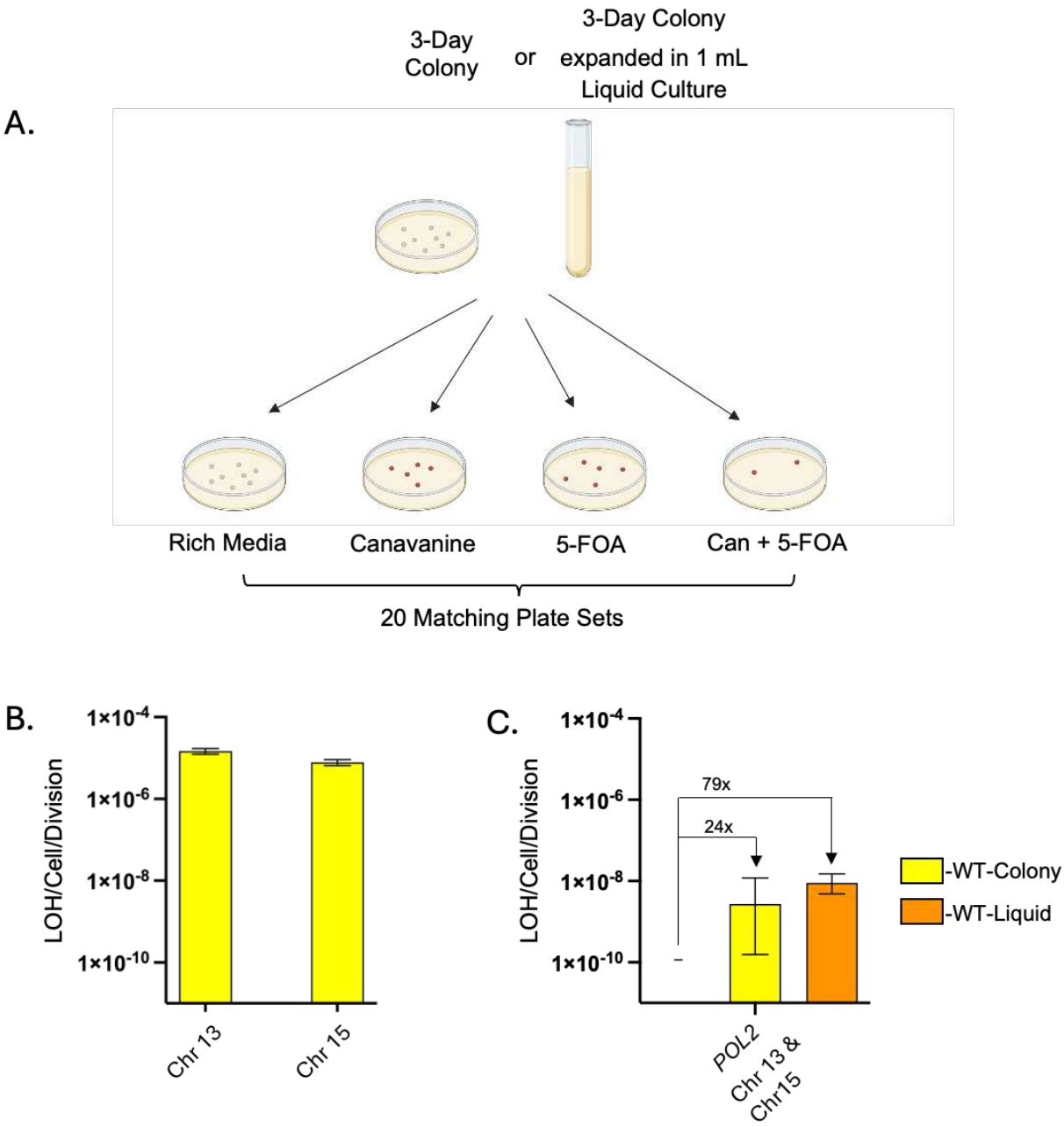

Figure 5. A. Counter selection experimental design. Cultures of the experimental strains are grown either on a rich media plate or in a liquid culture and then are aliquoted and plated onto a variety of plate types. Colony counts from these plates are then used to determine a rate through maximum likelihood estimations (MLE). **B, C.** Wild type strain LOH rates. Rates for single LOH at each loci are shown (B) for JAY3412-2. The observed double rate of LOH was determined to be 24-fold higher than expected (C).

Exploring a Relationship Between Ribonucleotide Excision Repair and SGI

As outlined in the Introduction, we hypothesize that an increase in GGE noise could lead to an increase in SGI. A recent report by Desai *et al* 2021 showed that GGE noise can be modulated by the frequency of base excision repair (BER). In their experiments, mouse embryonic stem cells in culture were treated with IDU, a thymine analogue, that was then mis-incorporated into the genome during DNA synthesis. Interestingly, this excess of inappropriate bases in DNA led to an elevation in GGE noise, and most importantly, this effect was dependent on BER removal of IDU from the genome. The authors hypothesized that the enzymatic transaction of repairing of DNA by BER has a consequence of interfering with the normal transcription of any gene where an IDU was inappropriately inserted, thus generating more opportunities for GGE noise between otherwise identical cells in a population. In other words, a relatively benign form of DNA damage that cells are well equipped to handle, may not lead to mutation, but the act of repair itself locally and transiently perturbs transcription in a given locus- and cell-specific manner, thus increasing inter-cell expression noise.

The above finding led us to attempt an analogous approach to GGE noise modulation in our yeast experiments, and to use it to inquire about a possible relationship to SGI. Due to *S. cerevisiae*'s natural inability to uptake IDU, we decided instead to pursue a natural and abundant source of endogenous DNA base damage, ribonucleotides. Ribonucleotides are estimated to be incorporated by various DNA polymerases in yeast around 13,000 times per cell cycle in yeast (Williams and Kunkel 2014). This makes them the most common form of DNA lesion. Even so, they are efficiently removed by ribonucleotide excision repair (RER). So, the high turnover nature

of this damage-repair system (*i.e.*, high incorporation and efficient removal) might represent an important source of GGE noise each time a mis incorporated ribonucleotide is removed. By extension, we hypothesized that altering the rate of ribonucleotide incorporation or blocking RER might also be utilized the tune GGE noise up or down in yeast. Specifically, high incorporation of ribonucleotides throughout the genome, including inside genes, would trigger an elevated level of RER activity, which would in turn enhance GGE noise genome wide. Conversely, deletion of key enzymes in the RER pathway might have the opposite effect of attenuating GGE noise.

To test this idea, we utilized a mutant allele of DNA polymerase delta, *pol2-M644G,* which results in 11-fold higher frequency of ribonucleotide incorporation during DNA synthesis (Nick McElhinny et al. 2010). We reasoned that strains containing this mutant polymerase would elicit higher rates of ribonucleotide excision repair (RER) to cope with the excess endogenous ribonucleotide burden, and thus also display higher GGE noise. If GGE noise is one of the contributing mechanisms underlying bursts of systemic and transient mutagenesis, then we predicted that *pol2-M644G* mutants might display a higher SGI ratio in the double LOH rate assay.

We created a homozygous *pol2-M644G* strain, JAY3441, using the same hybrid diploid strain background and the same dual-function LOH markers as described above. Using the same counter selection approach, we measured single LOH rates of 3.41×10^{-5} LOH/cell/division at Chr13R and 1.83×10^{-5} at Chr15R (Figure 6A). These rates both represented a 2-fold elevation of the LOH rate relative to *POL2* wild type, consistent with our own previously reported work (Cornelio et al. 2017).Assuming independent accumulation of LOH at these two regions, the expected the double rate of LOH in *pol2-*

M644G strain would be 6.23×10^{-10}. However, we measured the actual observed double LOH rate using colony-based cultures at 1.2×10^{-7}, resulting in an SGI ratio of ~193 (Figure 6B). This represented a substantial increase in the SGI ratio measured in the WT strain (~24), suggesting that the *pol2-M644G* genotype has a larger propensity for acquiring multiple mutations simultaneously.

To further investigate the role that *pol2-M644G* might be playing in SGI, we created two additional hybrid diploid strains, JAY3499 and JAY3501, containing the homozygous deletion of the *RNH201* gene that encodes the catalytic subunit of RNase H2. RNase H2 is the primary enzyme responsible for the removal of mis incorporated ribonucleotides in the genome through RER (Cerritelli and Crouch 2009). We hypothesized that if RER is playing a role in the increased SGI ratio in *pol2-M644G*, then deleting this key enzyme should attenuate this effect and bring the SGI ratio back down closer to WT levels. Strain JAY3499 contains *POL2* with *rnh201Δ*, making it RER defective but with base level ribonucleotide incorporation. JAY3501 is a *pol2-M644G rnh201Δ* double mutant, thus experiencing higher incorporation of ribonucleotides into its genome while also being unable to remove them through RER. We performed LOH counter selection assays with these strains and found that in the *rnh201Δ* strain the single LOH rates for Chr13 and Chr15 were 1.6- and 1.5-fold higher than WT (Figure 6A). Through our experiment, we were able to determine the colony-based double rate to have an SGI ratio of ~57 (Figure 6B). In the *pol2-M644G rnh201Δ* strain we found the LOH rates for Chr13 and Chr15 were 4.5- and 2.5-fold higher than WT respectively (Figure 6A). Through our experiment, we were able to determine the colony-based double LOH rate to have an SGI ratio of ~59 (Figure 6B). These results demonstrated

that by deleting *RNH201*, the SGI ratios decrease, due to the impairment of RER. Additionally, it is also important to note that even though the *pol2-M644G rnh201Δ* strain displayed the highest single LOH rates, its SGI ratio was relatively low. This uncoupling suggests that the factors that contribute to elevate the rate of single LOH events are not necessarily the same factors that lead to elevated coincident double LOH.

After calculating the double rates, we first compared them to those calculated by the colony-based approach and found that the rates were roughly the same for the *pol2-M644G* and *pol2-M644G rnh201Δ* genotypes (0.9- and 1.1- fold higher for the liquid cultures respectively), while *rnh201Δ* had slightly elevated rates (1.8-fold higher for the liquid cultures). Again, we believe them to be a better representation of the double LOH rates. We next compared them with the expected rates previously determined by our colony-based approach. We found that *pol2-M644G, rnh201Δ*, and *pol2-M644G rnh201Δ* had SGI ratios of ~178, ~99, and ~63 respectively (Figure 6C). The WT, *rnh201Δ*, and *pol2-M644G rnh201Δ* strains' SGI ratios all increased, while the *pol2-M644G* strain's SGI ratio decreased slightly. However, the main finding that the *pol2-M644G* genotype appears to raise the SGI ratio and while deleting *RNH201* brings it back down.

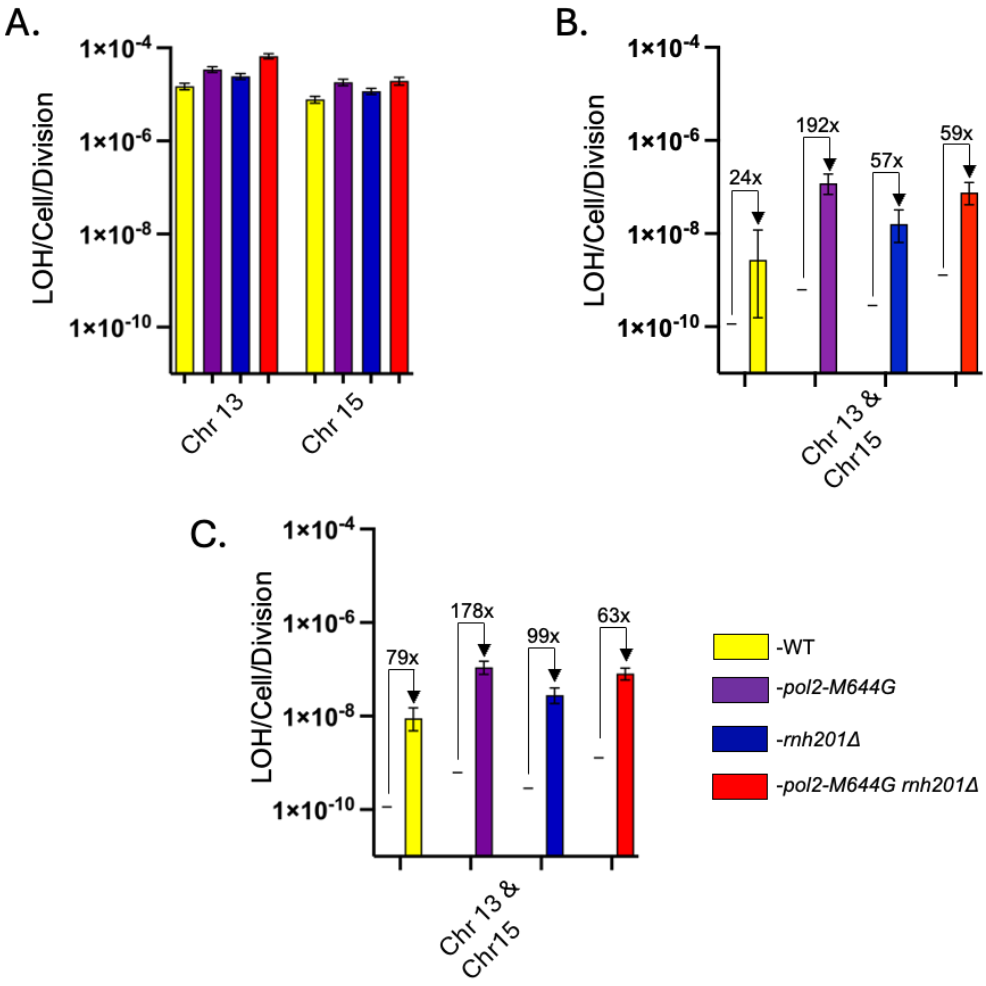

Figure 6. A, B. Four genotype single and double LOH rates through colony-based approach. Rates for individual and double LOH at the two different loci for various genotypes were measured using the MSS- MLE. The mutant allele *pol2-M644G,* which incorporates more ribonucleotides during DNA synthesis, had the highest observed/expected rate. By deleting *RNH201*, an important part of ribonucleotide excision repair, the observed/expected rate lowered back down. **C.** Four genotype double LOH rates through liquid culture-based approach. Expected rates calculated from the colony-based approach were compared to the double rates experimentally determined through liquid culture preparation. Patterns remain similar, with *pol2-M644G* having the highest amount of fold change.

Mutation Rate Assay in Homozygous Background

As an additional and independent test of a possible interaction between SGI, ribonucleotides, RER and GGE noise, we created new set of experimental diploid strains, including WT and the mutant genotypes above. In this case, the diploids were homozygous throughout their genomes for the S288c haploid strain background. These strains were derived from previous work reported by our group (Cornelio et al. 2017), however slightly modifying them to be amenable to the measurement of double LOH rates using both *CAN1* and *URA3*. These strains possessed a heterozygous *CAN1/can1* marker at its native loci on Chr5L, as well as the counter selectable CORE2 cassette ($_{Kl}$*URA3*-$_{Sc}$*URA3-KanMX4*) downstream of the *MAL13* gene, at a telomere proximal position on Chr7R (Figure 7A). We used the same colony-based approach as previously described for counter selection to determine both single and double LOH rates for Chr5L and Chr7R. Expected double rates were calculated in the same scheme as before by multiplying the colony-based single LOH rates together and were compared to the experimentally determined colony-based double LOH rates. We found that WT, *pol2-M644G, rnh201Δ*, and *pol2-M644G rnh201Δ* strains had double LOH rates with SGI ratios of ~58, ~99, ~53, and ~25 respectively (Figure 7B,C). Again, these results show the same trends in a homozygous background and with markers on different chromosomes. This independent experiment also corroborated the uncoupling between the rate of single LOH and SGI ratios. Specifically, the single LOH rates in *pol2-M644G rnh201Δ* were the highest, yet its SGI ratio was the lowest, reinforcing the suggestion that double LOH occurrence is driven by one or more processes that are distinct from those that determine single mutation.

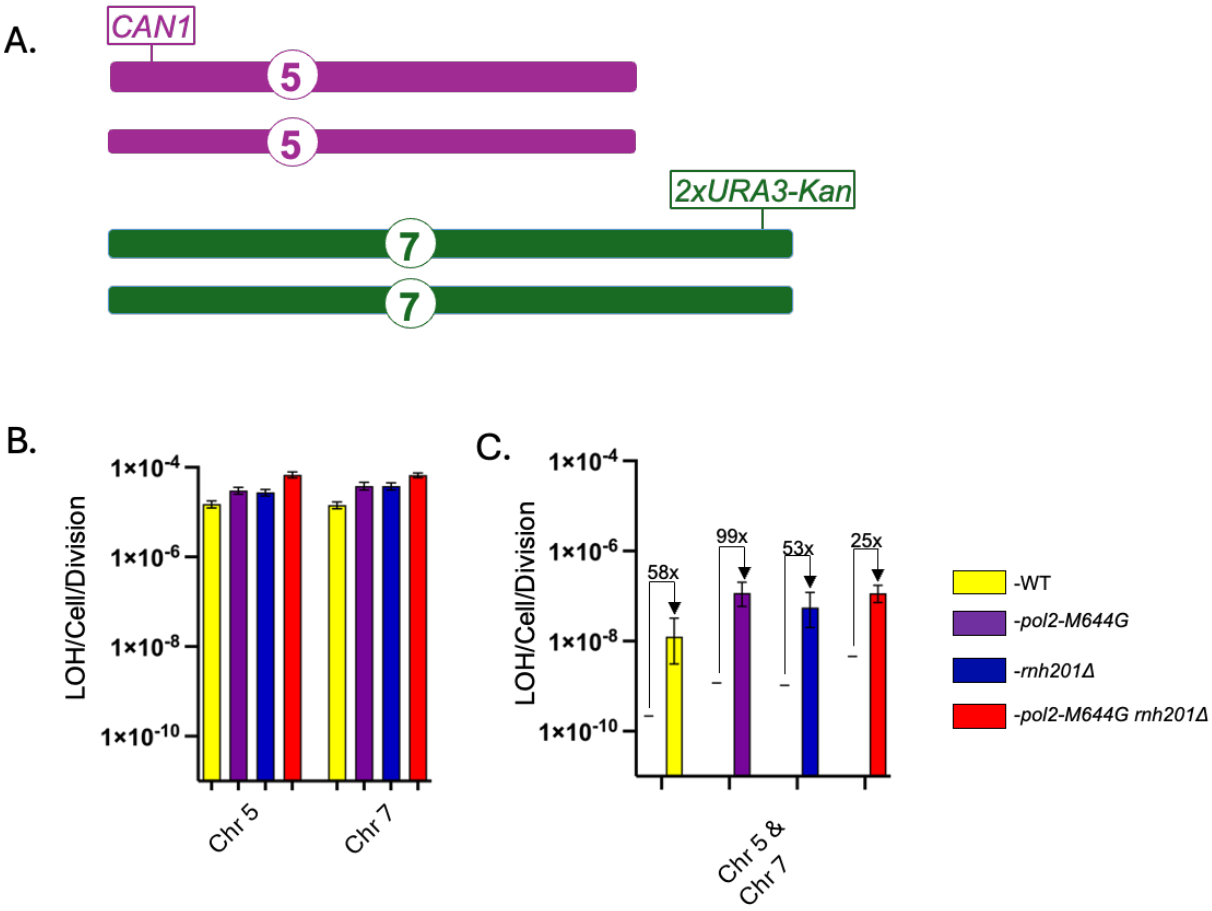

Figure 7. A. Homozygous strain background. Strains JAY3592, JAY3594, JAY3596, and JAY3598 are diploid homozygous S288c strains. They contain counter selectable markers *CAN1* and *URA3* on chromosomes 5 and 7 respectively. **B, C.** Colony-based LOH rates for homozygous strains. Single (A) and double (B) LOH rates are shown for the homozygous strain backgrounds. The pol2-M644G genotype again possesses the highest observed versus expected fold change at 99-fold higher.

Phylogenetic Screening in Defined Cellular Lineages

Earlier work from our group (Heasley et al. 2020; Sampaio et al. 2020), and the quantitative rate assays described above, strongly, albeit indirectly, suggested that LOH tracts can accumulate coincidently in bursts, and that these transient events most likely have brief durations, over one or two cell cycles. To directly test this model, we utilized the *ADE1* and *ADE2* screenable genes present in our dual function reporter cassettes (Figure 4). Compared to the counter-selection approach, screening for the presence of LOH tracts (red colonies that lost either *ADE1* or *ADE2*) requires permissive plating and visual inspection of hundreds of thousands of colonies and thus it is extremely laborious. However, it has the distinct advantage of preserving the viability of all cells involved, including non-LOH sibling (white) clones from the same cellular lineage as the LOH-carrying (red) clones. This permissive growth strategy in turn enables the subsequent genotyping analysis of all clones in the lineage and the resulting data can be used for the phylogenetic inference of the relative timing of LOH accumulation.

Another feature of this experimental approach was the ability to reduce as much as possible the overall time frame through which LOH mutations could accumulate in each culture. This was done in order to improve the time resolution of the phylogenetic inferences. We achieved this by growing thousands of nano (20 μl) cultures, each seeded from dilutions tuned to include a single yeast progenitor cell, and then incubated for 14 hours at 30C to allow a maximum of ~6 mitotic generations before being plated onto rich media with low adenine. For frame of reference, we estimate that the *CAN1* and *URA3* counter selection LOH rate assays described above involved yeast cell lineages that grew for between ~23 (colony-based) and ~28 (1 ml liquid-based)

consecutive cell divisions, producing total population sizes of ~10^7 and ~10^8 cells, respectively. Therefore, the nano cultures approach enabled an enormous reduction in the time and opportunities for single LOH to form, and most importantly for double LOH to co-accumulate.

We conducted control experiments in which nano cultures were started with the same dilution procedure but were plated immediately without allowing any incubation time for cell divisions in the liquid nano culture phase. These controls showed that most such-seeded nano cultures (85%) yielded zero or one colonies, providing confidence that most nano cultures that were used in the experiment were actually seeded by a single cell. In addition, for nano cultures that were allowed incubation time before plating, we limited our posterior analyses to only nano culture that yielded overall phylogeny sizes between 3 and 64 total colonies (red plus white). Fewer than 3 colonies meant that the nano culture was most likely stationary, whereas more than 64 colonies suggested that more than one live cell had seeded the nano culture, therefore plates below or above these colony number limits were discarded.

We carried out this procedure with both WT and *pol2-M644G* hybrid diploid strains, and between the two we plated and screened 7,510 nano cultures, containing a total of 370,300 colonies. Of these 1,544 produced plates with zero colonies, and another 637 produced plates with one or two colonies. 1,218 plates produced plates with 65 or more colonies. From the remaining 4,111 plates in the 3 to 64 colony range eligible for analysis, we identified 108 phylogenies containing one or more red colonies.

Each of these plates represented a single, complete, and independent phylogeny from which we screened for LOH by the presence of a red colony. While the frequency

of LOH is relatively high compared to other mutation classes (see Introduction), in absolute terms LOH is still quite rare (~1 in 3,000 red colonies). This, combined with the small number of colonies present in each eligible nano culture meant that the vast majority of plates consisted only of white colonies, and therefore were uninformative and discarded (Figure 8A). Occasionally (in 108 of the eligible cultures), red colonies were found, and they signaled that at least one LOH event had occurred in that cell lineage spanning either the *ADE1-CAN1* or *ADE2-$_{KI}$URA3* reporter insertion sites. Upon identification of a red colony, we phenotyped them to interrogate the presence of either counter-selectable marker and thus validate and distinguish the location of the primary screened LOH tract (Can^R Ura^+ for LOH on Chr13R or Can^S Ura^- for LOH on Chr15R). Next, we analyzed the screened red LOH-carrying colonies by WGS to characterize the precise location and nature of the screened/primary LOH mutation events using the many HetSNPs present between the two haploid parent strain's genomes. In addition, and most importantly, WGS allowed us to determine whether those red colonies also possessed one or more additional unselected/secondary structural variation tracts that could have accumulated either gradually or coincidently through a burst. Not surprisingly, in many cases the screened red colonies only contained one LOH tract, the primary one that gave them the red color phenotype. Since these were obviously uninformative for the study of mutation co-accumulation modes, those nano culture too were discarded (Figure 8B). All Scenario 2 LOH tracts are presumed to have occurred through random and independent mutational events that did not trigger other mutations elsewhere in the genome, and therefore were consistent with the classic Darwinian gradualistic process.

In other cases, 15 phylogenies derived from WT and 13 phylogenies derived from *pol2-M644G*, WGS did identify one or more unselected mutation tracts in the red colonies at additional genomic positions distinct from Chr13R or Chr15R (Figure 8 C,D). Because our nano culture screening approach allowed growth on the Petri plate of all living descendants of the single cell that founded that culture, whenever unselected LOH tracts were present in the red colony, the entire phylogeny (all sibling white colonies on the plate) was readily available for genotyping through PCR-RFLP and in some cases WGS. The summation of the genotyping was then used in a simple phylogenetic tree inference to deduce the relative timing of emergence between the screened primary (red-causing LOH tract) and the unselected secondary mutations. Mutations that were inferred to have occurred either in the same or in immediately consecutive cell division cycles were attributed to a punctuated accumulation mode (Figure 8D), whereas mutations separated in time by more than one cell generation where attributed to independent gradual accumulation (Figure 8C).

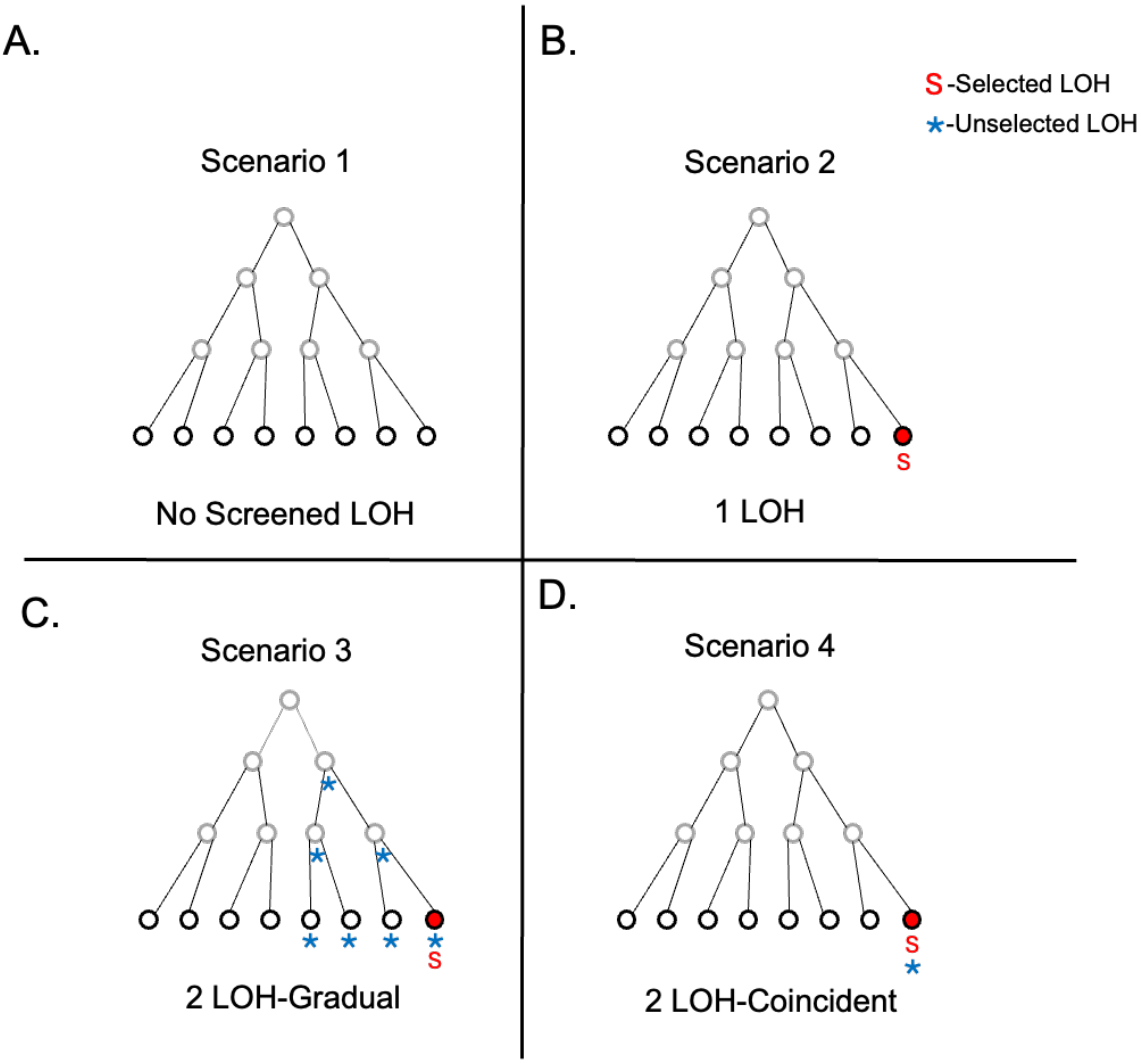

Figure 8. A. Scenario 1. A phylogeny where no colonies contain an LOH event, and all colonies appear white on a plate. **B.** Scenario 2. A phylogeny where there is one red colony present. Upon WGS, the LOH that turned the colony red is the only event. **C.** Scenario 3. A phylogeny where a red colony contains 2 LOH events, one selected and one unselected. Genotyping of the phylogeny reveals that other white colonies contain this unselected event, giving evidence of gradualism. **D.** Scenario 4. Another phylogeny that contains 2 LOH events, one selected and one unselected. Upon genotyping the rest of the phylogeny, none of the other colonies contain the unselected event, giving evidence of a mutational burst.

Phylogenetic Analysis of WT-Derived LOH Clones

Of our total 7,510 nano cultures, 5,025 were derived from the WT experimental strain. We found 63 eligible nano cultures containing at least one red colony, and through WGS we determined that 15 of these phylogenies possessed one or more secondary LOH tracts. Through genotyping of the white sibling colonies in these phylogenies we inferred whether or not evidence of bursts was present in those lineages. Overall, we detected direct and unambiguous evidence for coincident/punctuated LOH accumulation in 9 of 15 WT phylogenies. Below we describe in detail a few selected representative examples of the genotyping results and phylogenetic inferences. The reconstructed phylogenetic trees for all the remaining nano cultures are shown in Supplemental Information.

JS10 was a phylogeny that contained a total of 33 colonies with 1 being red (JS10R1). Upon WGS of JS10R1, we were able to detect 2 total LOH tracts on Chr13R and Chr4 (Figure 9A). The primary LOH on Chr13R was a terminal CN-LOH from position 554,724 to the end of the right arm of the chromosome, spanning the *ADE1-CAN1* reporter insertion site, and thus conferring the colony's red color and canavanine resistance. The secondary LOH is also a terminal CN-LOH on Chr4R from position 622,651 to the end of the chromosome (*TEL04R*) and made the region homozygous for the S288c alleles. We performed PCR-RFLP genotyping analysis (Figure 9B) for a HetSNP in the Chr4R CN-LOH region for the entire surviving phylogeny and found that 10 of the white clones were also homozygous S288c for this HetSNP. Together, this information implies that the unselected CN-LOH event on Chr4R happened first, and it was followed 3 cell divisions later by the screened CN-LOH event on Chr13R (Figure

10). This phylogeny provided a clear example of a linear, independent, sequential accumulation of two different mutations that is explained by gradualism. We found that 10 of the 15 WT phylogenies had similar patterns of gradualism.

A.

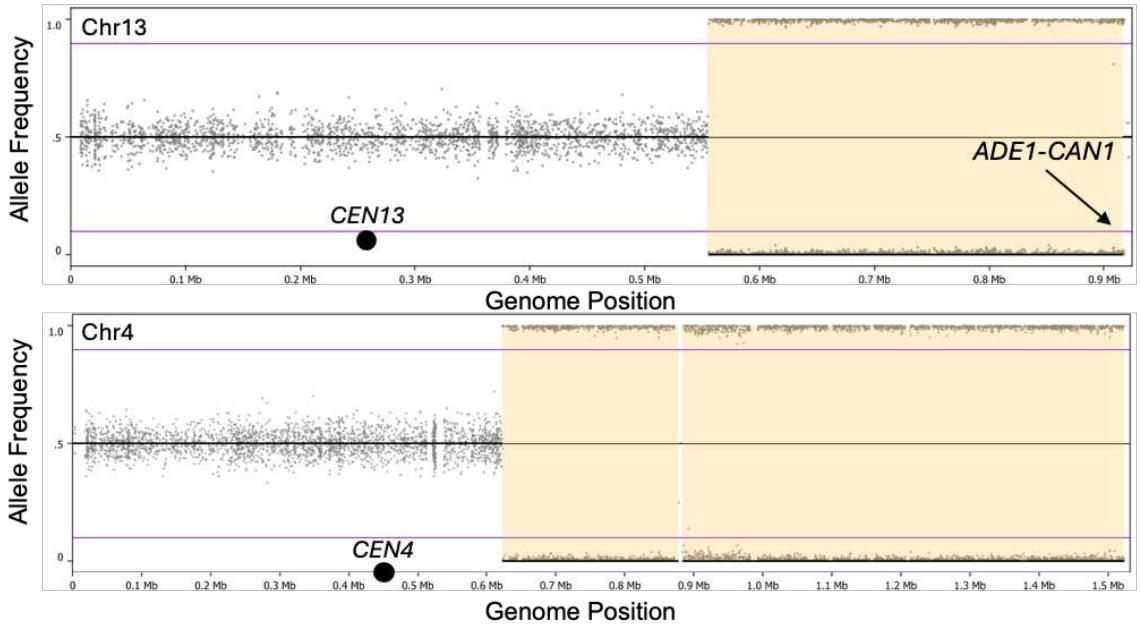

B.

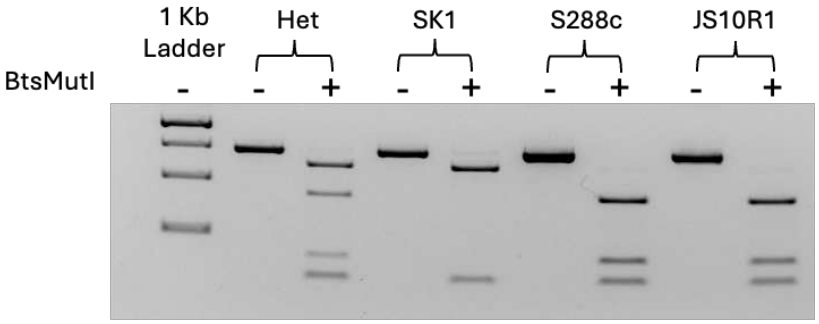

Figure 9. A. Sequencing Analysis of JS10 Family. A primary LOH was first detected on Chr13 both both the presence of a red colony in JS10R1 as well as a secondary LOH on Chr4. LOH events are colored yellow. **B.** Restriction Digest of JS10 Family. A portion of a an RFLP experiment done with the JS10 family is shown. The following lanes show the digestion patterns for the PCR product of the Chr4 LOH with BtsMutI. Lane 3 shows the digest pattern for a heterozygous diploid while lanes 5 and 7 show the digest patterns for either haploid parent, mimicking homozygous SK1 and S288c respectively. Lane 9 shows the digestion pattern for JS10R1, showing the same pattern as JAY3408, meaning it is homozygous S288c at this SNP.

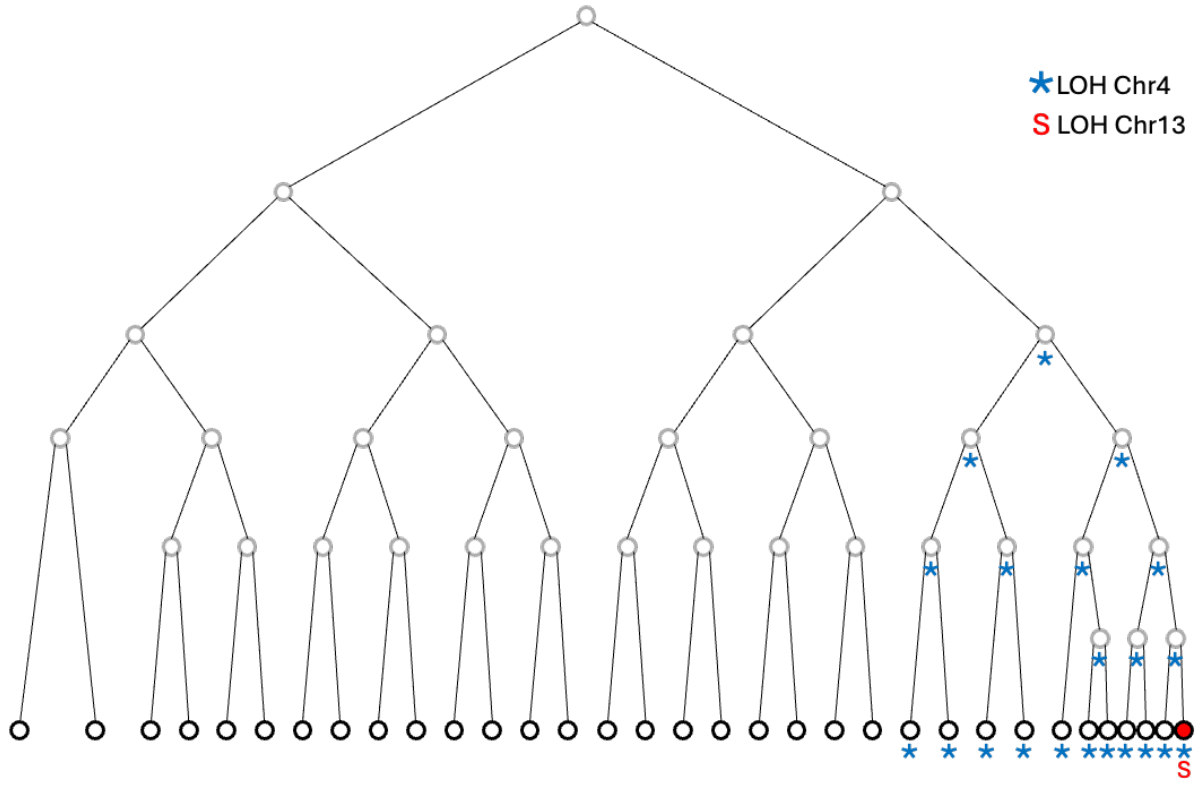

Figure 10. JS10 phylogenetic tree. The JS10 family contains 33 colonies with one red colony. There are two LOH events within the family on Chr4 and Chr13. Due to the presence of the LOH on Chr4 being in multiple colonies, we know that the event on Chr4 happened first followed by the event on Chr13 much later. This phylogeny arose from gradualism. Blue stars denote colonies containing the unselected Chr4 LOH while the red S denotes the colony with the screened LOH on Chr13.

JS39 was a phylogeny that contained only 5 total colonies with one being red (JS39R1). Due to the family's relatively small size, the entirety of the phylogeny, including the white clones, were all analyzed by WGS. We found that JS39R1 contained 4 total LOH events on Chr15, Chr11, and Chr12, all of them copy-neutral. The primary screen CN-LOH tract on Chr15 was a terminal event from 630,587 to *TEL15R* and conferred its red color and resistance to 5-FOA. There were two unselected LOH events on Chr11, one of them terminal LOH leading to S288c homozygosity from the left end of the chromosome (*TEL11L*) to position 92,948, and also a 23.5 Kb interstitial LOH between 225,909 to 249,447 leading to S288c homozygosity. The LOH tract on Chr12 was also a terminal LOH from 451,190 to the right end of the chromosome leading to S288c homozygosity. WGS analysis of all 4 sibling white clones showed that the regions corresponding to the JS39R1 LOH events on Chr11 and Chr12 remained heterozygous. Remarkably, one of the white clones, JS39W4, possessed an LOH tract at the exact same region on Chr15R in JS39R1, but homozygous for the SK1 alleles instead. This directly implies the two reciprocal products of a mitotic crossover event, and unequivocally ties JS39R1 and JS39W4 as direct siblings, separated in time by a single cell division of the same parent cell. With this particular pattern of mutation, the only explanation for the occurrence of the LOH tracts on Chr11 and Chr4 is a coincidental event, or burst, that also triggered the Chr15 crossover. This particular burst encompassed 4 LOH events in a single cell cycle (Figure 11). Overall, we found 10 of the 15 WT phylogenies had patterns of bursts.

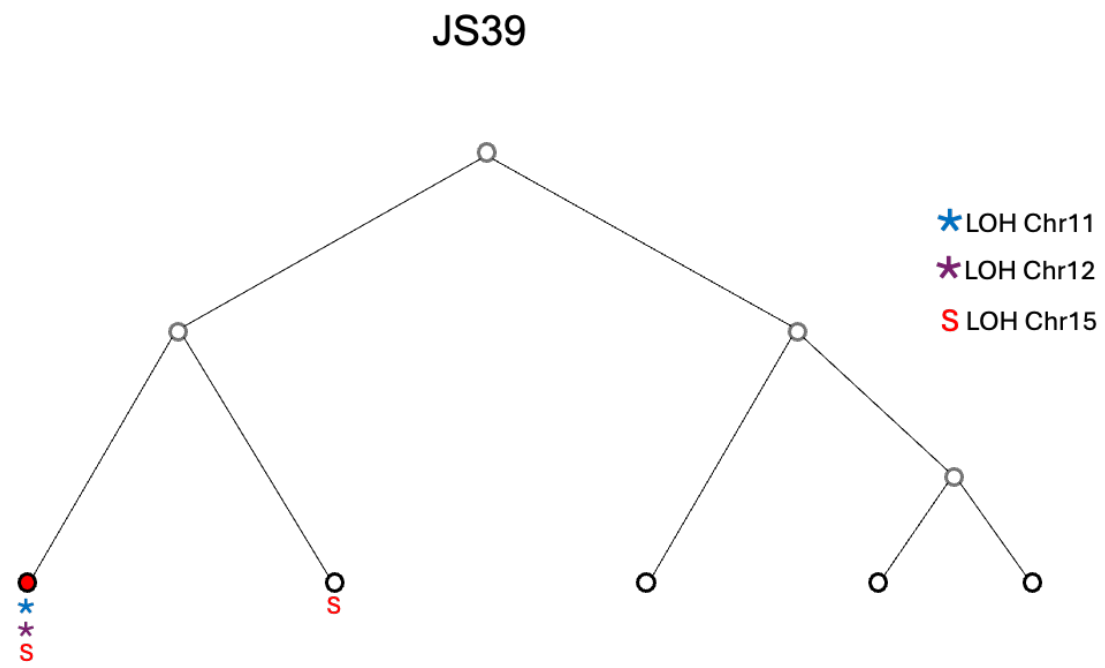

Figure 11. JS39 phylogenetic tree. The JS10 family contains 5 colonies with one red colony. There are 4 LOH events within the family on Chr11, Chr12, and Chr13. Due to the presence of the LOH events on Chr11 and Chr12 only being present in the red colony, these events most likely coincided. Additionally, one white colony possessed the other half a crossover that caused the event on Chr15. This phylogeny arose from bursts. Blue and purple stars denote colonies containing the unselected Chr11 and Chr12 events while the red S denotes the colonies with the screened LOH on Chr15.

JS3 was a phylogeny that consisted of a total of 40 colonies with 14 being red (JS3R1-R14). Upon WGS of JS3R1, we were able to detect 2 total LOH events on Chr15R and Chr11L. The screened LOH on Chr15R is a terminal LOH from position 653,057 to *TEL15R* and conferred the colony's red color and 5-FOA resistance. The unselected LOH was also a terminal LOH from the beginning of Chr11 (*TEL11L*) to position 129,862. We performed PCR-RFLP genotyping analysis for a HetSNP in the Chr11L region for the entire phylogeny and found that 8 of the red clones and all of the white clones were heterozygous for this marker SNP. However, 5 of the other red colonies possessed the same LOH event on Chr11. Together, this information implies that the LOH event on Chr15 happened first, followed immediately by the LOH event on Chr11. This is an example of a coincident burst event that took place over the span of two cell divisions (Figure 12). In our WT dataset, we found two phylogenies (JS3 and JS58) that contain similar inferred two-cell division burst.

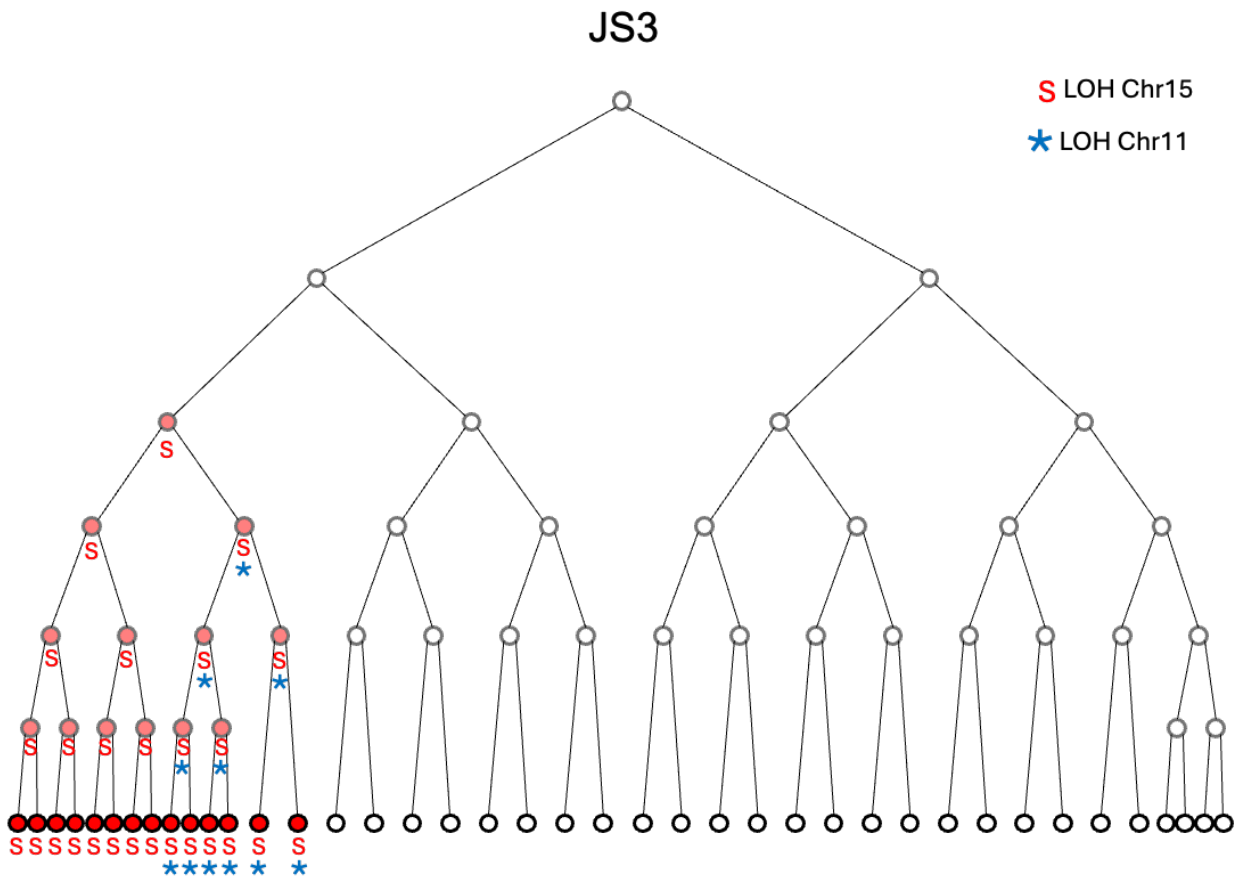

Figure 12. JS3 phylogenetic tree. The JS3 family contains 40 colonies with 14 red colony. There are 2 LOH events within the family on Chr15 and Chr11. Due to the presence of the unselected LOH being in about half of the red colonies, this demonstrates a burst that occurred over the course of two cell cycles. Blue stars denote colonies containing the unselected Chr11 events while the red S denotes the colonies with the screened LOH on Chr15.

JS56 was a phylogeny that contained a total of 64 colonies with only one being red (JS56R1). Upon WGS of JS56R1, we found 3 total LOH events on Chr13R, Chr2, and Chr11. The screened primary LOH on Chr13R is a terminal LOH from position 833,534 to *TEL13R* conferring the colony's red color and canavanine resistance (homozygous S288c). The other two LOH tracts were also terminal events, with Chr2R tract starting at 576,818 to the chromosome's right end (*TEL02R*) and Chr11L starting at the left end of the chromosome (*TEL11L*) up to position 338,559. We performed PCR-RFLP genotyping for HetSNPs in the respective Chr2 and Chr11 regions in all surviving white colonies in the phylogeny (JS56W1-W63). For the LOH event on Chr2, we found that 43 of the white colonies also contained the same event. Interestingly, for the LOH event on Chr11, only the red clone (JS56R1) possessed this tract. Collectively, this implied that the event on Chr2 happened first, early on in the lineage, followed by a coincidental event on Chr13 and Chr11 (Figure 13). This lineage demonstrates both gradualism and bursts, further supporting the idea that these mutation accumulation models are not mutually exclusive and rather play a cooperative role in the overall mutation landscape. We found 4 of the 15 WT phylogenies that had both gradualism and bursts.

An alternative explanation for this particular lineage is also possible. In this case, the nano culture would have been seeded by two cells, instead of a single cell as intended by our dilution approach. One of the two founding cells already carried the Chr2 LOH tract, while the other had no LOH tracts at all. The Chr2 LOH event would have happened on its own before the time window analyzed in this lineage, alter the Chr11 and Chr15 LOH tracts would coincide in one of the descendants of this founding

cell. In either case, however, the punctuated nature of Chr11 and Chr15 double LOH formation remains unchanged.

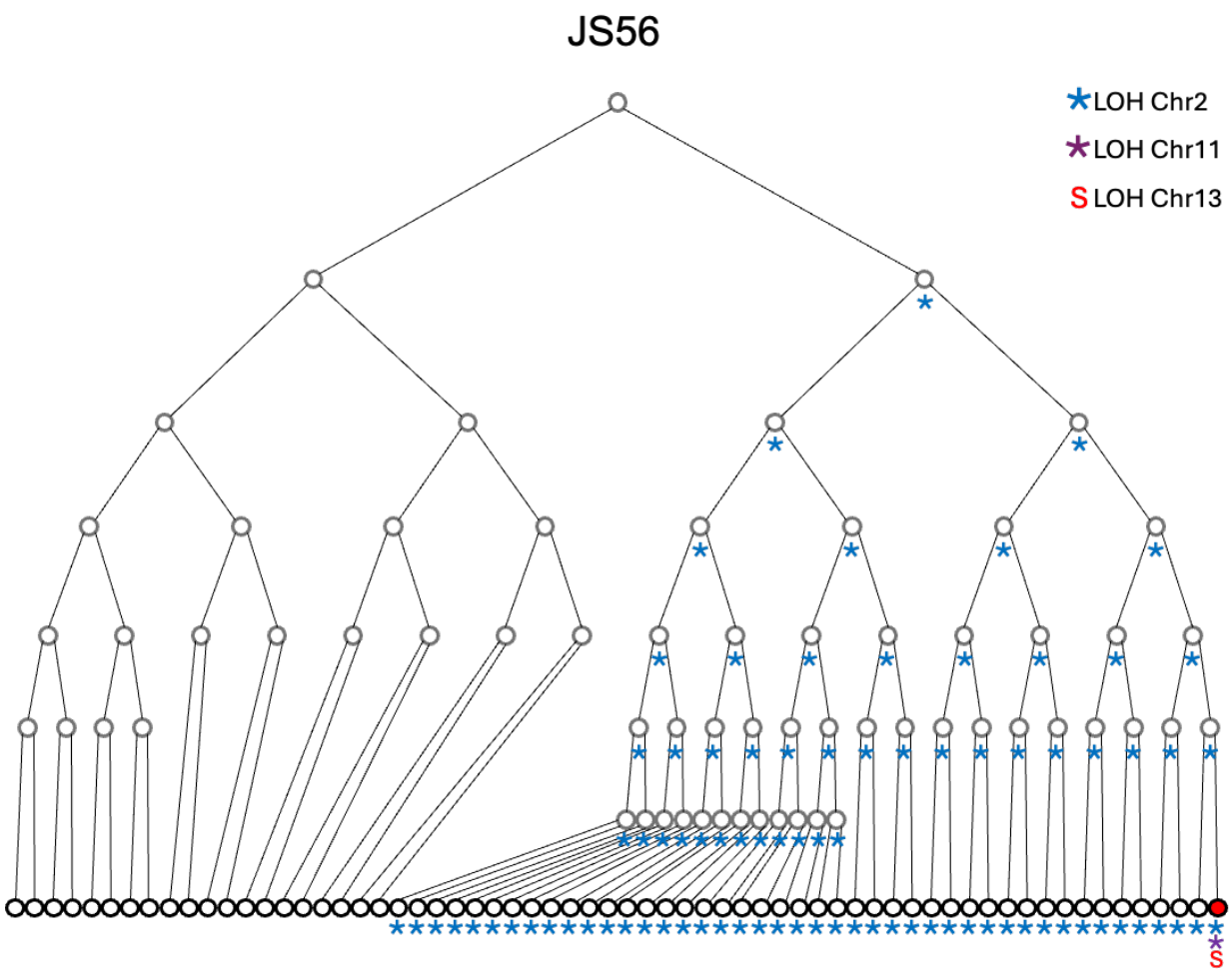

Figure 13. JS56 phylogenetic tree. The JS56 family contains 64 colonies with 1 red colony. There are 3 LOH events within the family on Chr2, Chr11, and Chr13. The unselected LOH on Chr2 was present in about 2/3 of the colonies, while the unselected LOH on Chr11 was only in the red colony. This is an example of a situation in which a phylogeny arose from both gradualism as well as a burst. Blue and purple stars denote colonies containing the unselected Chr2 and Chr11 events while the red S denotes the colonies with the screened LOH on Chr13.

Phylogenetic Analysis of pol2-M644G-Derived LOH Clones

Given the results the quantitative mutation rate assays described earlier (Fig X), we decided to also characterize the presence/frequency of punctuated bursts as well as their timing in the context of the *pol2-M644G* mutation, which we earlier observed resulted in a near 200-fold increase in the SGI ratio. Thus, we hypothesized that in *pol2-M644G* a higher proportion of coincident LOH tracts observed through our phylogenetic screen approach would be attributed to bursts compared to the WT control strain. We found that 9/15 WT phylogenies contained mutation bursts while *pol2-M644G* had a similar amount at 9/13 phylogenies. Below we describe the results from the analysis of a small number of representative and interesting examples of *pol2-M644G* phylogenies.

JSP45 was a phylogeny that contained a total of 34 colonies with 1 being red (JSP45R1). Upon WGS of JSP45R1, we were able to detect two total LOH tracts on Chr13R and Chr11. The screened primary LOH on Chr13R is a terminal LOH from 850,650 to TEL13R and conferred the colony's red color and 5-FOA resistance. The secondary LOH tract was also a terminal LOH from the left end of the chromosome (TEL11L) to position 83,549. We performed PCR-RFLP genotyping analysis for a HetSNP on Chr11 for the entire phylogeny and found that 5 of the white clones also carried this LOH tract. Together, this information implies that the event on Chr11 occurred first, followed by a brief period of stability, then the event on Chr13. This phylogeny is another example of gradualism (Figure 14). We found 7 of the 13 *pol2-M644G* phylogenies had patterns of gradualism.

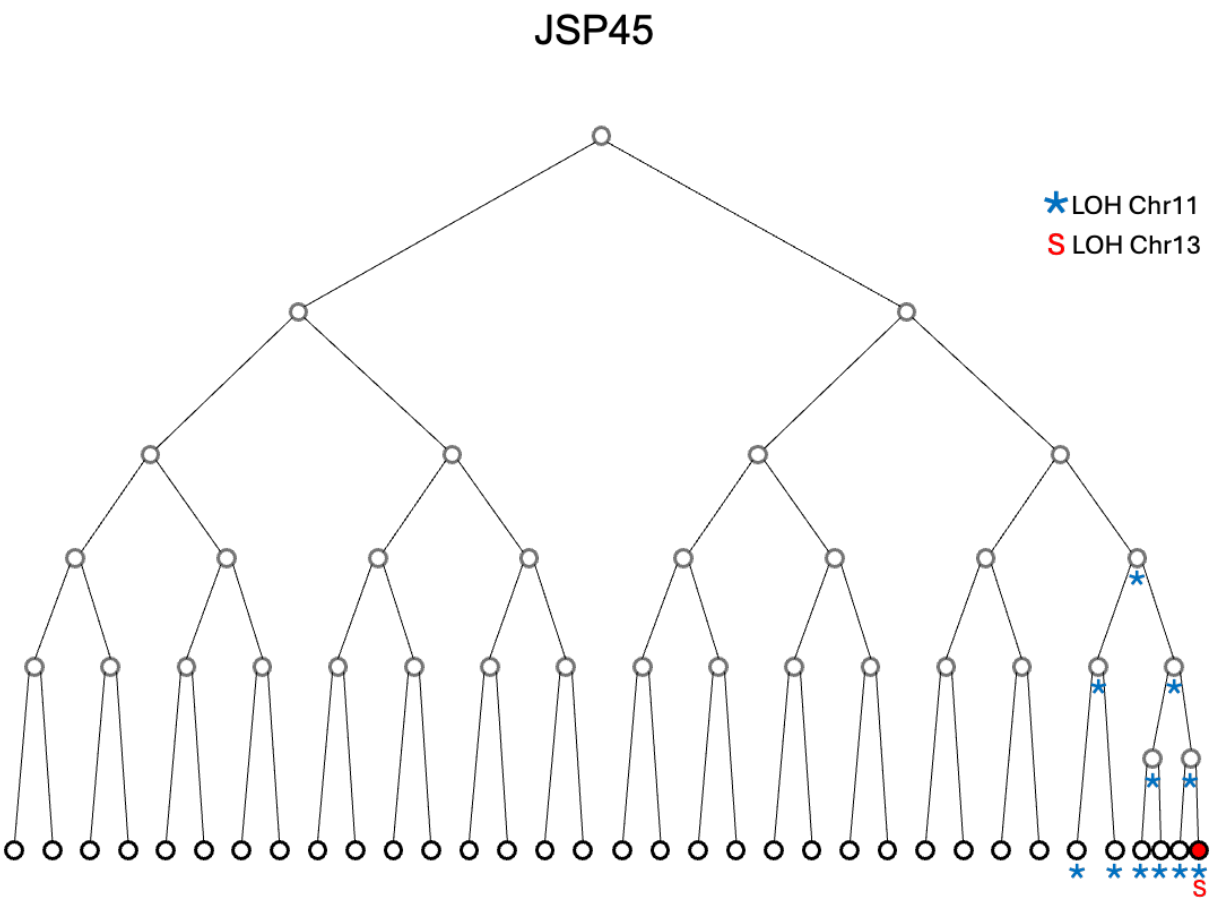

Figure 14. JSP45 phylogenetic tree. The JSP45 family contains 34 colonies with one red colony. There are two LOH events within the family on Chr11 and Chr13. Due to the presence of the LOH on Chr11 being in multiple colonies, we know that the event on Chr4 happened first followed by the event on Chr13 much later. This phylogeny arose from gradualism. Blue stars denote colonies containing the unselected Chr11 LOH while the red S denotes the colony with the screened LOH on Chr13.

JSP23 was a phylogeny that contained a total of 20 colonies with only one being red (JSP23R1). Upon WGS of JSP23R1, we were able to detect two total LOH tracts on Chr13R and Chr7. The screened primary LOH on Chr13 is a terminal LOH from 264,034 to *TEL13R* and conferred the colony's red color and canavanine resistance. The secondary LOH tract on Chr7 was also a terminal LOH from 528,828 to the end of the chromosome (*TEL07R*). We performed PCR-RFLP genotyping analysis for a HetSNP on the corresponding Chr7 region for the entire phylogeny and found that all white colonies in the phylogeny were heterozygous at this HetSNP. Together, this information implies that the events on Chr7 and Chr13 must necessarily have happened coincidentally in the same division, providing another clear example of a burst (Figure 15). We found that 9 of the 13 *pol2-M644G* phylogenies had bursts.

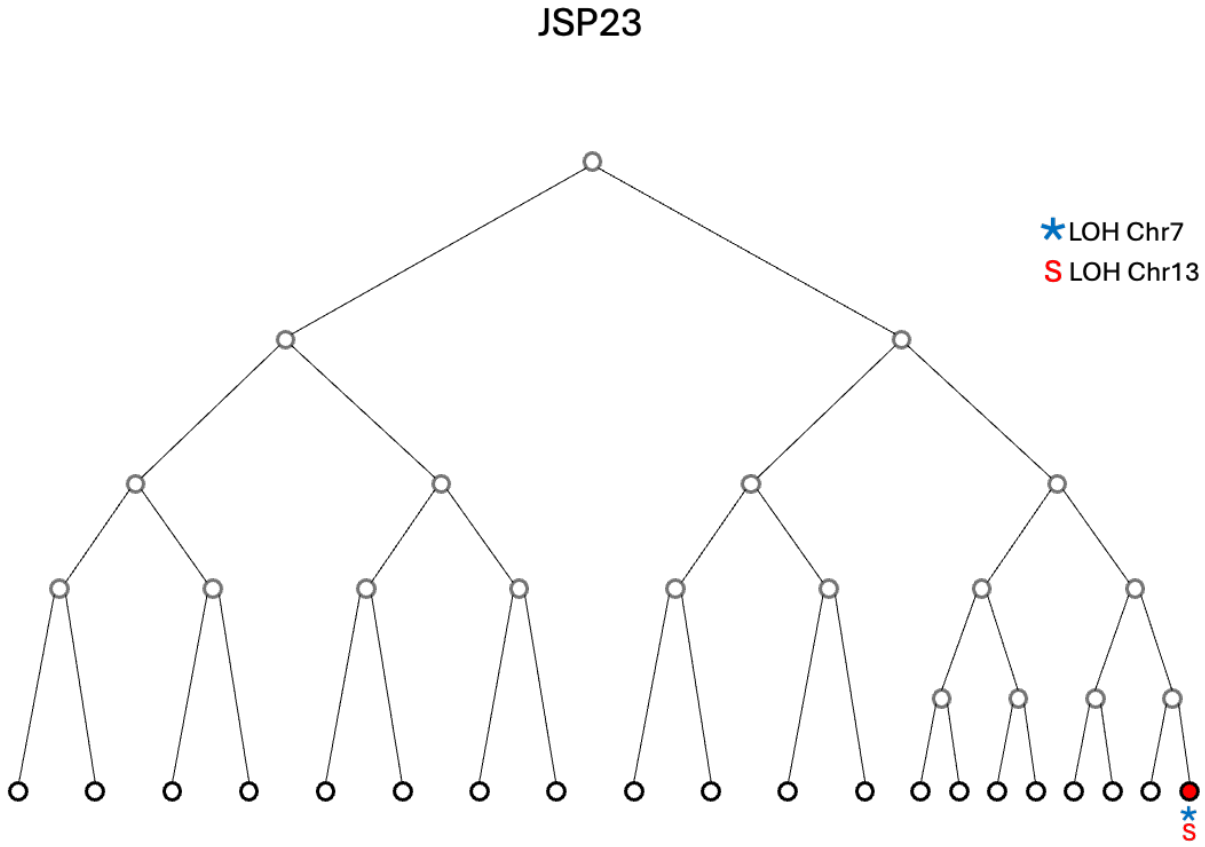

Figure 15. JS39 phylogenetic tree. The JS10 family contains 20 colonies with one red colony. There are two LOH events within the family on Chr7 and Chr13. Due to the presence of the LOH events on Chr7 and Chr13 only being present in the red colony, these events most likely coincided. This phylogeny arose from bursts. Blue stars denote colonies containing the unselected Chr7 event while the red S denotes the colonies with the screened LOH on Chr13.

JSP20 is a phylogeny that contains a total of 20 colonies with two being red (JSP20R1 and R2). Upon WGS of JSP19R1 and R2, we found a total of 3 LOH events on Chr13, Chr16, and Chr4. The primary LOH on Chr13 is a terminal LOH from 447,488 to *TEL13R*. The LOH events on Chr16 and Chr4 are also terminal LOH events, with the Chr4 event from position 656,349 to the end of the chromosome (*TEL4R*) and the Chr16 event from the beginning of the chromosome (*TEL16L*) to position 292,215. We performed PCR-RFLP analysis for the HetSNPs on Chr16 and Chr14 for the remaining white colonies and found that the LOH on Chr14 was shared with two white colonies, and the LOH on Chr16 with four white colonies. Together, this information implies the LOH event on Chr16 occurred first, immediately followed by the event on Chr4, and then again immediately followed by the event on Chr13 (Figure 16). Due to the relatively short time period for this to occur, we infer that this particular phylogeny also is the product of a mutation burst that took multiple cell cycles to complete, much like JS58. In our *pol2-M644G* dataset, this multi cell division burst occurred in two (JSP20 and JSP32) of the 13 phylogenies.

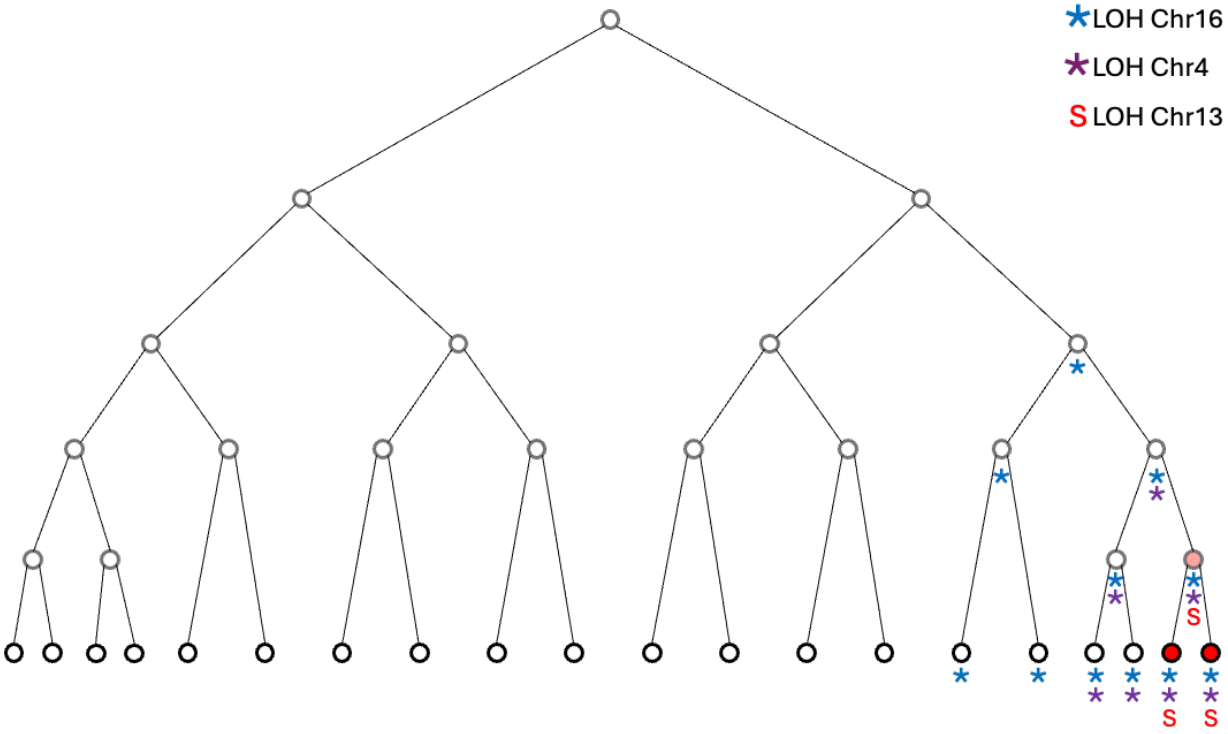

Figure 16. JSP20 phylogenetic tree. The JSP20 family contains 20 colonies with two red colonies. There are three LOH events within the family on Chr16, Chr4 and Chr13. This tree shows all three of the events happening all immediately after each other. This phylogeny arose from a multi cell division burst. Blue and purple stars denote colonies containing the unselected Chr16 and Chr 4 events while the red S denotes the colonies with the screened LOH on Chr13.

JSP43 is a phylogeny that contains a total of 58 colonies with one being red (JSP43R1). Upon WGS of JSP43R1, we found 3 total LOH events on Chr13, Chr11, and Chr16. The primary LOH on Chr13 is a terminal LOH from 735,170 to *TEL13R* and conferred the colony's red color and canavanine resistance. The other two LOH events were interstitial LOH events, with Chr11 from positions 74,603 to 79,688 and Chr16 from 393,808 to 405,804. We performed PCR-RFLP for HetSNPs in Chr11 and Chr16 in the remaining white colonies in the phylogeny (JSP43W1-W57). For the LOH event on Chr11, we found that 14 of the white colonies also possessed this LOH event. However, only the red colony in this family possessed the LOH on Chr16. Together, this information implies that the event on Chr11 occurred first, followed by the events on Chr13 and Chr16 together. This phylogeny is another example of both gradualism and bursts both contributing to a mutational landscape (Figure 17). We found that 3 of the 13 *pol2-M644G* phylogenies had patterns of both gradualism and bursts.

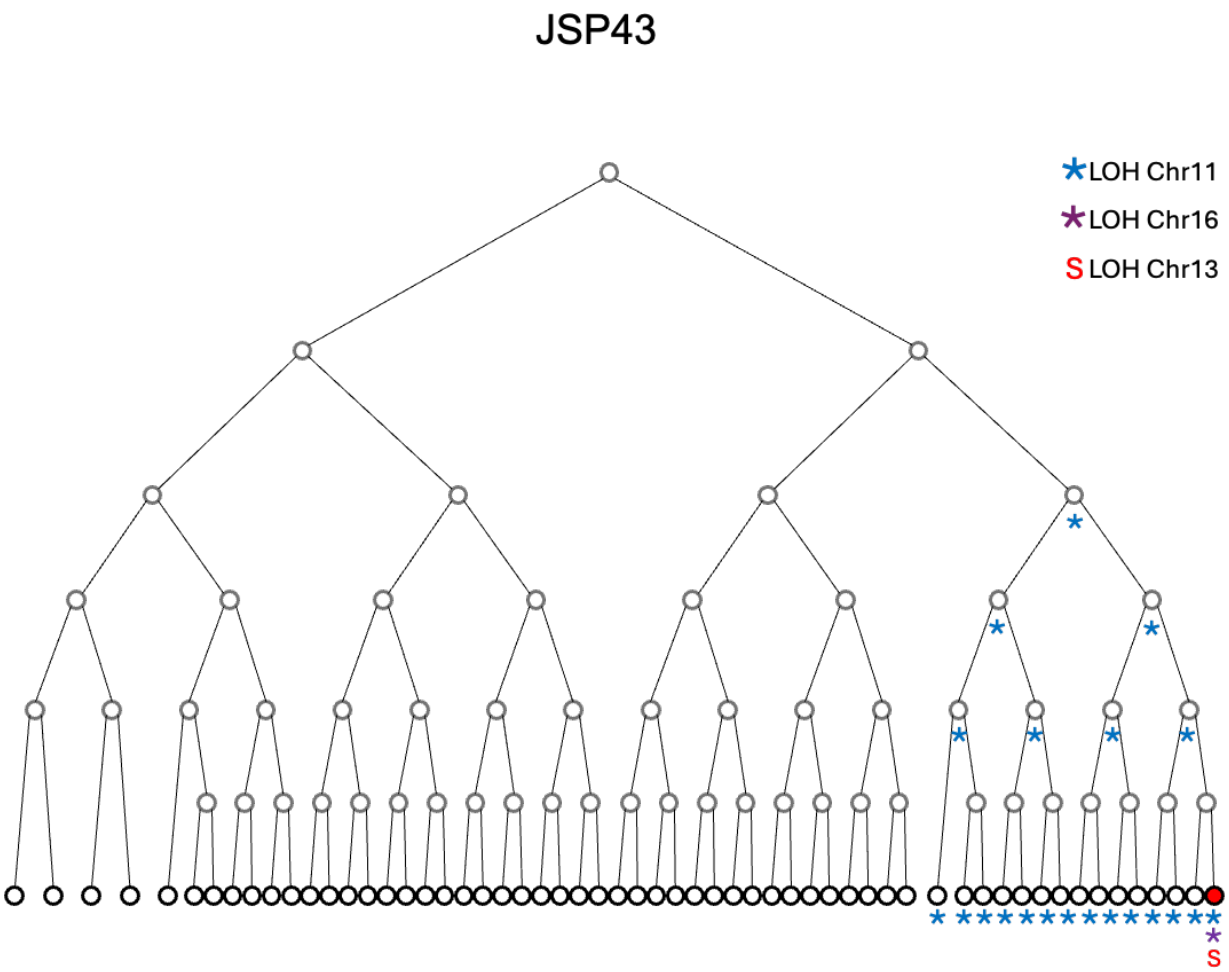

Figure 17. JSP43 phylogenetic tree. The JSP43 family contains 58 colonies with one red colonies. There are three LOH events within the family on Chr11, Chr16 and Chr11. This tree shows the event happening on Chr11 first and then the events on Chr14 and Chr13 happening coincidentally later. This phylogeny arose from both gradualism and bursts. Blue and purple stars denote colonies containing the unselected Chr11 and Chr 16 events while the red S denotes the colonies with the screened LOH on Chr13.

We investigated 15 WT phylogenies and 13 *pol2-M644G* phylogenies. Out of the 15 WT phylogenies, bursts were present in 10 (67%), while in the *pol2-M644G* phylogenies, bursts were present in 8 (62%). These experiments demonstrate that not only are bursts present, but they happen at a relatively high frequency. Additional LOH analysis information can be found in Supplementary Tables 2 and 3.

Single Cell RNA-Sequencing Analysis of GGE Noise

GGE noise modulation in Desai *et al* 2021 was determined by using single cell RNA-sequencing (scRNA-seq) in mammalian cells exposed to either DMSO or IDU. They were able to determine that the IDU treatment cause in increase in GGE noise by comparing population variance of the mean transcript count for all the expressed genes detected in their study. They found that for each gene, cells treated with IDU had a two-fold higher measurement of variance of transcript counts between individual cells within the cell population compared to the DMSO controls, and that this elevation was dependent on an active BER pathway. However, the mean number of transcripts for the total cell populations remained largely unaltered between IDU and DMSO treatments, with or without BER inhibition. In other words, the introduction of highly repairable DNA damage (IDU) elevated GGE noise. We used this principle as the motivation to ask whether or not the robust SGI ratio modulation phenotype uncovered in our previous experiments with *pol2-M644G* (high endogenous ribonucleotide incorporation damage) and *rnh201Δ* (absence of the corresponding repair pathway) mutants might also be associated with increased or attenuated GGE noise in yeast, respectively.

We carried out scRNA-seq in a set of four S288c-isogenic haploid strains (WT, single *pol2-M644G* and *rnh201Δ* mutants, and the *pol2-M644G rnh201Δ* double mutant. Single cell transcript counts for each genotype were then obtained, and count variance between cells was measure as measure of GGE noise. Using the scRNA-Seq described in Jackson *et al* 2020, we were able to obtain transcript counts for a total of roughly 15,000 cells, including internal controls standards. On average, there were 2,444 unique transcripts counted per cell. We calculated the population variance as well as the mean

transcript count for each gene per cell. When comparing GGE noise for all genes in WT versus *pol2-M644G,* there was no clear difference in transcript count variance (Figure 18A).

Next, we focused on a smaller specific set of individual genes of interest and compared their expression profiles and inter-cell expression heterogeneity (noise). The genes we chose included some to ones with highest expression, which make up a large proportion of the per-cell transcriptome. We also analyzed the single cell transcription profiles of genes previously identified in a systematic screen to participate in suppression of LOH (*i.e.*, their deletion resulted in increased in LOH rates) (Andersen et al. 2008). Genes *ENO2* (encoding Enolase II, a phosphopyruvate hydratase involved in glycolysis) and *RPL3* (encoding Ribosomal 60S subunit protein L3) were identified to be among the most highly expressed in our data and showed no noticeable difference in the distribution in their transcript count between WT and *pol2-M644G* (Figure 18B). Transcripts from these two genes corresponded to disproportionately large proportions, 4% and 1% respectively, of the total detected per cell transcriptomes among the ~6,000 genes in *S. cerevisiae*. In such extreme cases, it may be that transcription rates are so high that they become inherently buffered from noise modulation effects.

In stark contrast, the genome stability genes we focused on (known to be involved in LOH suppression) displayed far lower absolute expression levels (Figure 18C). Among these, genes *DPB3*, *TOP1*, *RAD51*, and *RAD54* each also did not show noticeable differences in the distribution in their transcript counts per cell between WT and *pol2-M644G*. However, these 4 genes also had extremely low numbers of transcripts counted per cell, in fact with the majority of cells having no transcripts

detected at all (inset numbers in Figure 18C histograms). The analysis of scRNA-Seq data from the *rnh201Δ* single mutant cells, and from *pol2-M644G rnh201Δ* double mutants also displayed very similar results, compared to WT, *pol2-M644G* single mutant, and to each other, thus are not shown.

Taken together, while in general the scRNA-Seq dataset did not reveal any evidence of up or down modulation of GGE noise by ribonucleotide damage or the RER pathway, the ultimate interpretation of results was hampered by the fact that we could not adequately measure noise for lowly expressed genes, including those most likely to impact LOH mutagenesis. Despite its overall high quality, the scRNA-Seq data generated in our study did not have enough resolution to capture enough transcripts from these key genes to support a robust interpretation. On one hand, GGE noise may simply not be affected by excessive ribonucleotide or lack of RER at all. On the other hand, noise modulation by ribonucleotides/RER may be buffered in highly expressed genes and undetectable in lowly expressed ones due to current technical limitations of scRNA-Seq.

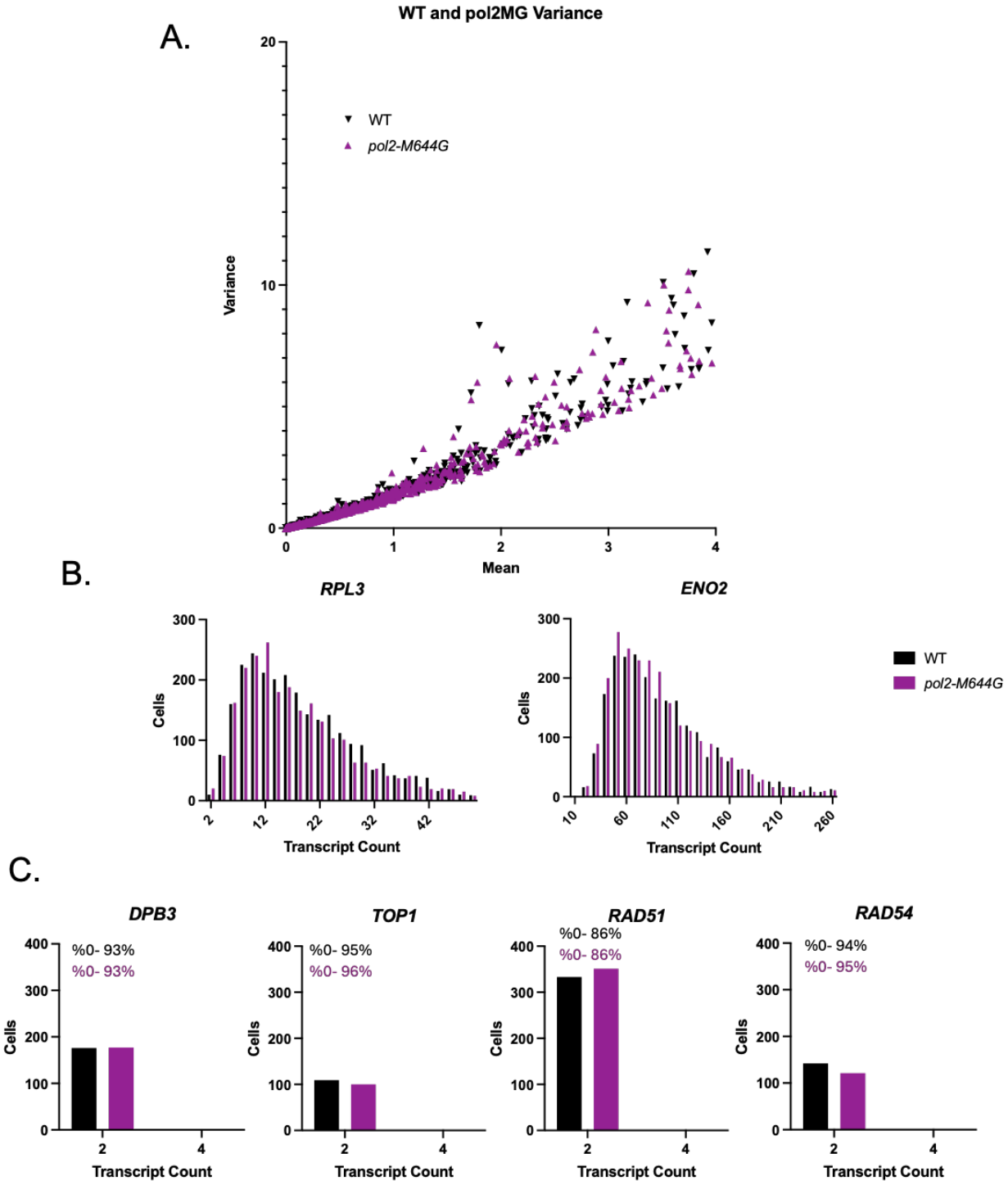

Figure 18. A. Single Cell RNA-Sequencing. Population variance of all yeast genes was calculated and compared to mean transcript count. There appears to be no difference between WT and *pol2-M644G* strains in terms of noise in GGE. **B., C.** Transcription distribution of individual genes. The transcript counts for select **B.** highly expressed genes and **C.** genes important in LOH are shown. Inlets display the percentage of cells that had zero total transcripts for the specific gene.

CHAPTER 3 – DISCUSSION

Through the use of our unique dual purpose gene cassettes, we were able to address multiple questions concerning SGI and mutation bursts. The mutation rate assays were able to show that the assumption of independence still gives rise to an excess in observed rate of double LOH, agreeing with our previous findings by earlier studies. Interestingly, these new experiments allowed for the testing and identification of a mutant that we hypothesized to lead to a larger SGI ratio. The *pol2-M644G* mutant showed the highest SGI ratio of ~178, the largest we have observed in terms of LOH. We hypothesized that this increase in SGI ratio was likely due to noise in GGE, although further experiments done to test this leave this question open-ended.

The phylogenies through nano cultures were able to show directly and unambiguously yeast clones where multiple LOH tracts must necessarily have formed through a mutational burst, something we have previously not been able to show at this resolution. Out of our 28 phylogenies collected between our two genotypes, 18 (64%) exhibited some type of burst event. This evidence shows that bursts contribute a major role in the accumulation of multiple mutations. Our experiments were also able to identify potential lengths of burst events. While the majority of bursts took place over a single cell cycle, we saw four phylogenies that exhibited a burst that took place over two cell cycles. We hypothesize that whatever is causing SGI, in some cases may linger within the cell for a few cell divisions before becoming resolved, giving rise to a multi cell division burst. Surprisingly, our *pol2-M644G* strain phylogenies did not have a higher incidence of mutation bursts. We hypothesized that since the SGI ratio was twice as

high as the WT, we would observe more phylogenies with bursts, although this is not what we observed. This could be explained either by the relatively small sample size or the already high affinity for bursts that the WT strain has. Additionally, while break points of the primary LOH on Chr13 and Chr15 seemed random, there appeared to be a bias in our study as to the chromosome of the secondary unselected LOH. Of the 28 phylogenies, 14 of them had an LOH on Chr11, 7 of these being one of the chromosomes involved in a burst. There does not currently appear to be any literature on Chr11 being a hotspot for recombination or containing a common fragile site. Further experimentation could be done to try to resolve this bias.

Noise in GGE serves as a potential mechanism for SGI, as it is both transient and has the ability to indiscriminately cause genome instability in a very short time frame. Our experiments hoped to address this potential cause through the use of our *pol2-M644G* strains. As mentioned previously in our mutation rate assays, the *pol2-M644G* strains had the highest SGI ratio. We hypothesized that this was due to noise in GGE caused by RER, further supported by our other strains showing a lower SGI ratio where we impaired RER by deleting *RNH201*. However, when we directly tested this hypothesis through our ScRNA-seq experiments, we found no notable difference in noise by measuring population variance for each gene. These results either suggest that the method we utilized to detect noise in GGE in yeast was not sensitive enough or our *pol2-M644G* strains do not have a higher level of noise. The ScRNA-seq experiments were only able to capture an average of 2,444 transcripts per cell, which his standard for *S. cerevisiae* studies (Gasch et al. 2017; Nadal-Ribelles et al. 2019; Jariani et al. 2020). Current literature suggests a range of 15,000-30,000 transcripts per

yeast cell (Hereford and Rosbash 1977; Miura et al. 2008; Pelechano et al. 2010). This relatively low level of recovery may not best represent the amount of noise in these strains. It is also possible that our *pol2-M644G* strains do not have more noise than the WT. This leaves open the door to alternate explanations we see in the mutation rate assays, such as replication stress, something that this genotype was originally found to raise in its initial publication. Further experiments such as using a GFP-reporter system to check the variance in fluorescence or treating WT cells with drugs that induce replication stress may help elucidate the actual systems at play.

Some literature seems to give the impression that the idea of gradualism and punctuated equilibrium at are odds with each other, that it must be one model or the other. This idea that they oppose each other is a false one, as the present study shows that these events are not mutually exclusive. There were a number of phylogenies within this study that demonstrated both gradualistic and burst-like patterns. Rather than being separate ideas, we propose that the idea of punctuated equilibrium adds onto the idea of gradualism to fill in situations where either one is weaker.

Not only will these experiments provide a further understanding on how life evolved into having the complex genomes we have today, but also help us understand how the genomes of tumors found in cancer patients may arise (Casasent et al. 2018; Gao et al. 2021). LOH events have been linked to a multitude of genetic diseases such as cancer, neurological diseases, and more (Steinmann et al. 2009; Nichols et al. 2020). In this investigation, we aimed to tie together the role of systemic instability in causing these burst mutations that can lead to a more complex genome. Our system in yeast

will be able to add on to the current understanding of how systemic genomic instability occurs and its consequences.

CHAPTER 4 – MATERIALS AND METHODS

Media and Growth

Standard procedures for yeast transformation, crossing, and sporulation were followed. Strains were grown either in liquid or solid YPD, synthetic minimal media (SC) plus canavanine (60 mg/L), SC plus 5-FOA (1 g/L), or SC plus canavanine and 5-FOA where specified.

Strain Construction

The strains constructed for this study are hybrid, diploid *Saccharomyces cerevisiae.* The two haploid parents of the hybrid came from two different genetic backgrounds, S288c and SK1. These two strains are evolutionarily diverged from each other and contain approximately 4 single nucleotide polymorphisms (SNPs) about every 1 kb (SK1 references). This highly heterozygous genome allows for the ease of sequencing resolution when it comes to detecting LOH events. Two gene cassettes were placed at the ends to two of the longest chromosome arms in *S. cerevisiae.* Each of these cassettes contained two genes (*ADE1-CAN1* or *ADE2-*$_{KI}$*URA3*) that were first deleted from their native loci before being transformed to their experimental loci. *ADE1* and *ADE2* were utilized for screening for LOH while *CAN1* and $_{KI}$*URA3* were used for counterselection. *ADE1* and *ADE2* are naturally occurring yeast genes that are involved in the adenine synthesis pathway. If either of these genes become nonfunctional, a buildup of a red pigmented adenine intermediate (CAIR and SAICAR) forms in the cells that turns colonies from white to red (Rébora et al. 2001), an essential phenotype for our screening experiments. *CAN1* and $_{KI}$*URA3* are also native yeast genes that when

lost allow for the resistance of either the drug canavanine or 5-fluoroorotic acid (5-FOA) respectively. These counter selectable genes allowed us to perform LOH rate assays. The cassette containing *ADE1* and *CAN1* was placed at the end of chromosome 13, between *YMR317W* and *ADH6* at position 910,871, while the cassette containing *ADE2* and $_{KI}$*URA3* was placed at the end of chromosome 15, between *PHR1* and *YOR387C* at position 1,068,920. These loci were chosen due to previous literature showing they were subject to high amounts of natural recombination (Sui et al. 2020). When an LOH event spans the loci that contains either of these gene cassettes, colonies on a plate turn from white to red and obtain either resistance to canavanine (event on 13) or 5-FOA (event on 15). To ensure all events come from mitotic recombination and not meiotic, the experimental strains are *ime1Δ* preventing them from entering meiosis. This also prevents the return to growth phenotype often seen in yeast that could be mistaken for a mutation burst. We also made the strains *mss11Δ* to prevent any flocculation and to ensure colonies were started by a single cell.

For our experiments addressing noise in gene expression, we created *POL2* mutant strains with the same background as our initial experiments. We utilized the mutant polymerase *pol2-M644G,* found to incorporate ribonucleotides at a level 11 times higher than wildtype (Pursell et al. 2007). This polymerase has a point mutation that changes a methionine next to the steric gate of the enzyme to a glycine. In previous experiments done by our lab, *pol2-M644G* has been shown to increase the rates of LOH. Additionally, we also created *rnh201Δ* strains, a subunit of RNase H2, effectively limiting the ability of ribonucleotide excision repair. The genotypes for all strains used in these experiments is shown in Table 1.

Table 1. Strains constructed for this study

Strain Name	Ploidy	*MAT* A/α	Genotype
JAY3364	1n	a	*ura3::TY, cup1Δ, sfa::hisG, trp1Δ, leu2Δ, mss11Δ, hoΔ, ade1Δ, ade2Δ, lys2Δ, tkl2Δ, PHR1::ADE2-klURA3, can1::NAT, ADH6::ADE1-CAN1, ime1::TRP1*
JAY3408	1n	α	*ura3-52, leu2D1, trp1D63, ade2D::natMX, ade1D::hphMX, can1, ime1D::TRP1, mss11Δ*
JAY3412-0	2n	a/α	JAY3364xJAY3408
JAY3412-1	2n	a/α	JAY3364xJAY3408
JAY3412-2	2n	a/α	JAY3364xJAY3408
JAY3412-3	2n	a/α	JAY3364xJAY3408
JAY3439	1n	α	*ura3-52, leu2D1, trp1D63, ade2D::natMX, ade1D::hphMX, can1, ime1D::TRP1, mss11Δ, KanMX-pol2M644G*
JAY3378	1n	a	*ura3::TY, cup1Δ, sfa::hisG, trp1Δ, leu2Δ, mss11Δ, hoΔ, ade1Δ, ade2Δ, lys2Δ, tkl2Δ, PHR1::ADE2-klURA3, can1::NAT, ADH6::ADE1-CAN1, ime1::TRP1, pol2-M644G::Kan*
JAY3441	2n	a/α	JAY3378xJAY3439
JAY3487	1n	a	*ura3::TY, cup1Δ, sfa::hisG, trp1Δ, leu2Δ, mss11Δ, hoΔ, ade1Δ, ade2Δ, lys2Δ, tkl2Δ, PHR1::ADE2-klURA3, can1::NAT, ADH6::ADE1-CAN1, ime1::TRP1, rnh201::skLEU2*
JAY3489	1n	α	*ura3-52, leu2D1, trp1D63, ade2D::natMX, ade1D::hphMX, can1, ime1D::TRP1, mss11Δ, rnh201::skLEU2*
JAY3499	2n	a/α	JAY3487xJAY3489
JAY3492	1n	a	*ura3::TY, cup1Δ, sfa::hisG, trp1Δ, leu2Δ, mss11Δ, hoΔ, ade1Δ, ade2Δ, lys2Δ, tkl2Δ, PHR1::ADE2-klURA3, can1::NAT, ADH6::ADE1-CAN1, ime1::TRP1, pol2-M644G::Kan, rnh201::skLEU2*
JAY3494	1n	α	*ura3-52, leu2D1, trp1D63, ade2D::natMX, ade1D::hphMX, can1, ime1D::TRP1, mss11Δ, KanMX-pol2M644G, rnh201::skLEU2*
JAY3501	2n	a/α	JAY3492xJAY3494
JAY1321	1n	a	*MAL13::Kan-URA3x2, ura3Δ, PEX17, pol2-M644G, rnh201D::HYG*
JAY3590	1n	α	*MAL13, ura3Δ, PEX17, pol2-M644G, rnh201D::HYG can1*
JAY3592	2n	a/α	JAY1321xJAY3590
JAY1168	1n	a	*ade5-1, his7-2, leu2-3,112,* Leu+, *trp1-289, cup1D, RSC30, sfa1D::hisG, lys2Δ, ura3Δ, MAL13::CORE2*
JAY3586	1n	α	*ade5-1, his7-2, leu2-3,112,* Leu+, *trp1-289, cup1D, RSC30, sfa1D::hisG, lys2Δ, ura3Δ, can1*
JAY3594	2n	a/α	JAY1168xJAY3586
JAY1318	1n	a	*MAL13::Kan-URA3x2, ura3Δ, PEX17, pol2-M644G*
JAY3588	1n	α	*ade5-1, his7-2, leu2-3,112, LEU+, trp1-289, cup1D, RSC30, sfa1D::hisG, ura3Δ, pol2- M644G, can1*
JAY3596	2n	a/α	JAY1318xJAY3588
JAY1165	1n	a	*ade5-1, his7-2, leu2-3,112, LEU+, trp1-289, cup1D, RSC30, sfa1D::hisG, lys2Δ, ura3Δ, rhn201D::Hyg,* Ura+
JAY3584	1n	α	*ade5-1, his7-2, leu2-3,112, LEU+, trp1-289, cup1D, RSC30, sfa1D::hisG, lys2Δ, ura3Δ, rnh201D:: Hyg, can1*
JAY3598	2n	a/α	JAY1165xJAY3584

Mutation Rate Assays

Our counter selective approach is adapted from the experiments depicted in Sampaio 2020. Cells for these experiments were prepared in either of two different methods. To generate the most effective single LOH rates, cells were struck to single colonies on YPD and allowed to grow for 3 days at 30° C. For effective double LOH rates, our hybrid strains were grown until saturation in 1 mL of liquid YPD. These liquid cultures were then spun to pellet the cells and cells were washed twice with water. Individual colonies or spun down pellets were then dissolved into 1 mL of water. Dilutions from aliquots of these cultures will be plated onto four separate plates: 50 μl at 10^{-4} dilution onto YPD, 50 μl at 10^{-1} dilution onto 5-FOA, 25 μl at 10^{-4} dilution onto canavanine, and 450 μl undiluted onto two plates of 5-FOA + canavanine. We determined the rates of LOH for each marker loci by counting the colonies on their corresponding plate types. Colony counts were then used by the R program mlemur (Łazowski 2023) to generate maximum likelihood estimates (MSS-MLEs) (Luria and Delbrück 1943) for each single and double rate. Expected frequencies for double LOH were calculated by multiplying the corresponding single rates for each genotype (Sampaio et al. 2020). Fold change shown is a measurement of the observed double rates divided by the expected.

Nano Culture Phylogenies

To prepare cells for plating, we prepared 10 mL liquid cultures of YPD for both our wild type and *pol2-M644G* strains and allowed them to grow to saturation. These cultures were then diluted to 10 mL at 10^{-6} concentration. We filled 96-well plates with 20 μl of this culture into each of the wells, creating nano cultures. The nano cultures

grew for 14 hours at 30° C. After growth (5 or 6 cell divisions), we added 100 μl of water to each well to increase their volume. Each well was plated onto its own SC low adenine plate. These plates grew for 2 days at 30° C. We counted and recorded the colony count for each plate and screened them for the presence of a red colony. Plates that were eligible for continued phylogenetic analysis contained at least one red colony and less than 64 total colonies on the plate. Sectored colonies appeared during this experiment, but were not counted for analysis, as the events leading to a sectored colony occurred outside the timing for the experiment.

Whole Genome Sequencing

Colonies were sequenced using Illumina whole genome sequencing in the same methods described in previous studies by our lab (Heasley et al. 2021). We used YeaStar Genomic DNA kits to extract high quality DNA and prepared the multiplex libraries using seqWell plexWell 96 kits. The University of Colorado Cancer Center Genomics Core and Novogene completed the sequencing for 150 bp paired reads at an average of 100X coverage. Sequencing reads were mapped to the S288c genome using CLC Genomics Workbench and LOH were identified using Nexus Copy Number.

PCR-Restriction Fragment Length Polymorphism (RFLP) Assays

RFLP was utilized to both verify as well as determine the presence of LOH tracts in both red colonies and their accompanying white colony siblings. PCR primers were created that would cross at least two restriction sites as well as a corresponding SNP that would be affected by the LOH and remove/add a restriction site. PCR products were then cut using the recommended conditions per enzyme. The resultant products were run on a 1.7% agarose gel where genotypes for the LOH tracts were determined.

Single Cell RNA-Sequencing

scRNA-Seq was performed by the David Gresham Lab at NYU using the protocol described in their work (Jackson et al. 2020).

REFERENCES

Aksenova A, Volkov K, Maceluch J, Pursell ZF, Rogozin IB, Kunkel TA, Pavlov YI, Johansson E. 2010. Mismatch repair-independent increase in spontaneous mutagenesis in yeast lacking non-essential subunits of DNA polymerase ε. *PLoS Genet* **6**: e1001209.

Andersen MP, Nelson ZW, Hetrick ED, Gottschling DE. 2008. A genetic screen for increased loss of heterozygosity in Saccharomyces cerevisiae. *Genetics* **179**: 1179-1195.

Araki H, Hamatake RK, Morrison A, Johnson AL, Johnston LH, Sugino A. 1991. Cloning DPB3, the gene encoding the third subunit of DNA polymerase II of Saccharomyces cerevisiae. *Nucleic Acids Res* **19**: 4867-4872.

Argueso JL, Alani E. 2020. Hundreds of thousands of cell generations reveal a treasure chest of genome alterations. *Proc Natl Acad Sci U S A* **117**: 31567-31569.

Bell MA. 2009. Implications of a fossil stickleback assemblage for Darwinian gradualism. *J Fish Biol* **75**: 1977-1999.

Bentley RA. 2022. Prehistory of Kinship. *Annual Review of Anthropology* **51**: 137-154.

Bull HJ, McKenzie GJ, Hastings PJ, Rosenberg SM. 2000. Evidence that stationary-phase hypermutation in the Escherichia coli chromosome is promoted by recombination. *Genetics* **154**: 1427-1437.

Casanova EL, Konkel MK. 2020. The Developmental Gene Hypothesis for Punctuated Equilibrium: Combined Roles of Developmental Regulatory Genes and Transposable Elements. *Bioessays* **42**: e1900173.

Casasent AK, Schalck A, Gao R, Sei E, Long A, Pangburn W, Casasent T, Meric-Bernstam F, Edgerton ME, Navin NE. 2018. Multiclonal Invasion in Breast Tumors Identified by Topographic Single Cell Sequencing. *Cell* **172**: 205-217.e212.

Cerritelli SM, Crouch RJ. 2009. Ribonuclease H: the enzymes in eukaryotes. *FEBS J* **276**: 1494-1505.

Choate KA, Lu Y, Zhou J, Choi M, Elias PM, Farhi A, Nelson-Williams C, Crumrine D, Williams ML, Nopper AJ et al. 2010. Mitotic recombination in patients with ichthyosis causes reversion of dominant mutations in KRT10. *Science* **330**: 94-97.

Chumki SA, Dunn MK, Coates TF, Mishler JD, Younkin EM, Casper AM. 2016. Remarkably Long-Tract Gene Conversion Induced by Fragile Site Instability in Saccharomyces cerevisiae. *Genetics* **204**: 115-128.

Cornelio DA, Sedam HN, Ferrarezi JA, Sampaio NM, Argueso JL. 2017. Both R-loop removal and ribonucleotide excision repair activities of RNase H2 contribute substantially to chromosome stability. *DNA Repair (Amst)* **52**: 110-114.

Cross WCh, Graham TA, Wright NA. 2016. New paradigms in clonal evolution: punctuated equilibrium in cancer. *J Pathol* **240**: 126-136.

Darwin C. 1859. On the origin of species by means of natural selection, or preservation of favoured 274 races in the struggle for life.

Dennis MY, Eichler EE. 2016. Human adaptation and evolution by segmental duplication. *Curr Opin Genet Dev* **41**: 44-52.

Dutta A, Dutreux F, Schacherer J. 2021. Loss of heterozygosity results in rapid but variable genome homogenization across yeast genetic backgrounds. *Elife* **10**.

-. 2022. Loss of Heterozygosity Spectrum Depends on Ploidy Level in Natural Yeast Populations. *Mol Biol Evol* **39**.

Eldredge N, Gould S. 1972. Punctuated Equilibria: An Alternative to Phyletic Gradualism. Models of Paleobiology.

Field MG, Durante MA, Anbunathan H, Cai LZ, Decatur CL, Bowcock AM, Kurtenbach S, Harbour JW. 2018. Punctuated evolution of canonical genomic aberrations in uveal melanoma. *Nat Commun* **9**: 116.

Gao R, Bai S, Henderson YC, Lin Y, Schalck A, Yan Y, Kumar T, Hu M, Sei E, Davis A et al. 2021. Delineating copy number and clonal substructure in human tumors from single-cell transcriptomes. *Nat Biotechnol* **39**: 599-608.

Gao R, Davis A, McDonald TO, Sei E, Shi X, Wang Y, Tsai PC, Casasent A, Waters J, Zhang H et al. 2016. Punctuated copy number evolution and clonal stasis in triple-negative breast cancer. *Nat Genet* **48**: 1119-1130.

Gasch AP, Yu FB, Hose J, Escalante LE, Place M, Bacher R, Kanbar J, Ciobanu D, Sandor L, Grigoriev IV et al. 2017. Single-cell RNA sequencing reveals intrinsic and extrinsic regulatory heterogeneity in yeast responding to stress. *PLoS Biol* **15**: e2004050.

Gould SJ, Eldredge N. 1993. Punctuated equilibrium comes of age. *Nature* **366**: 223-227.

Heasley LR, Sampaio NMV, Argueso JL. 2021. Genome-Wide Analysis of Mitotic Recombination in Budding Yeast. *Methods Mol Biol* **2153**: 201-219.

Heasley LR, Watson RA, Argueso JL. 2020. Punctuated Aneuploidization of the Budding Yeast Genome. *Genetics* **216**: 43-50.

Hereford LM, Rosbash M. 1977. Number and distribution of polyadenylated RNA sequences in yeast. *Cell* **10**: 453-462.

Hwang MS, Mog BJ, Douglass J, Pearlman AH, Hsiue EH, Paul S, DiNapoli SR, Konig MF, Pardoll DM, Gabelli SB et al. 2021. Targeting loss of heterozygosity for cancer-specific immunotherapy. *Proc Natl Acad Sci U S A* **118**.

Jackson CA, Castro DM, Saldi GA, Bonneau R, Gresham D. 2020. Gene regulatory network reconstruction using single-cell RNA sequencing of barcoded genotypes in diverse environments. *Elife* **9**.

Jangam D, Feschotte C, Betrán E. 2017. Transposable Element Domestication As an Adaptation to Evolutionary Conflicts. *Trends Genet* **33**: 817-831.

Jariani A, Vermeersch L, Cerulus B, Perez-Samper G, Voordeckers K, Van Brussel T, Thienpont B, Lambrechts D, Verstrepen KJ. 2020. A new protocol for single-cell RNA-seq reveals stochastic gene expression during lag phase in budding yeast. *Elife* **9**.

Jinks-Robertson S, Petes TD. 2021. Mitotic recombination in yeast: what we know and what we don't know. *Curr Opin Genet Dev* **71**: 78-85.

Leighton J, Hu M, Sei E, Meric-Bernstam F, Navin NE. 2023. Reconstructing mutational lineages in breast cancer by multi-patient-targeted single-cell DNA sequencing. *Cell Genom* **3**: 100215.

Loeb LA. 2011. Human cancers express mutator phenotypes: origin, consequences and targeting. *Nat Rev Cancer* **11**: 450-457.

Loeillet S, Herzog M, Puddu F, Legoix P, Baulande S, Jackson SP, Nicolas AG. 2020. Trajectory and uniqueness of mutational signatures in yeast mutators. *Proc Natl Acad Sci U S A* **117**: 24947-24956.

Luria SE, Delbrück M. 1943. Mutations of Bacteria from Virus Sensitivity to Virus Resistance. *Genetics* **28**: 491-511.

Lynch M. 2010. Evolution of the mutation rate. *Trends Genet* **26**: 345-352.

Lynch M, Sung W, Morris K, Coffey N, Landry CR, Dopman EB, Dickinson WJ, Okamoto K, Kulkarni S, Hartl DL et al. 2008. A genome-wide view of the spectrum of spontaneous mutations in yeast. *Proc Natl Acad Sci U S A* **105**: 9272-9277.

Miura F, Kawaguchi N, Yoshida M, Uematsu C, Kito K, Sakaki Y, Ito T. 2008. Absolute quantification of the budding yeast transcriptome by means of competitive PCR between genomic and complementary DNAs. *BMC Genomics* **9**: 574.

Mokyr J. 1990. Punctuated Equilibria and Technological Progress. *The American Economic Review* **80**: 350-354.

Nadal-Ribelles M, Islam S, Wei W, Latorre P, Nguyen M, de Nadal E, Posas F, Steinmetz LM. 2019. Sensitive high-throughput single-cell RNA-seq reveals within-clonal transcript correlations in yeast populations. *Nat Microbiol* **4**: 683-692.

Natali F, Rancati G. 2019. The Mutator Phenotype: Adapting Microbial Evolution to Cancer Biology. *Front Genet* **10**: 713.

Newman CM, Cohen JE, Kipnis C. 1985. Neo-darwinian evolution implies punctuated equilibria. *Nature* **315**: 400-401.

Nichols CA, Gibson WJ, Brown MS, Kosmicki JA, Busanovich JP, Wei H, Urbanski LM, Curimjee N, Berger AC, Gao GF et al. 2020. Loss of heterozygosity of essential genes represents a widespread class of potential cancer vulnerabilities. *Nat Commun* **11**: 2517.

Nick McElhinny SA, Kumar D, Clark AB, Watt DL, Watts BE, Lundström EB, Johansson E, Chabes A, Kunkel TA. 2010. Genome instability due to ribonucleotide incorporation into DNA. *Nat Chem Biol* **6**: 774-781.

Ninio J. 1991. Transient mutators: a semiquantitative analysis of the influence of translation and transcription errors on mutation rates. *Genetics* **129**: 957-962.

Nomura T. 2020. Recombination-induced revertant mosaicism in ichthyosis with confetti and loricrin keratoderma. *J Dermatol Sci* **97**: 94-100.

Nowell PC. 1976. The clonal evolution of tumor cell populations. *Science* **194**: 23-28.

Pelechano V, Chávez S, Pérez-Ortín JE. 2010. A complete set of nascent transcription rates for yeast genes. *PLoS One* **5**: e15442.

Podlaha O, Riester M, De S, Michor F. 2012. Evolution of the cancer genome. *Trends Genet* **28**: 155-163.

Pribis JP, García-Villada L, Zhai Y, Lewin-Epstein O, Wang AZ, Liu J, Xia J, Mei Q, Fitzgerald DM, Bos J et al. 2019. Gamblers: An Antibiotic-Induced Evolvable Cell Subpopulation Differentiated by Reactive-Oxygen-Induced General Stress Response. *Mol Cell* **74**: 785-800.e787.

Pursell ZF, Isoz I, Lundström EB, Johansson E, Kunkel TA. 2007. Yeast DNA polymerase epsilon participates in leading-strand DNA replication. *Science* **317**: 127-130.

Raser JM, O'Shea EK. 2005. Noise in gene expression: origins, consequences, and control. *Science* **309**: 2010-2013.

Rodrigues-Prause A, Sampaio NMV, Gurol TM, Aguirre GM, Sedam HNC, Chapman MJ, Malc EP, Ajith VP, Chakraborty P, Tizei PA et al. 2018. A Case Study of Genomic Instability in an Industrial Strain of. *G3 (Bethesda)* **8**: 3703-3713.

Rose KD, Bown TM, Flanagan KM, Lillegraven JA. 1986. Gradual evolution and species discrimination in the fossil record. in *Vertebrates, Phylogeny, and Philosophy*, p. 0. University of Wyoming.

Rosen DM, Younkin EM, Miller SD, Casper AM. 2013. Fragile site instability in Saccharomyces cerevisiae causes loss of heterozygosity by mitotic crossovers and break-induced replication. *PLoS Genet* **9**: e1003817.

Rosenberg SM, Thulin C, Harris RS. 1998. Transient and heritable mutators in adaptive evolution in the lab and in nature. *Genetics* **148**: 1559-1566.

Ryland GL, Doyle MA, Goode D, Boyle SE, Choong DY, Rowley SM, Li J, Bowtell DD, Tothill RW, Campbell IG et al. 2015. Loss of heterozygosity: what is it good for? *BMC Med Genomics* **8**: 45.

Rébora K, Desmoucelles C, Borne F, Pinson B, Daignan-Fornier B. 2001. Yeast AMP pathway genes respond to adenine through regulated synthesis of a metabolic intermediate. *Mol Cell Biol* **21**: 7901-7912.

Sampaio NMV, Ajith VP, Watson RA, Heasley LR, Chakraborty P, Rodrigues-Prause A, Malc EP, Mieczkowski PA, Nishant KT, Argueso JL. 2020. Characterization of systemic genomic instability in budding yeast. *Proc Natl Acad Sci U S A* **117**: 28221-28231.

Seferbekova Z, Lomakin A, Yates LR, Gerstung M. 2023. Spatial biology of cancer evolution. *Nat Rev Genet* **24**: 295-313.

Sievers CK, Grady WM, Halberg RB, Pickhardt PJ. 2017. New insights into the earliest stages of colorectal tumorigenesis. *Expert Rev Gastroenterol Hepatol* **11**: 723-729.

Smukowski Heil C. 2023. Loss of Heterozygosity and Its Importance in Evolution. *J Mol Evol* **91**: 369-377.

Steinmann K, Kluwe L, Friedrich RE, Mautner VF, Cooper DN, Kehrer-Sawatzki H. 2009. Mechanisms of loss of heterozygosity in neurofibromatosis type 1-associated plexiform neurofibromas. *J Invest Dermatol* **129**: 615-621.

Stewart JA, Hillegass MB, Oberlitner JH, Younkin EM, Wasserman BF, Casper AM. 2021. Noncanonical outcomes of break-induced replication produce complex, extremely long-tract gene conversion events in yeast. *G3 (Bethesda)* **11**.

Sui Y, Qi L, Wu JK, Wen XP, Tang XX, Ma ZJ, Wu XC, Zhang K, Kokoska RJ, Zheng DQ et al. 2020. Genome-wide mapping of spontaneous genetic alterations in diploid yeast cells. *Proc Natl Acad Sci U S A* **117**: 28191-28200.

Symington LS, Rothstein R, Lisby M. 2014. Mechanisms and regulation of mitotic recombination in Saccharomyces cerevisiae. *Genetics* **198**: 795-835.

Torkelson J, Harris RS, Lombardo MJ, Nagendran J, Thulin C, Rosenberg SM. 1997. Genome-wide hypermutation in a subpopulation of stationary-phase cells underlies recombination-dependent adaptive mutation. *EMBO J* **16**: 3303-3311.

Vallania FL, Sherman M, Goodwin Z, Mogno I, Cohen BA, Mitra RD. 2014. Origin and consequences of the relationship between protein mean and variance. *PLoS One* **9**: e102202.

van Dijk D, Dhar R, Missarova AM, Espinar L, Blevins WR, Lehner B, Carey LB. 2015. Slow-growing cells within isogenic populations have increased RNA polymerase error rates and DNA damage. *Nat Commun* **6**: 7972.

Van Etten J, Bhattacharya D. 2020. Horizontal Gene Transfer in Eukaryotes: Not if, but How Much? *Trends Genet* **36**: 915-925.

Wei W, Ho WC, Behringer MG, Miller SF, Bcharah G, Lynch M. 2022. Rapid evolution of mutation rate and spectrum in response to environmental and population-genetic challenges. *Nat Commun* **13**: 4752.

Williams JS, Kunkel TA. 2014. Ribonucleotides in DNA: origins, repair and consequences. *DNA Repair (Amst)* **19**: 27-37.

Woo AC, Faure L, Dapa T, Matic I. 2018. Heterogeneity of spontaneous DNA replication errors in single isogenic. *Sci Adv* **4**: eaat1608.

Zhai Y, Minnick PJ, Pribis JP, Garcia-Villada L, Hastings PJ, Herman C, Rosenberg SM. 2023. ppGpp and RNA-polymerase backtracking guide antibiotic-induced mutable gambler cells. *Mol Cell* **83**: 1298-1310.e1294.

Zhang X, Sjöblom T. 2021. Targeting Loss of Heterozygosity: A Novel Paradigm for Cancer Therapy. *Pharmaceuticals (Basel)* **14**.

Zhu X, Dunn JM, Goddard AD, Squire JA, Becker A, Phillips RA, Gallie BL. 1992. Mechanisms of loss of heterozygosity in retinoblastoma. *Cytogenet Cell Genet* **59**: 248-252.

Łazowski K. 2023. Efficient, robust, and versatile fluctuation data analysis using MLE MUtation Rate calculator (mlemur). *Mutat Res* **826**: 111816.

APPENDIX: SUPPLEMENTARY FIGURES

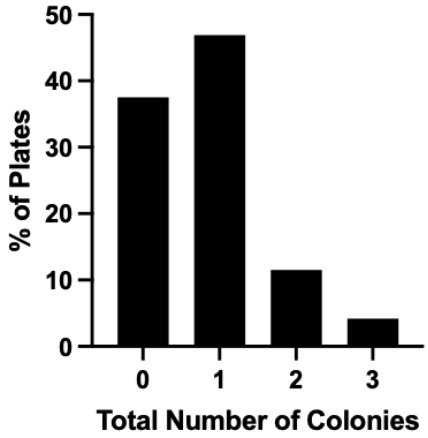

Supplementary Figure 1. Control experiment for phylogeny growth. Number of colonies for 0 hr growth is shown. Plates with 0 or 1 total colony made up 85% of the plates.

Supplementary Table 1.1 Numerical results for colony-based mutation rate assays.

Strain	Genotype	LOH Rate-Chr13	95% CI	LOH Rate-Chr15	95% CI	Expected Double LOH Rate	Observed LOH Rate	95% CI	SGI Ratio
3412-2	*POL2 RNH201*	1.47E-05	1.23E-05–1.70E-05	7.81E-06	6.5E-06 – 9.13E-06	1.15E-10	2.72642e-09	1.56E-10 – 1.2E-08	23.8
3441	*pol2-M644G RNH201*	3.41E-05	3.05E-05 – 4.404E-5	1.83E-05	1.53E-05 – 2.16E-05	6.23E-10	1.20224e-07	7.17E-08 – 1.98E-07	193
3499	*POL2 rnh201Δ*	2.42E-05	1.79E-05–2.49E-05	1.18E-05	1.00E-05 – 1.33E-05	2.85E-10	1.61E-08	6.30E-09 – 3.18E-08	56.6
3501	*pol2-M644G rnh201Δ*	6.56E-05	5.73E-05 – 7.35E-05	1.97E-05	1.19E-05 - 2.75E-05	1.29E-09	7.60E-08	4.14E-08 – 1.25 E -07	58.9
3594	*POL2 RNH201*	1.52E-05	1.24E-05 – 1.79E-05	1.43E-05	1.18E-05–1.69E-05	2.18E-10	1.25E-08	3.12E-09 – 3.24E-08	57.5
3596	*pol2-M644G RNH201*	3.06E-05	2.53E-05 – 3.60E-05	3.85E-05	3.11E-05 – 4.59E-05	1.18E-09	1.17E-07	5.91E-08 – 2.03E-07	99.3
3598	*POL2 rnh201Δ*	2.76e-05	2.31E-05 – 3.22E-05	3.81E-05	3.11E-05 – 4.52E-05	1.05E-09	5.60E-08	2.01E-08 – 1.20E-07	53.2
3592	*pol2-M644G rnh201Δ*	6.69E-05	5.78E-05 – 7.88E-05	6.84E-05	5.86E-05 – 7.46E -05	4.58E-09	1.16E-07	7.23E-08 – 1.72E-07	25.4

Supplementary Table 1.2 Numerical results for liquid culture-based mutation rate assays.

Strain	Genotype	Expected Double LOH Rate	Observed LOH Rate	95% CI	SGI Ratio
3412-2	*POL2 RNH201*	1.15E-10	9.04E-09	4.85E-09 – 1.49E-08	78.6
3441	*pol2-M644G RNH201*	6.23E-10	1.11E-07	7.84E-08 – 1.49E-07	178.2
3499	*POL2 rnh201Δ*	2.85E-10	2.82E-08	1.85E-08 – 4.02E-08	98.9
3501	*pol2-M644G rnh201Δ*	1.29E-09	8.12E-08	5.88E-08 – 1.07E-07	62.9

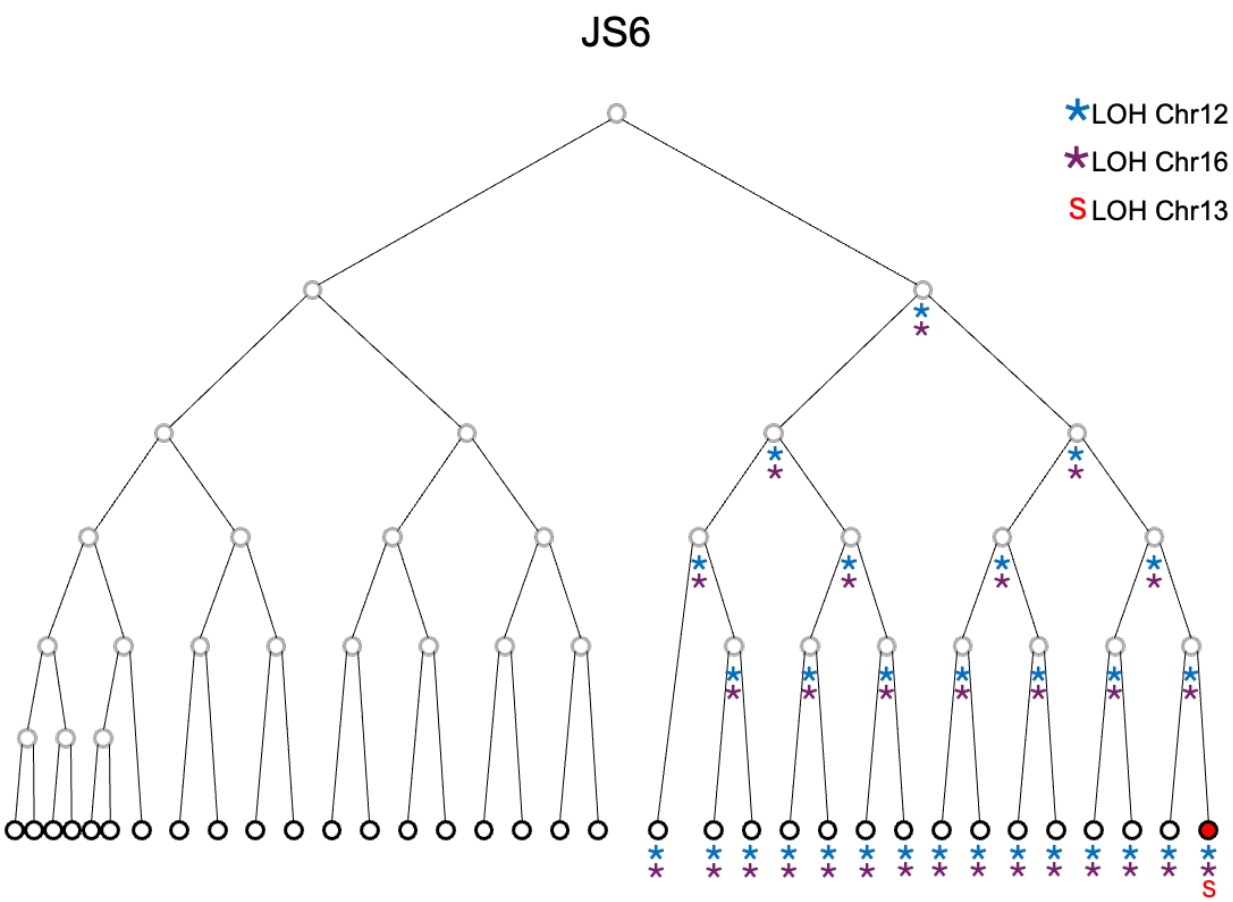

Supplementary Figure 2. JS6 Phylogeny. JS6 shows coincidental as well as independent accumulation of mutations.

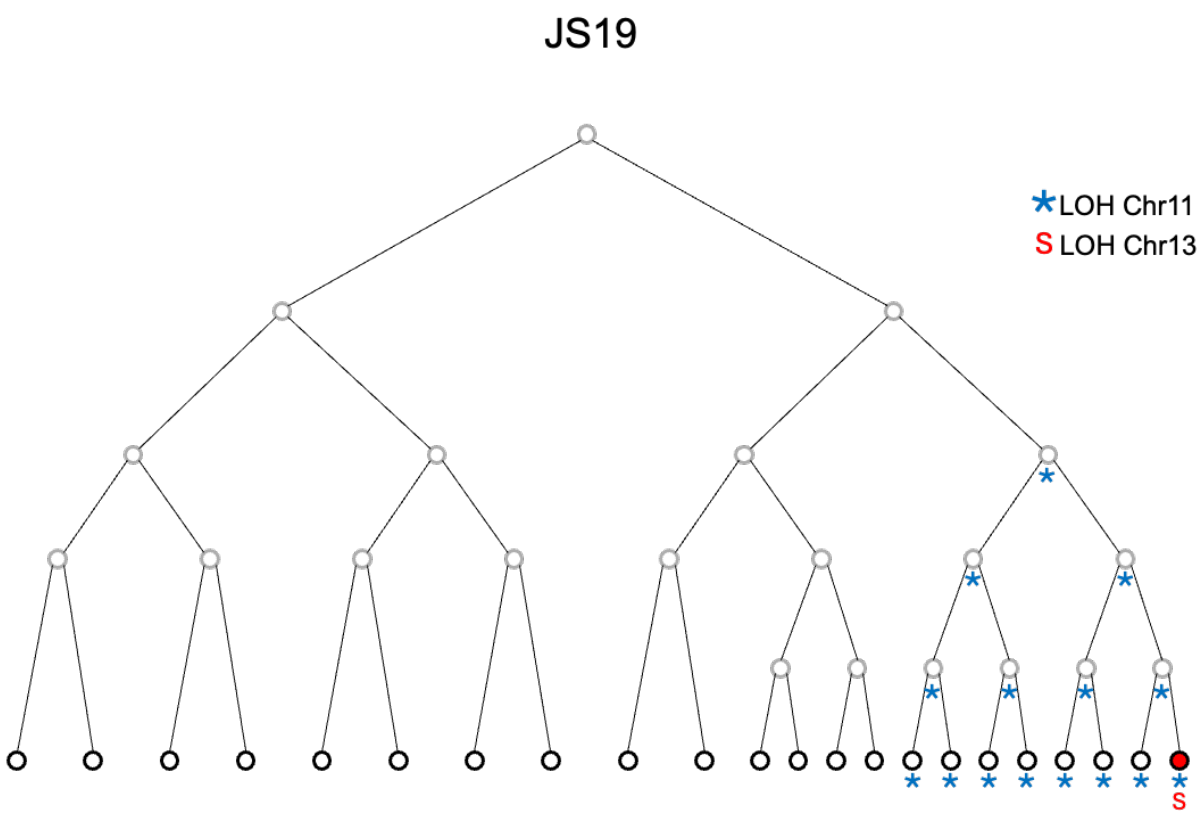

Supplementary Figure 3. JS19 Phylogeny. JS19 shows independent accumulation of mutations.

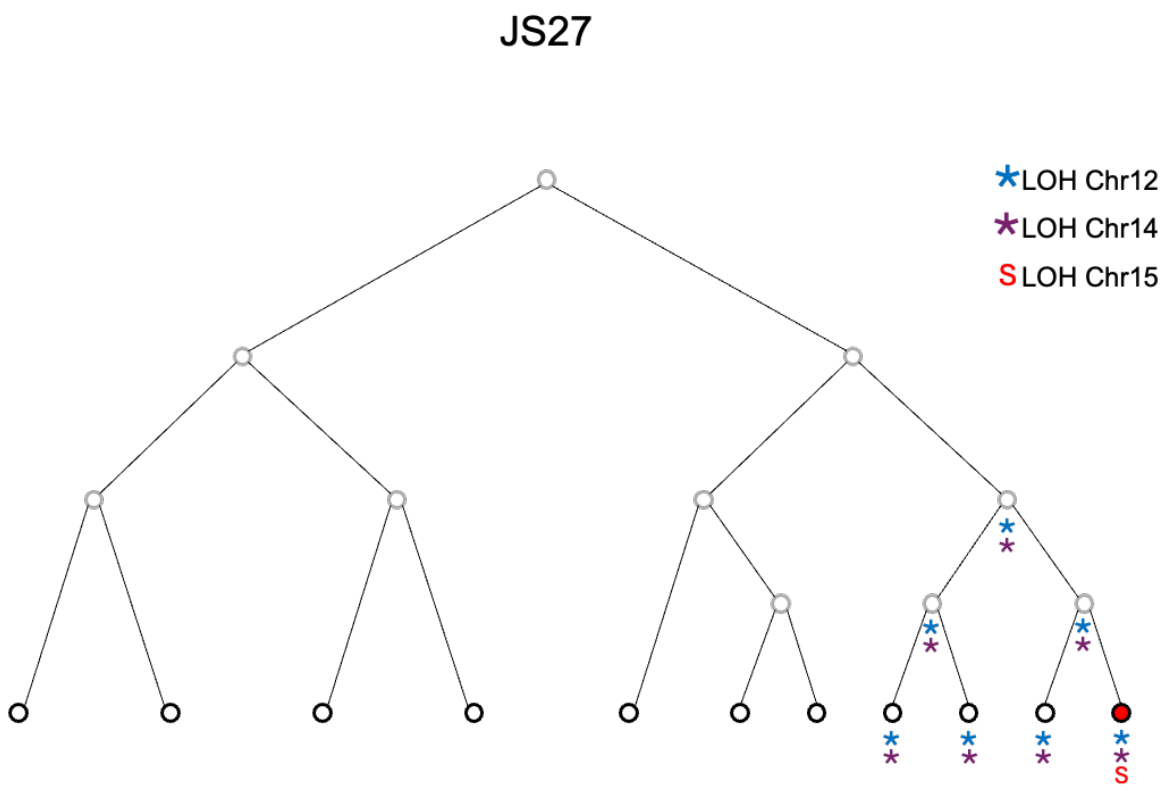

Supplementary Figure 4. JS27 Phylogeny. JS27 shows coincidental as well as independent accumulation of mutations.

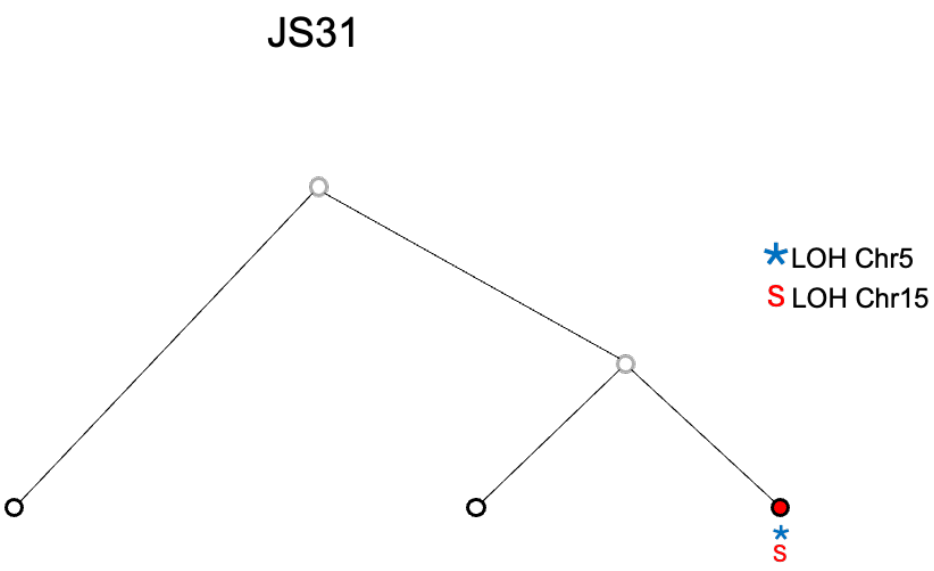

Supplementary Figure 5. JS31 Phylogeny. JS31 shows a coincidental accumulation of mutations.

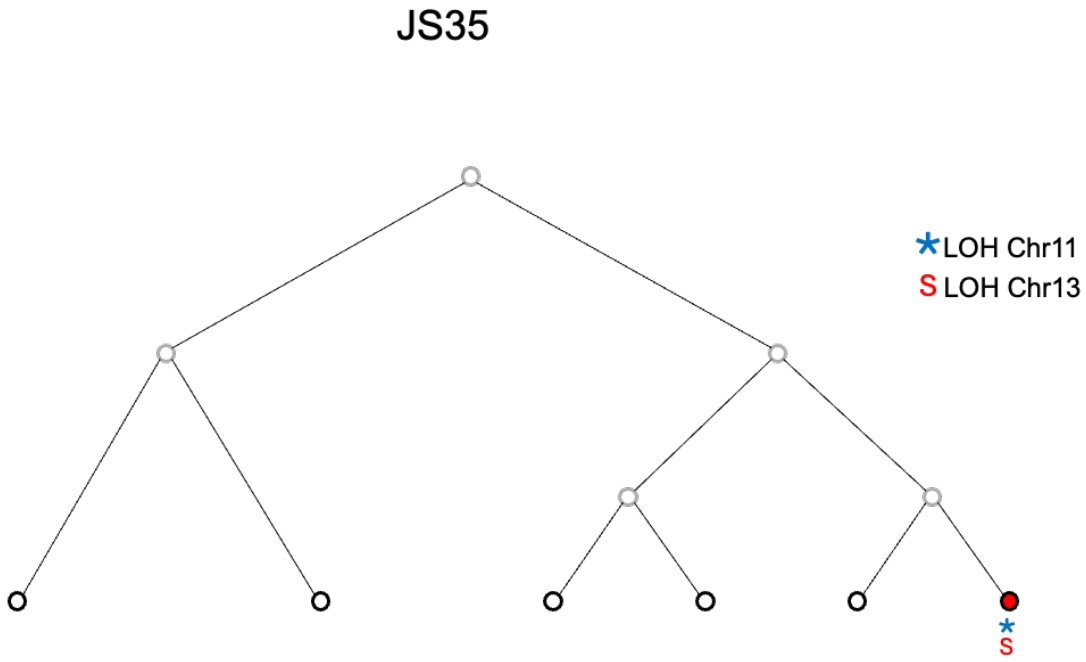

Supplementary Figure 6. JS35 Phylogeny. JS35 shows a coincidental accumulation of mutations.

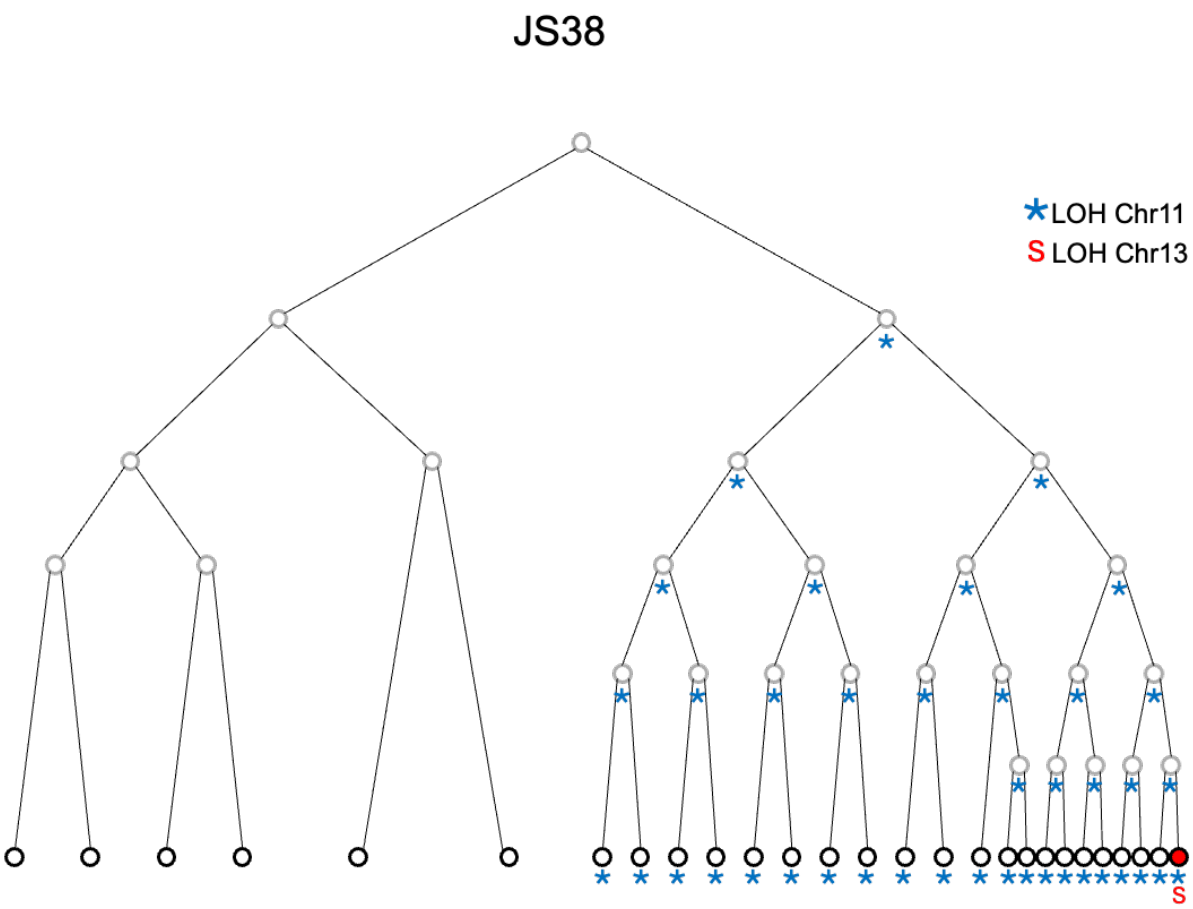

Supplementary Figure 7. JS38 Phylogeny. JS38 shows independent accumulation of mutations.

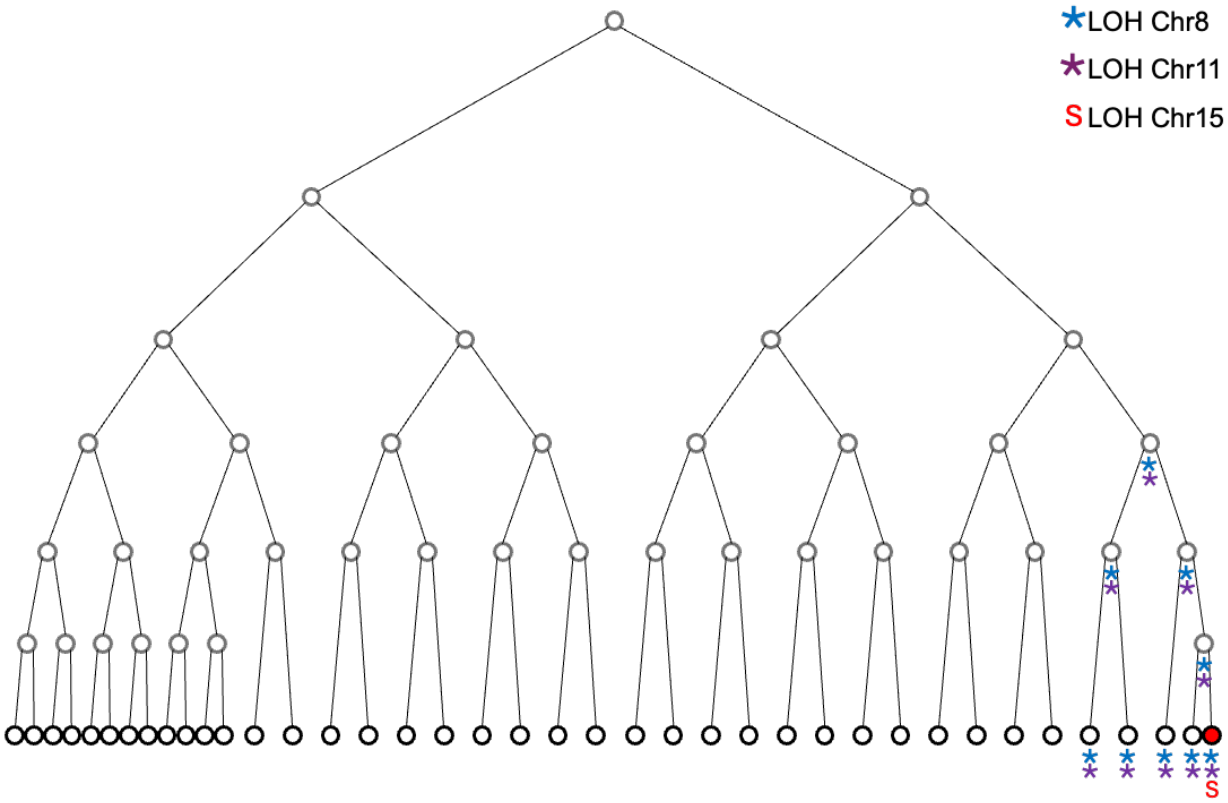

Supplementary Figure 8. JS46 Phylogeny. JS46 shows independent as well as coincidental accumulation of mutations.

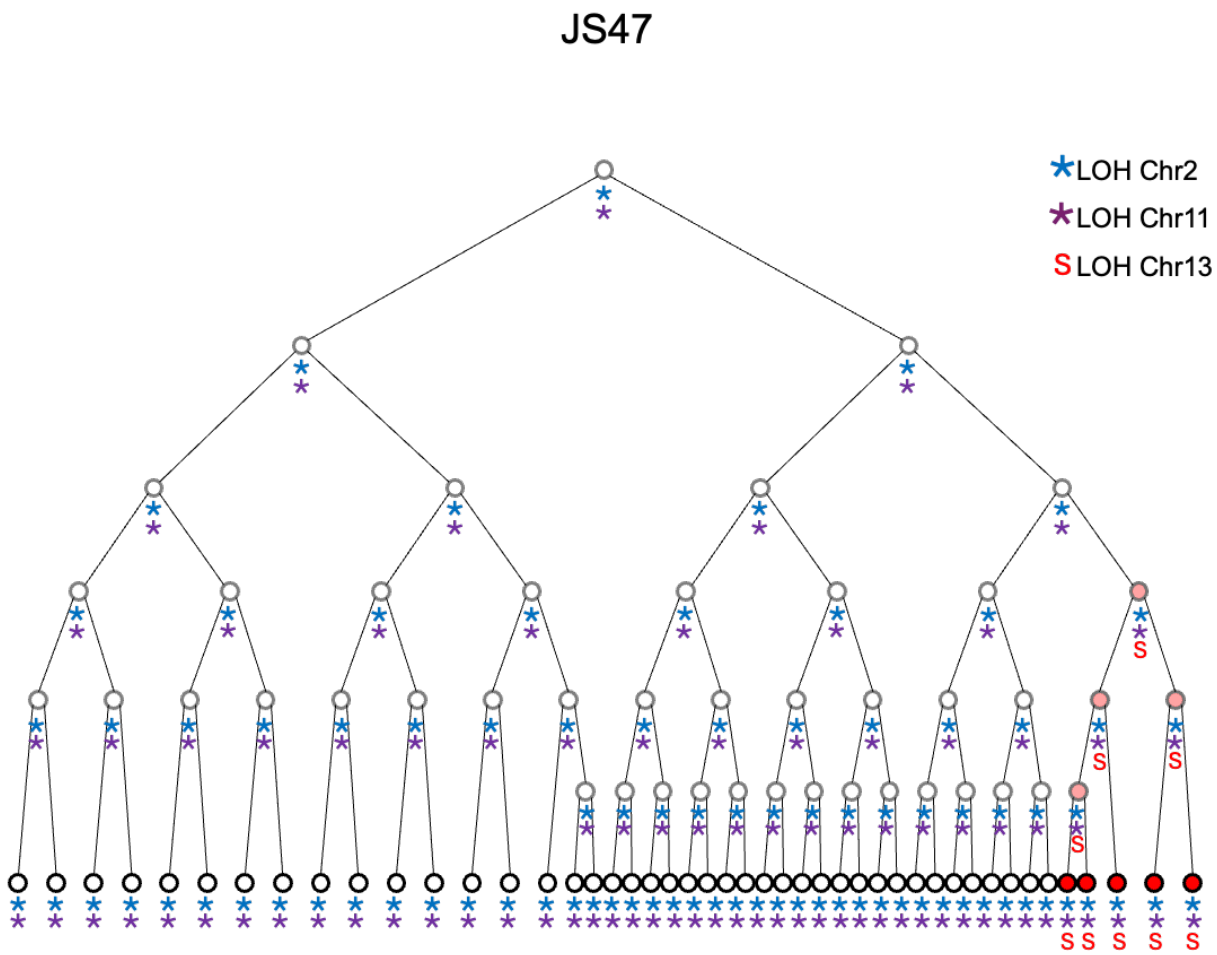

Supplementary Figure 9. JS47 Phylogeny. JS47 shows independent accumulation of mutations.

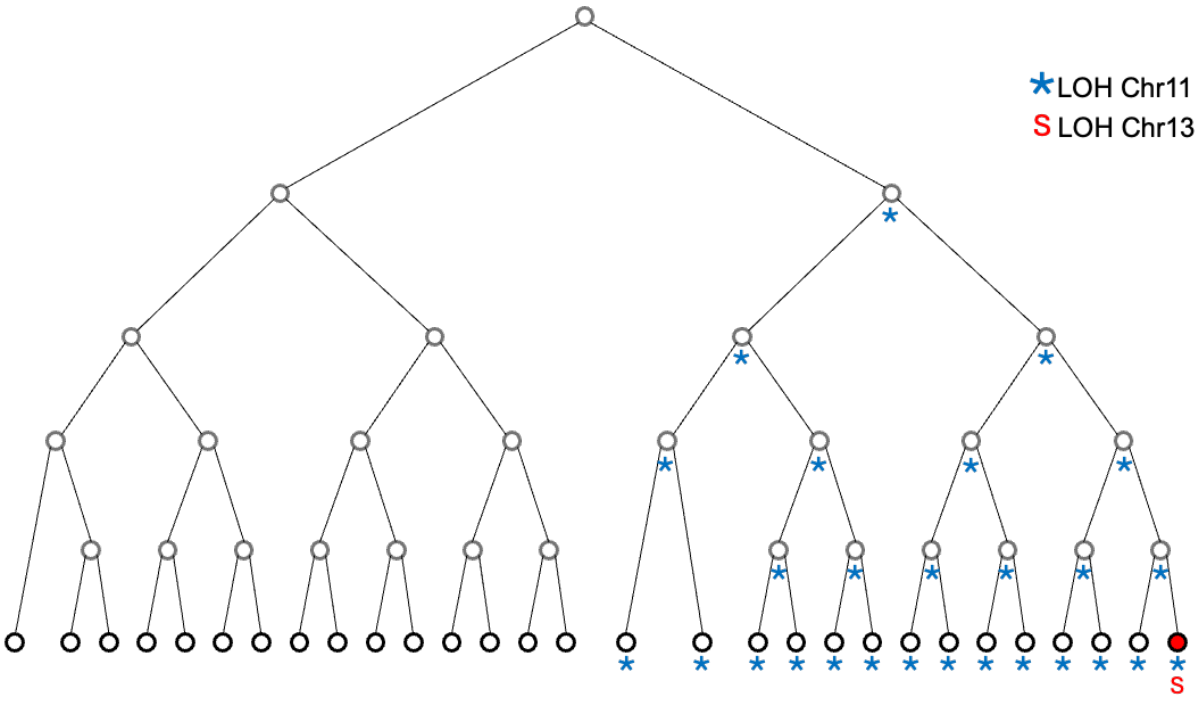

Supplementary Figure 10. JS51 Phylogeny. JS51 shows independent accumulation of mutations.

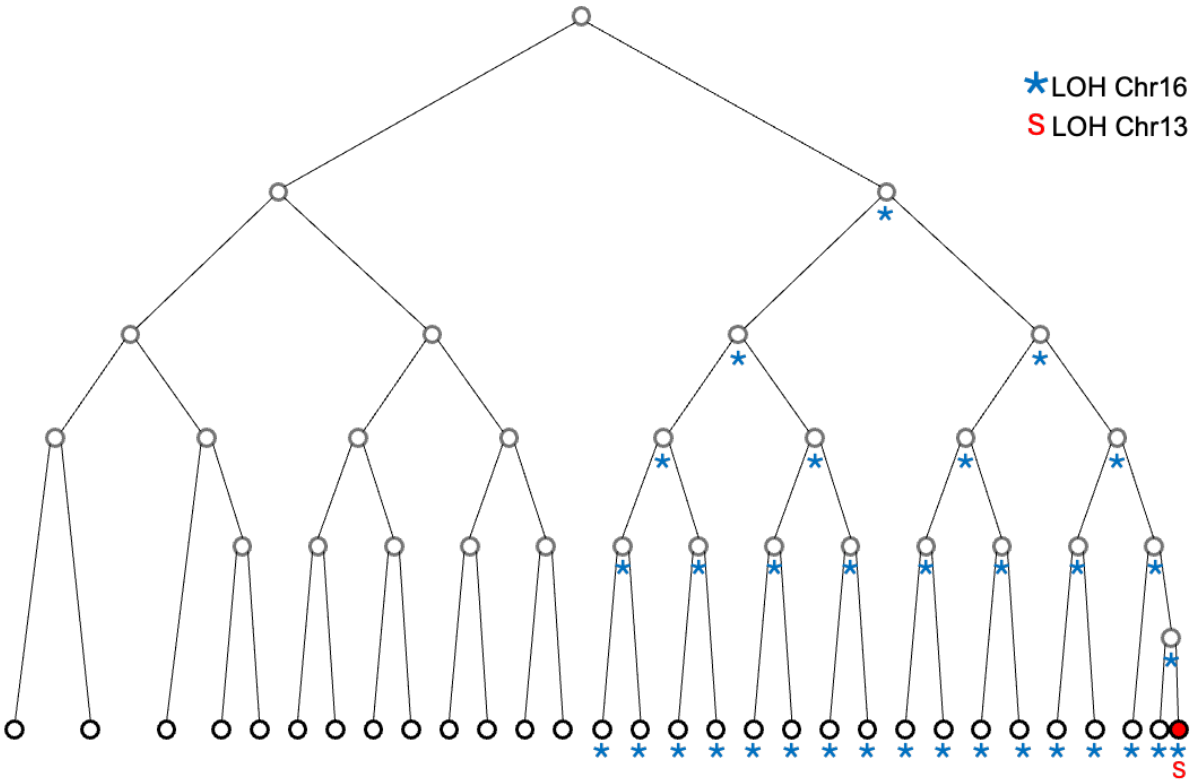

Supplementary Figure 11. JS55 Phylogeny. JS55 shows independent accumulation of mutations.

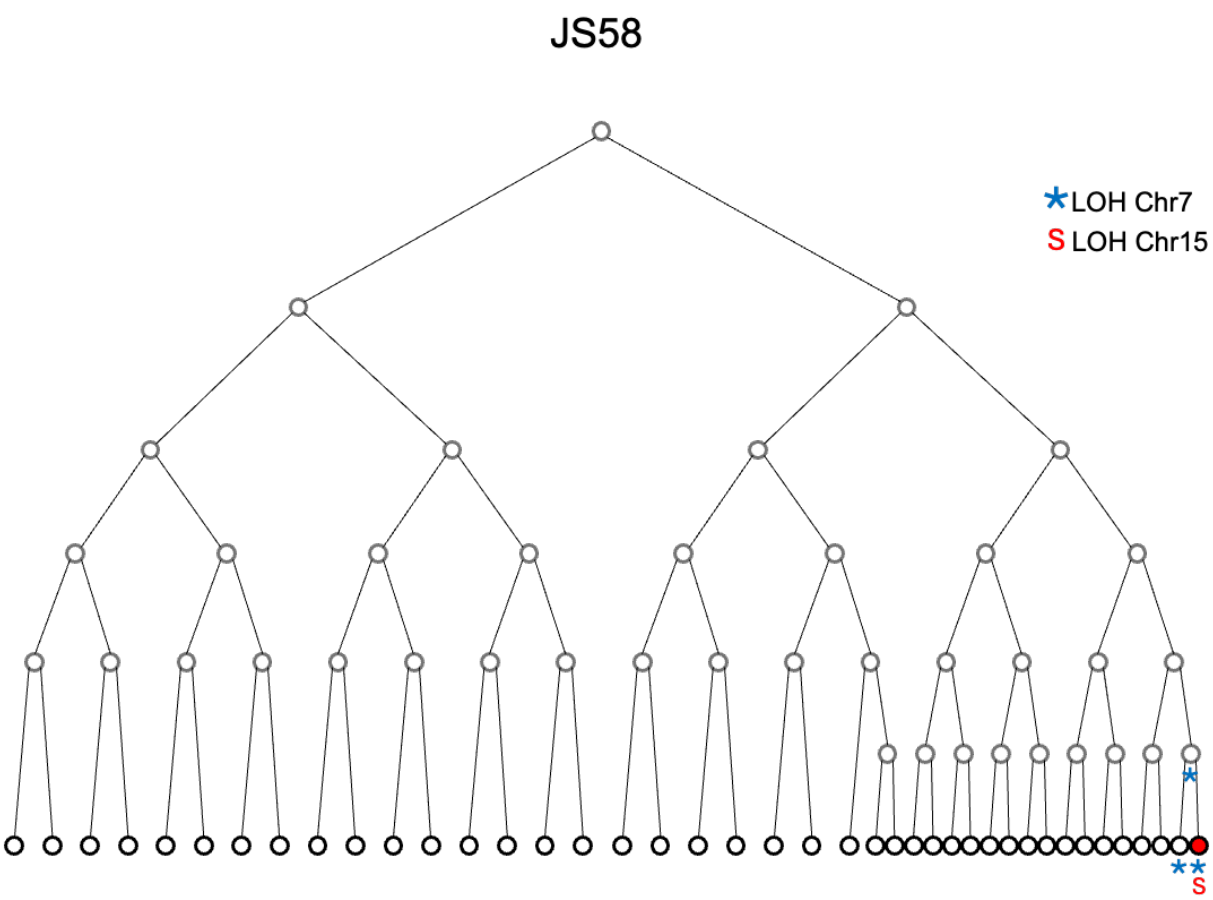

Supplementary Figure 12. JS58 Phylogeny. JS58 shows coincidental mutation accumulation over two cell cycles.

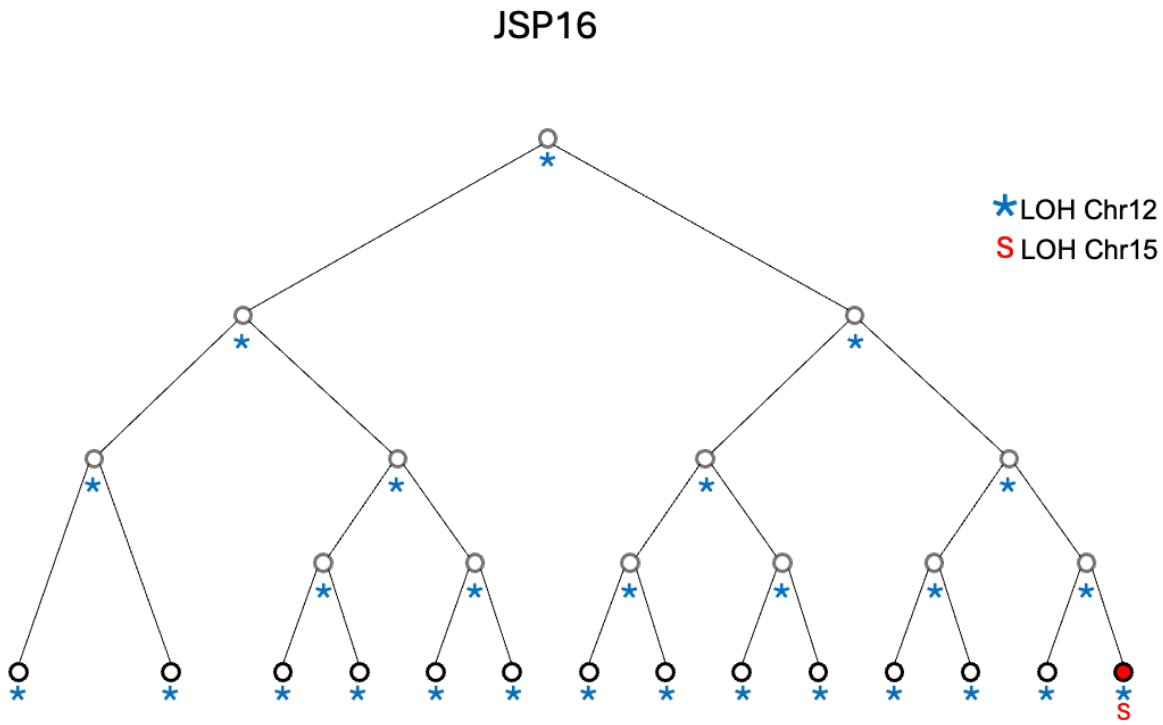

Supplementary Figure 13. JSP16 Phylogeny. JSP16 shows independent accumulation of mutations.

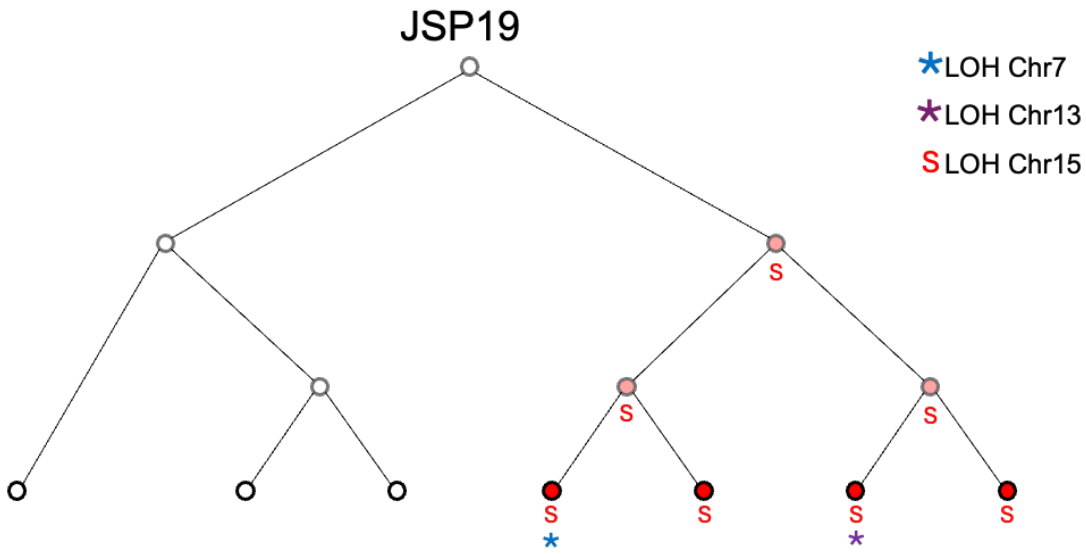

Supplementary Figure 14. JSP19 Phylogeny. JSP19 shows independent accumulation of mutations.

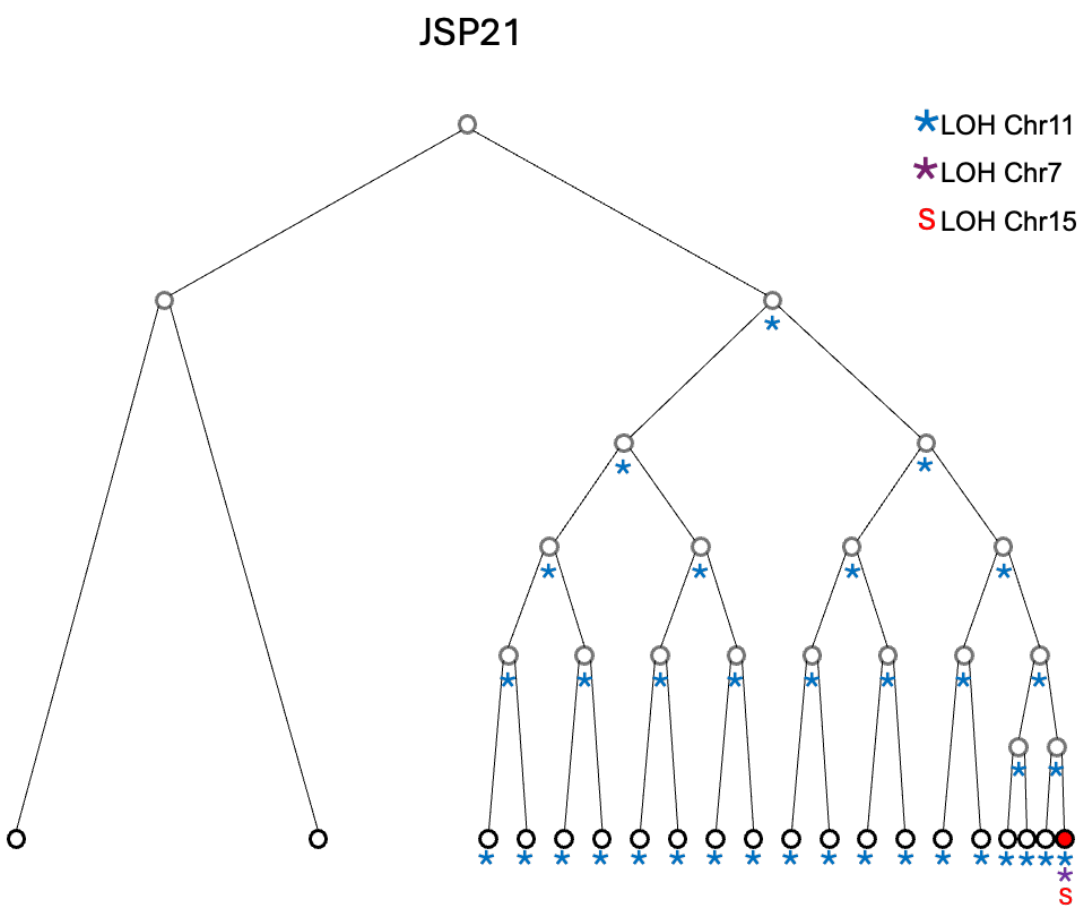

Supplementary Figure 15. JSP21 Phylogeny. JSP21 shows independent as well as coincidental accumulation of mutations.

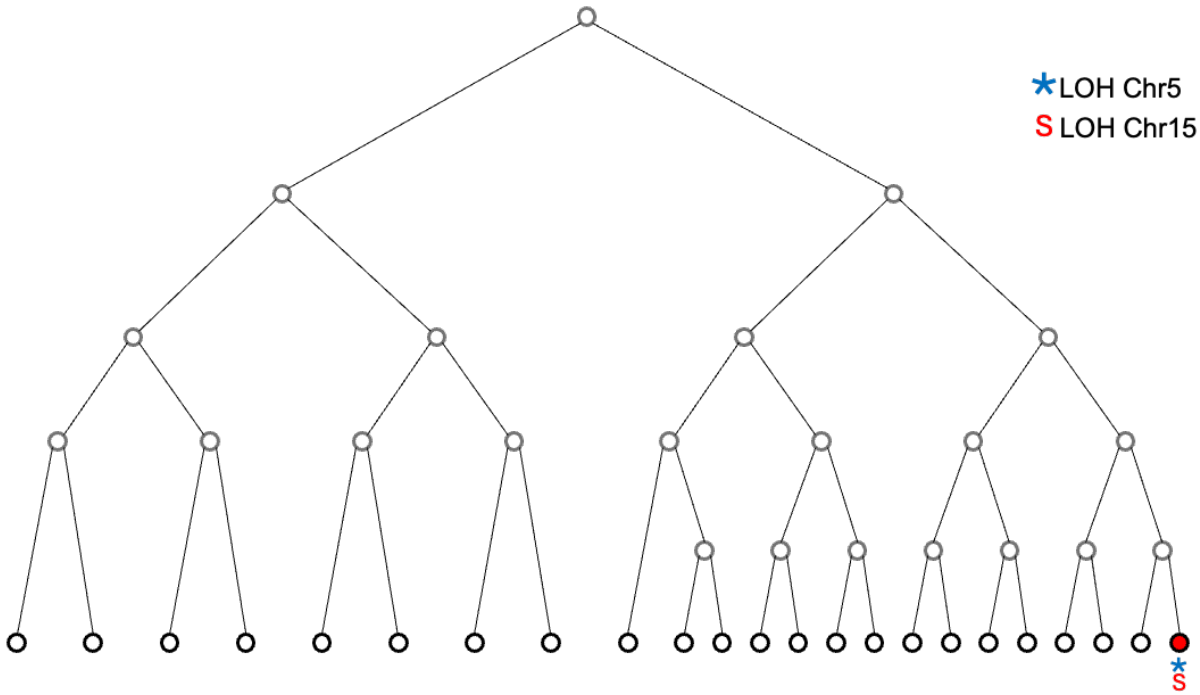

Supplementary Figure 16. JSP30 Phylogeny. JSP30 shows a coincidental accumulation of mutations.

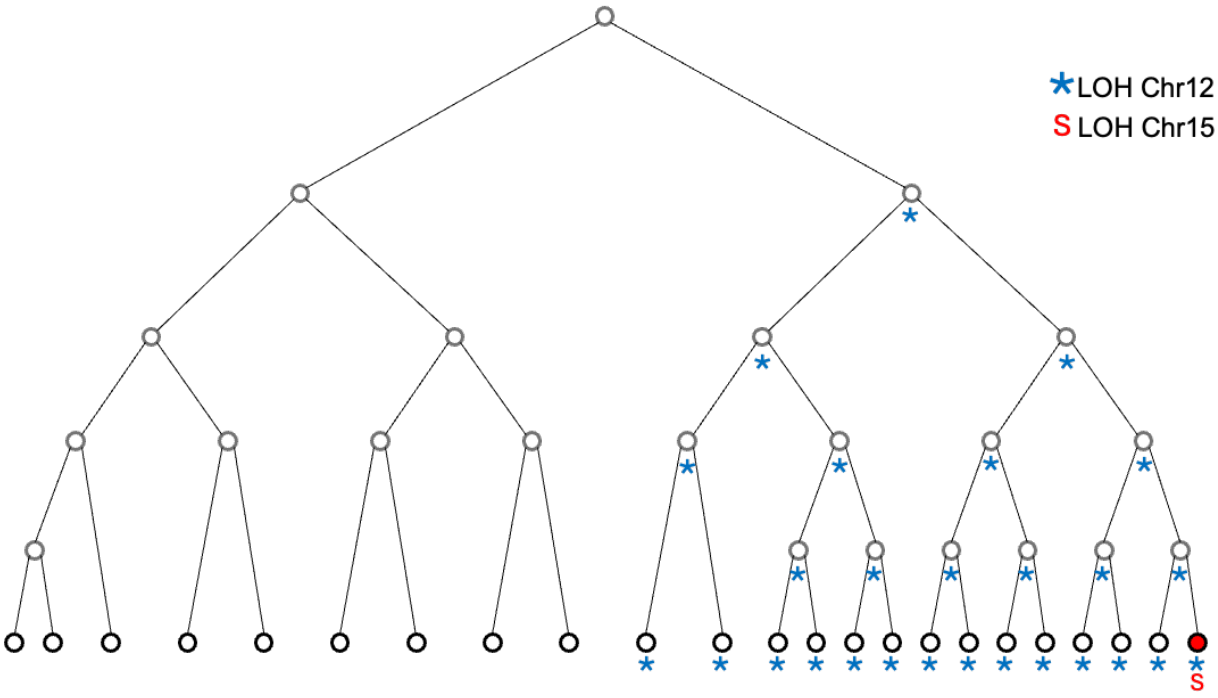

Supplementary Figure 17. JSP31 Phylogeny. JSP31 shows independent accumulation of mutations.

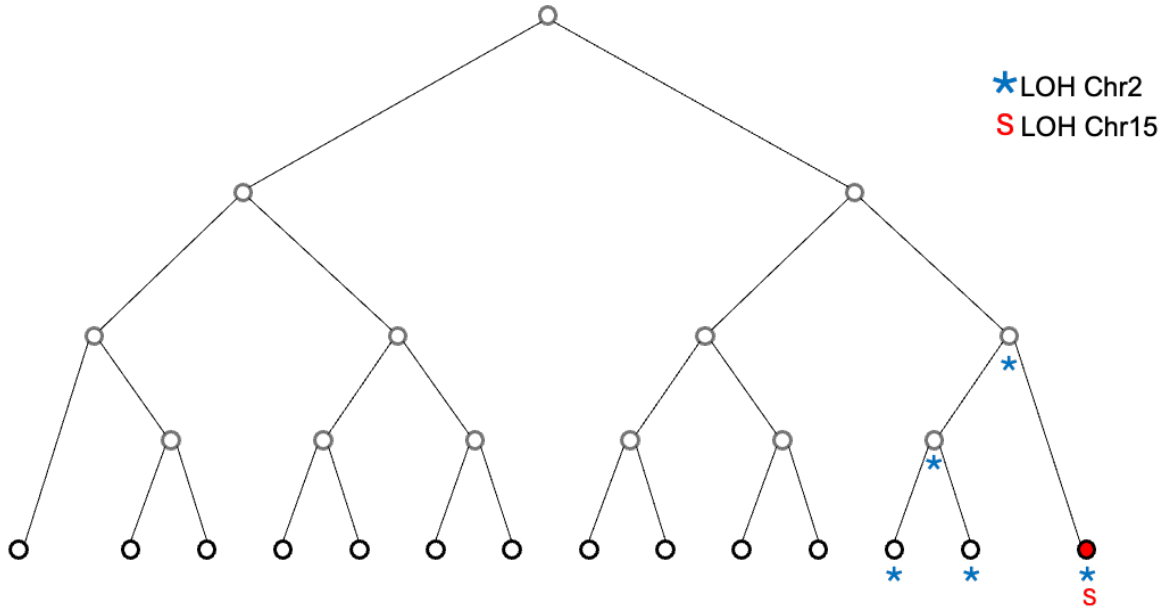

Supplementary Figure 18. JSP32 Phylogeny. JSP32 shows a coincidental mutation accumulation over two cell cycles.

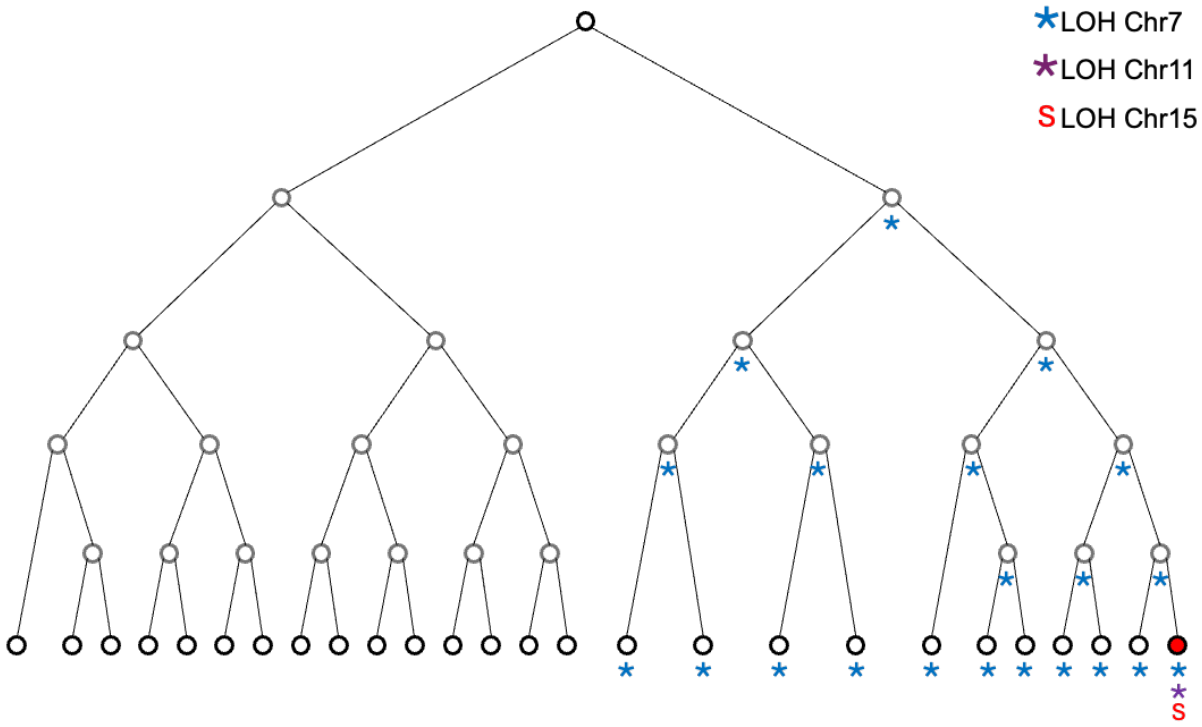

Supplementary Figure 19. JSP39 Phylogeny. JSP39 shows independent and coincidental mutation accumulation.

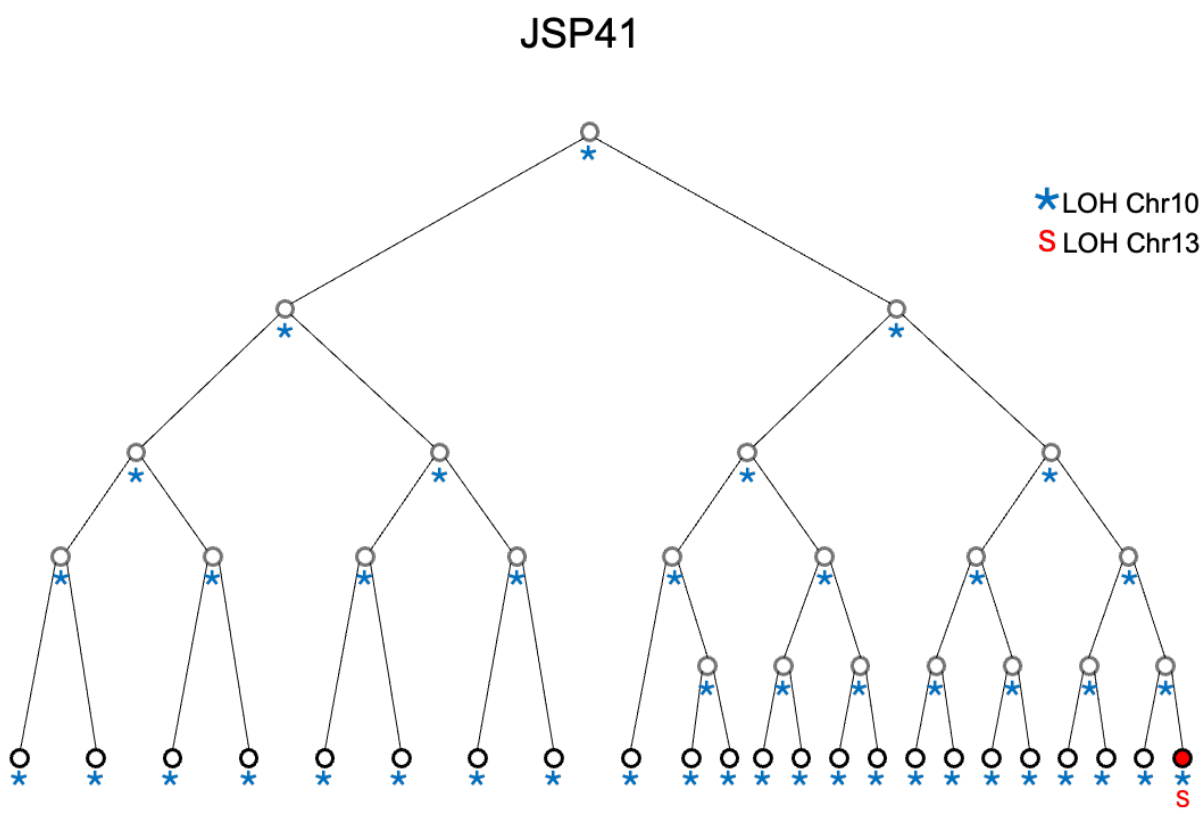

Supplementary Figure 20. JSP41 Phylogeny. JSP41 shows independent mutation accumulation.

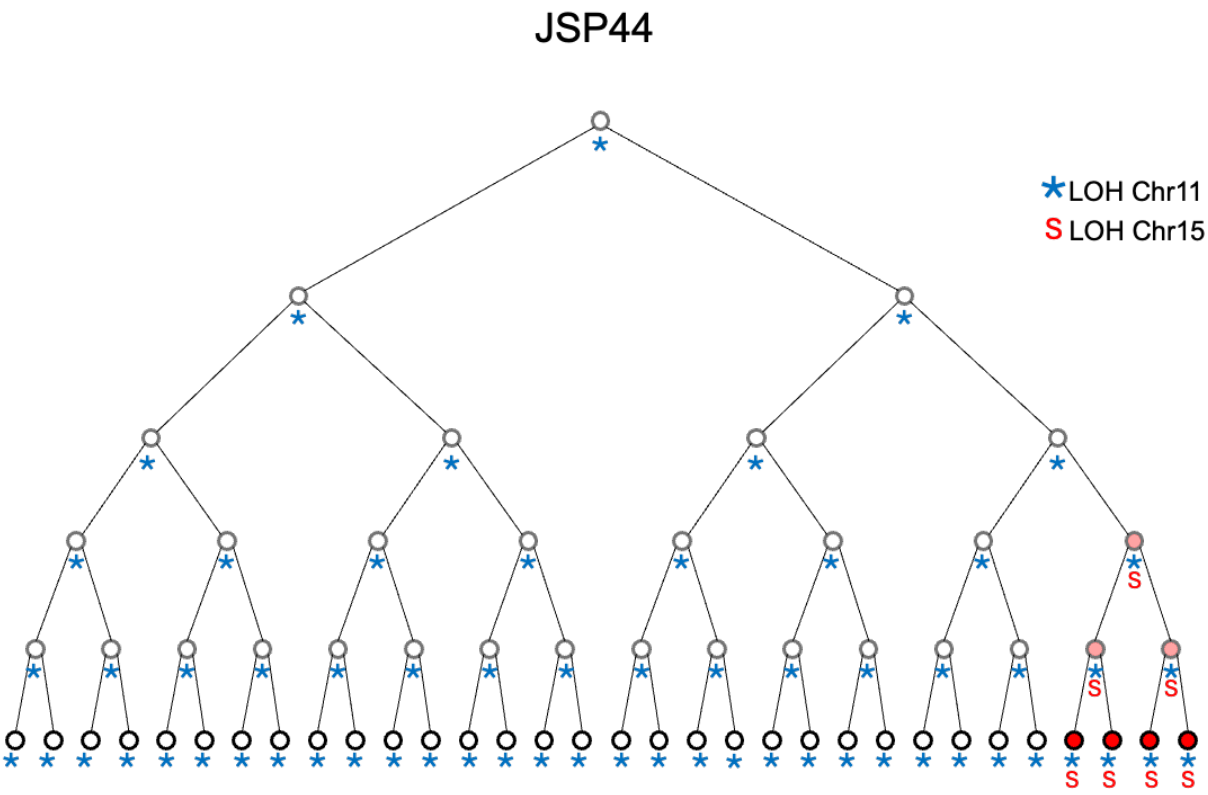

Supplementary Figure 21. JSP44 Phylogeny. JSP44 shows independent mutation accumulation.

Supplementary Table 2. JS phylogenies (WT) sequencing notes. This table shows all LOH events detected through our analysis of WGS.

Parent Strain	Family Name	LOH Chromosome	LOH Range	LOH Tract Length	# of SNPS	Genotype	Type (Interstitial, Terminal, Whole)	Copy Number
JAY3412-0	JS2R1	15	783587 - END	284940	877	Homozygous for S288c	Terminal	Normal (2)
JAY3412-0	JS2R2	15	646794 - END	421733	1081	Homozygous for S288c	Terminal	Normal (2)
JAY3412-0	JS3R1	11	0 - 129862	129862	419	Homozygous for S288c	Terminal	Normal (2)
JAY3412-0	JS3R1	15	653075 - END	415452	2263	Homozygous for S288c	Terminal	Normal (2)
JAY3412-0	JS3R2	11	0 - 134200	134200	270	Homozygous for S288c	Terminal	Normal (2)
JAY3412-0	JS3R2	15	653075 - END	415452	2270	Homozygous for S288c	Terminal	Normal (2)
JAY3412-0	JS3R3	15	653075 - END	415452	2313	Homozygous for S288c	Terminal	Normal (2)
JAY3412-0	JS3R4	11	0 - 180504	180504		Homozygous for S288c	Terminal	Normal (2)
JAY3412-0	JS3R4	15	653075 - END	415452	2063	Homozygous for S288c	Terminal	Normal (2)
JAY3412-0	JS3R5	11	0 - 79688	134200	272	Homozygous for S288c	Terminal	Normal (2)
JAY3412-0	JS3R5	11	100670 -134200	134200	272	Homozygous for S288c	Terminal	Normal (2)
JAY3412-0	JS3R5	15	653075 - END	415452	2304	Homozygous for S288c	Terminal	Normal (2)
JAY3412-0	JS3R6	15	653075 - END	415452	1955	Homozygous for S288c	Terminal	Normal (2)
JAY3412-0	JS3R6	11	0 - 146540	146540	373	Homozygous for S288c	Terminal	Normal (2)
JAY3412-0	JS4R1	13	460255 - END	447064	546	Homozygous for S288c	Interstitial	Normal (2)
JAY3412-0	JS4R2	13	462388 - END	444931	2370	Homozygous for S288c	Terminal	Normal (2)
JAY3412-0	JS4R3	13	461567 - END	445752	746	Homozygous for S288c	Interstitial	Normal (2)
JAY3412-0	JS4R4	13	462388 - END	444931	2477	Homozygous for S288c	Terminal	Normal (2)
JAY3412-0	JS4R5	13	462388 - END	444931	2414	Homozygous for S288c	Terminal	Normal (2)
JAY3412-0	JS4R6	13	461567 - END	445752	2370	Homozygous for S288c	Terminal	Normal (2)
JAY3412-0	JS6R1	12	526397 - 535113	8716	40	Homozygous for SK1	Interstitial	Normal (2)
JAY3412-0	JS6R1	16	661680 - 683285	21605	109	Homozygous for S288c	Interstitial	Normal (2)
JAY3412-0	JS6R1	13	451502 - END	455817	2243	Homozygous for S288c	Terminal	Normal (2)
JAY3412-0	JS7R1	11	19902 - END	626238	1153	Homozygous for S288c	Terminal	Deletion (1)
JAY3412-0	JS7R2	4	926285 - 951132	24847	144	Homozygous for SK1	Interstitial	Normal (2)
JAY3412-0	JS7R2	11	20382 - END	625758	1631	Homozygous for S288c	Interstitial	Deletion (1)
JAY3412-0	JS7R3	4	926737 - 971153	44416	244	Homozygous for SK1	Interstitial	Normal (2)
JAY3412-0	JS7R3	11	19563 - END	626577	1701	Homozygous for S288c	Terminal	Deletion (1)
JAY3412-0	JS8R1	15	554987 - END	513540	1997	Homozygous for S288c	Interstitial	Normal (2)
JAY3412-0	JS9R1	15	617892 - END	450635	2411	Homozygous for S288c	Terminal	Normal (2)
JAY3412-0	JS9R2	15	617892 - END	450635	2453	Homozygous for S288c	Terminal	Normal (2)
JAY3412-0	JS10R1	13	554724 - END	352595	1995	Homozygous for S288c	Terminal	Normal (2)
JAY3412-0	JS10R1	4	622651 - END	900179	4632	Homozygous for S288c	Terminal	Deletion (1)
JAY3412-0	JS12R1	15	507308 - END	561219	2667	Homozygous for S288c	Terminal	Normal (2)
JAY3412-0	JS13R1	13	610099 - END	297220	1409	Homozygous for S288c	Terminal	Normal (2)
JAY3412-0	JS13R2	13	610099 - END	297220	1257	Homozygous for S288c	Terminal	Normal (2)
JAY3412-0	JS13R3	13	610099 - END	297220	1660	Homozygous for S288c	Terminal	Normal (2)
JAY3412-0	JS13R4	13	608020 - END	299299	1322	Homozygous for S288c	Terminal	Normal (2)
JAY3412-0	JS13R5	13	610099 - END	297220	1449	Homozygous for S288c	Terminal	Normal (2)
JAY3412-0	JS13R6	13	610099 - END	297220	1644	Homozygous for S288c	Terminal	Normal (2)
JAY3412-0	JS14R2	11	19020 - END	627120	2424	Homozygous for S288c	Whole	Deletion (1)
JAY3412-0	JS14R4	4	21113 - 560715	539602	288	Homozygous for SK1	Interstitial	Deletion (1)
JAY3412-0	JS14R4	4	769356 - 1326543	557187	119	Homozygous for SK1	Interstitial	Deletion (1)
JAY3412-0	JS14R4	4	769356 - END	753474	210	Homozygous for SK1	Interstitial	Deletion (1)
JAY3412-0	JS14R4	4	374909 - 1326543	951634	148	Homozygous for SK1	Interstitial	Deletion (1)
JAY3412-0	JS15R1	12	830945 - 835013	4068	4	Homozygous for S288c	Interstitial	Duplication (3)
JAY3412-0	JS16R1	11	60173 - 88618	28445	29	Homozygous for S288c	Interstitial	Normal (2)
JAY3412-0	JS16R1	15	926925 - 969234	42309	148	Homozygous for S288c	Interstitial	Normal (2)
JAY3412-0	JS17R1	15	531379 - END	537148	2527	Homozygous for S288c	Terminal	Normal (2)
JAY3412-0	JS19R1	11	636244 - END	9896	45	Homozygous for S288c	Terminal	Normal (2)
JAY3412-0	JS19R1	3	136789 - END	170250	468	Homozygous for SK1	Terminal	Deletion (1)
JAY3412-0	JS19R1	13	531193 - END	376126	2136	Homozygous for S288c	Terminal	Normal (2)
JAY3412-0	JS20R1	15	383156 - END	685371	3523	Homozygous for S288c	Terminal	Normal (2)
JAY3412-0	JS20R2	15	383156 - END	685371	3601	Homozygous for S288c	Terminal	Normal (2)
JAY3412-0	JS21R1	11	19020 - END	627120	3093	Homozygous for S288c	Whole	Deletion (1)
JAY3412-0	JS22R1	8	469510 - 525043	55533	40	Homozygous for SK1	Interstitial	Normal (2)
JAY3412-0	JS22R1	4	18882 - 613744	594862	2661	Homozygous for SK1	Terminal	Deletion (1)
JAY3412-0	JS22R1	4	360631 - END	1162199	5417	Homozygous for SK1	Terminal	Deletion (1)
JAY3412-0	JS23R1	15	688719 - END	379808	2138	Homozygous for S288c	Terminal	Normal (2)
JAY3412-0	JS23R2	15	688719 - END	379808	2139	Homozygous for S288c	Terminal	Normal (2)
JAY3412-0	JS24R1	3	9392 - 32547	23155	16	Homozygous for S288c	Interstitial	Normal (2)
JAY3412-0	JS24R1	11	173878 - 200908	27030	646	Homozygous for S288c	Interstitial	Normal (2)
JAY3412-0	JS24R1	13	549484 - END	357835	1915	Homozygous for S288c	Terminal	Normal (2)
JAY3412-0	JS24R2	11	149388 - 200908	51520	131	Homozygous for S288c	Interstitial	Normal (2)
JAY3412-0	JS24R2	11	0 - 200908	200908	473	Homozygous for S288c	Interstitial	Normal (2)
JAY3412-0	JS24R2	13	619660 - END	287659	1339	Homozygous for S288c	Terminal	Normal (2)
JAY3412-0	JS24R2	13	549484 - 907319	357835	451	Homozygous for S288c	Terminal	Normal (2)
JAY3412-0	JS24R3	11	173878 - 200908	27030	679	Homozygous for S288c	Interstitial	Normal (2)
JAY3412-0	JS24R3	13	549484 - END	357835	2024	Homozygous for S288c	Terminal	Normal (2)
JAY3412-0	JS24R4	11	173878 - 200908	27030	132	Homozygous for S288c	Interstitial	Normal (2)
JAY3412-0	JS24R4	11	0 - 200908	200908	517	Homozygous for S288c	Terminal	Normal (2)
JAY3412-0	JS24R4	13	629060 - END	278259	1436	Homozygous for S288c	Terminal	Normal (2)
JAY3412-0	JS24R4	13	549484 - 970319	420835	509	Homozygous for S288c	Terminal	Normal (2)
JAY3412-0	JS24R5	11	174085 - 200908	26823	133	Homozygous for S288c	Interstitial	Normal (2)
JAY3412-0	JS24R5	11	0 - 200908	200908	519	Homozygous for S288c	Terminal	Normal (2)
JAY3412-0	JS24R5	13	634256 - END	273063	1422	Homozygous for S288c	Terminal	Normal (2)
JAY3412-0	JS24R5	13	549484 - 907319	357835	490	Homozygous for S288c	Terminal	Normal (2)
JAY3412-0	JS24R6	11	173878 - 200908	27030	139	Homozygous for S288c	Interstitial	Normal (2)
JAY3412-0	JS24R6	11	0 - 200908	200908	541	Homozygous for S288c	Terminal	Normal (2)
JAY3412-0	JS24R6	13	549484 - END	357835	2024	Homozygous for S288c	Terminal	Normal (2)

JAY3412-0	JS25R1	13	628415 - END	278904	1594	Homozygous for S288c	Terminal	Normal (2)
JAY3412-0	JS25R2	13	628415 - END	278904	1611	Homozygous for S288c	Terminal	Normal (2)
JAY3412-0	JS25R3	13	628415 - END	278904	1611	Homozygous for S288c	Terminal	Normal (2)
JAY3412-0	JS25W1	1	126902 - 135319	8417	15	Homozygous for SK1	Interstitial	Normal (2)
JAY3412-0	JS25W5	1	126902 - 135319	8417	15	Homozygous for SK1	Interstitial	Normal (2)
JAY3412-0	JS27R1	11	75663 - 79688	4025	8	Homozygous for S288c	Interstitial	Normal (2)
JAY3412-0	JS27R1	12	401372 - 407572	6200	43	Homozygous for S288c	Interstitial	Normal (2)
JAY3412-0	JS27R1	14	483741 - 516034	32293	120	Homozygous for SK1	Interstitial	Normal (2)
JAY3412-0	JS27R1	15	363824 - END	704703	3678	Homozygous for S288c	Terminal	Normal (2)
JAY3412-0	JS29R1	15	624868 - 652865	27997	11	Homozygous for S288c	Interstitial	Normal (2)
JAY3412-0	JS30R1	11	76124- 79688	3564	6	Homozygous for S288c	Interstitial	Normal (2)
JAY3412-0	JS30R1	2	49999 - 59500	9501	4	Homozygous for S288c	Interstitial	Normal (2)
JAY3412-0	JS30R1	13	282022 - END	625297	3189	Homozygous for S288c	Terminal	Normal (2)
JAY3412-0	JS31R1	15	1001411 - END	67116	478	Homozygous for S288c	Terminal	Normal (2)
JAY3412-0	JS31R1	5	333114 - END	233342	970	Homozygous for SK1	Terminal	Normal (2)
JAY3412-0	JS31W1	16	127009 - 132681	5672	24	Homozygous for S288c	Interstitial	Normal (2)
JAY3412-0	JS31W2	4	418803 - 422005	3202	15	Homozygous for S288c	Interstitial	Normal (2)
JAY3412-3	JS32R1	4	1018775 - 1043299	24524	4	Homozygous for SK1	Interstitial	Duplication (3)
JAY3412-3	JS32R1	15	811738 - END	256789	1427	Homozygous for S288c	Terminal	Normal (2)
JAY3412-3	JS33R1	13	675697 - END	231622	736	Homozygous for S288c	Interstitial	Normal (2)
JAY3412-3	JS34R1	4	1008685 - 1024375	15690	4	Homozygous for SK1	Interstitial	Duplication (3)
JAY3412-3	JS34R1	13	886590 - END	20729	35	Homozygous for S288c	Interstitial	Normal (2)
JAY3412-3	JS35R1	11	19020 - 79688	60668	194	Homozygous for S288c	Terminal	Normal (2)
JAY3412-3	JS35R1	15	622291 - END	446236	2497	Homozygous for SK1	Terminal	Normal (2)
JAY3412-3	JS35W5	3	77505 - 82365	4860	11	Homozygous for S288c	Interstitial	Normal (2)
JAY3412-3	JS37R1	11	460937 - 476611	15674	3065	Homozygous for S288c	Interstitial	Duplication (3)
JAY3412-3	JS37R1	15	735678 - END	332849	1759	Homozygous for S288c	Interstitial	Normal (2)
JAY3412-3	JS38R1	11	73701 - 83934	10233	29	Homozygous for S288c	Interstitial	Normal (2)
JAY3412-3	JS39R1	11	225909 - 249447	23538	280	Homozygous for S288c	Interstitial	Normal (2)
JAY3412-3	JS39R1	11	0 - 92948	92948	95	Homozygous for S288c	Terminal	Normal (2)
JAY3412-3	JS39R1	15	630587 - END	437940	2466	Homozygous for S288c	Terminal	Normal (2)
JAY3412-3	JS39R1	12	451190 - END	607434	1825	Homozygous for S288c	Interstitial	Normal (2)
JAY3412-3	JS39R1	12	451190 - END	607434	570	Homozygous for S288c	Terminal	Normal (2)
JAY3412-3	JS39W2	13	175682 - 179112	3430	24	Homozygous for SK1	Interstitial	Normal (2)
JAY3412-3	JS39W2	11	19020 - 373379	354359	1603	Homozygous for S288c	Terminal	Normal (2)
JAY3412-3	JS39W4	15	630587 - END	437940	2460	Homozygous for SK1	Terminal	Normal (2)
JAY3412-3	JS40R1	15	375315 - END	693212	3417	Homozygous for S288c	Terminal	Normal (2)
JAY3412-3	JS41W2	6	251438 - 255164	3726	27	Homozygous for SK1	Interstitial	Normal (2)
JAY3412-3	JS42R1	13	339889 - END	567430	3098	Homozygous for S288c	Terminal	Normal (2)
JAY3412-3	JS42R2	7	969608 - 989383	19775	4	Homozygous for S288c	Interstitial	Normal (2)
JAY3412-3	JS42R2	13	339328 - END	567991	1880	Homozygous for S288c	Terminal	Normal (2)
JAY3412-3	JS43R1	15	444406 - 449205	4799	13	Homozygous for SK1	Interstitial	Normal (2)
JAY3412-3	JS43R1	13	853802 - END	53517	81	Homozygous for S288c	Terminal	Normal (2)
JAY3412-3	JS44R1	14	147716 - 150779	3063	6	Homozygous for S288c	Interstitial	Normal (2)
JAY3412-3	JS44R1	13	560374 - 569867	9493	4	Homozygous for S288c	Interstitial	Normal (2)
JAY3412-3	JS44R1	13	601760 - END	305559	1000	Homozygous for S288c	Terminal	Normal (2)
JAY3412-2	JS45R1	13	417524 - END	489795	2701	Homozygous for S288c	Terminal	Normal (2)
JAY3412-2	JS46R1	8	496531 - END	28558	211	Homozygous for S288c	Terminal	Normal (2)
JAY3412-2	JS46R1	15	804884 - END	263643	1488	Homozygous for S288c	Terminal	Normal (2)
JAY3412-2	JS46R1	11	19020 - 381640	362620	1652	Homozygous for S288c	Terminal	Normal (2)
JAY3412-2	JS47R1	11	76124 - 92069	15945	51	Homozygous for S288c	Interstitial	Normal (2)
JAY3412-2	JS47R1	13	707980 - END	199339	1107	Homozygous for S288c	Terminal	Normal (2)
JAY3412-2	JS47R1	2	9859 - END	783283	4029	Homozygous for S288c	Whole	Normal (2)
JAY3412-2	JS47R2	11	76124 - 92069	15945	51	Homozygous for S288c	Interstitial	Normal (2)
JAY3412-2	JS47R2	13	707980 - END	199339	1108	Homozygous for S288c	Terminal	Normal (2)
JAY3412-2	JS47R2	2	9859 - END	783283	4029	Homozygous for S288c	Whole	Normal (2)
JAY3412-2	JS47R3	11	76124 - 92069	15945	51	Homozygous for S288c	Interstitial	Normal (2)
JAY3412-2	JS47R3	13	707980 - END	199339	1108	Homozygous for S288c	Terminal	Normal (2)
JAY3412-2	JS47R3	2	9859 - END	783283	4030	Homozygous for S288c	Whole	Normal (2)
JAY3412-2	JS47R4	11	76124 - 92069	15945	51	Homozygous for S288c	Interstitial	Normal (2)
JAY3412-2	JS47R4	13	707980 - END	199339	1107	Homozygous for S288c	Terminal	Normal (2)
JAY3412-2	JS47R4	2	9859 - END	783283	4030	Homozygous for S288c	Whole	Normal (2)
JAY3412-2	JS47R5	11	76124 - 92069	15945	51	Homozygous for S288c	Interstitial	Normal (2)
JAY3412-2	JS47R5	13	707980 - END	199339	1107	Homozygous for S288c	Terminal	Normal (2)
JAY3412-2	JS47R5	2	9859 - END	783283	4030	Homozygous for S288c	Whole	Normal (2)
JAY3412-1	JS48R1	4	367564 - 369971	2407	6	Homozygous for SK1	Interstitial	Normal (2)
JAY3412-1	JS48R1	13	904263 - END	3056	21	Homozygous for S288c	Terminal	Normal (2)
JAY3412-1	JS48R1	15	400447 - 427980	27533	3474	Homozygous for SK1	Interstitial	Normal (2)
JAY3412-1	JS49R1	4	367564 - 369971	2407	6	Homozygous for SK1	Interstitial	Normal (2)
JAY3412-1	JS49R1	13	619353 - END	287966	1669	Homozygous for S288c	Terminal	Normal (2)
JAY3412-1	JS49R1	15	400447 - 940002	539555	3475	Homozygous for SK1	Interstitial	Normal (2)
JAY3412-1	JS49R10	4	367564 - 369971	2407	6	Homozygous for SK1	Interstitial	Cresent Poidy
JAY3412-1	JS49R10	15	400447 - 511738	111291	3473	Homozygous for SK1	Interstitial	Normal (2) - Scattered
JAY3412-1	JS49R10	13	619353 - END	287966	1669	Homozygous for S288c	Terminal	Normal (2) - Scattered
JAY3412-1	JS49R11	4	367564 - 369971	2407	6	Homozygous for SK1	Interstitial	Cresent Poidy
JAY3412-1	JS49R11	15	400447 - 427926	27479	3473	Homozygous for SK1	Interstitial	Cresent Poidy
JAY3412-1	JS49R11	13	619353 - END	287966	1669	Homozygous for S288c	Terminal	Cresent Poidy
JAY3412-1	JS49R2	4	367564 - 369971	2407	6	Homozygous for SK1	Interstitial	Normal (2)
JAY3412-1	JS49R2	13	619353 - END	287966	1669	Homozygous for S288c	Terminal	Normal (2)
JAY3412-1	JS49R2	15	400447 - 940002	539555	3475	Homozygous for SK1	Interstitial	Normal (2)
JAY3412-1	JS49R3	4	367564 - 369971	2407	6	Homozygous for SK1	Interstitial	Normal (2)

JAY3412-1	JS49R3	15	400447 - 427917	27470	3473	Homozygous for SK1	Interstitial	Normal (2)
JAY3412-1	JS49R3	13	619353 - END	287966	1670	Homozygous for S288c	Terminal	Normal (2)
JAY3412-1	JS49R4	4	367564 - 369971	2407	6	Homozygous for SK1	Interstitial	Normal (2)
JAY3412-1	JS49R4	15	400447 - 427926	27479	3475	Homozygous for SK1	Interstitial	Normal (2)
JAY3412-1	JS49R4	13	619353 - END	287966	1670	Homozygous for S288c	Terminal	Normal (2)
JAY3412-1	JS49R5	4	367564 - 369971	2407	6	Homozygous for SK1	Interstitial	Normal (2)
JAY3412-1	JS49R5	15	400447 - 427926	27479	3475	Homozygous for SK1	Interstitial	Normal (2)
JAY3412-1	JS49R5	13	619353 - END	287966	1670	Homozygous for S288c	Terminal	Normal (2)
JAY3412-1	JS49R6	4	367564 - 369971	2407	6	Homozygous for SK1	Interstitial	Normal (2)
JAY3412-1	JS49R6	15	400447 - 427926	27479	3475	Homozygous for SK1	Interstitial	Normal (2)
JAY3412-1	JS49R6	13	619353 - END	287966	1669	Homozygous for S288c	Terminal	Normal (2)
JAY3412-1	JS49R7	4	367564 - 369971	2407	6	Homozygous for SK1	Interstitial	Normal (2)
JAY3412-1	JS49R7	15	400447 - 427926	27479	3474	Homozygous for SK1	Interstitial	Normal (2)
JAY3412-1	JS49R7	13	619353 - END	287966	1669	Homozygous for S288c	Terminal	Normal (2)
JAY3412-1	JS49R8	4	367564 - 369971	2407	6	Homozygous for SK1	Interstitial	Normal (2)
JAY3412-1	JS49R8	13	619353 - END	287966	1669	Homozygous for S288c	Terminal	Normal (2)
JAY3412-1	JS49R8	15	400447 - 940002	539555	3476	Homozygous for SK1	Interstitial	Normal (2)
JAY3412-1	JS49R9	4	367564 - 369971	2407	6	Homozygous for SK1	Interstitial	Cresent Poidy
JAY3412-1	JS49R9	15	400447 - 427980	27533	3473	Homozygous for SK1	Interstitial	Cresent Poidy
JAY3412-1	JS49R9	13	619353 - END	287966	1669	Homozygous for S288c	Terminal	Cresent Poidy
JAY3412-1	JS50R1	4	367564 - 369971	2407	6	Homozygous for SK1	Interstitial	Normal (2)
JAY3412-1	JS50R1	15	400447 - 427980	27533	3469	Homozygous for SK1	Interstitial	Normal (2)
JAY3412-1	JS50R1	13	334870 - END	572449	3198	Homozygous for S288c	Terminal	Normal (2)
JAY3412-1	JS51R1	4	367564 - 369971	2407	6	Homozygous for SK1	Interstitial	Normal (2)
JAY3412-1	JS51R1	15	400447 - 427926	27479	3471	Homozygous for SK1	Interstitial	Normal (2)
JAY3412-1	JS51R1	11	19020 - 127396	108376	425	Homozygous for S288c	Terminal	Normal (2)
JAY3412-1	JS51R1	13	8537 - END	898782	4789	Homozygous for S288c	Whole	Normal (2)
JAY3412-2	JS52R1	11	66776 - 81361	14585	16	Homozygous for S288c	Interstitial	Normal (2)
JAY3412-2	JS52R1	13	286312 - END	621007	3448	Homozygous for S288c	Terminal	Normal (2)
JAY3412-1	JS53R1	4	367564 - 369971	2407	6	Homozygous for SK1	Interstitial	Normal (2)
JAY3412-1	JS53R1	15	400447 - 427917	27470	3457	Homozygous for SK1	Interstitial	Normal (2)
JAY3412-1	JS53R1	13	435813 - END	471506	2490	Homozygous for S288c	Terminal	Normal (2)
JAY3412-1	JS54R1	4	367564 - 369971	2407	6	Homozygous for SK1	Interstitial	Normal (2)
JAY3412-1	JS54R1	15	400447 - 427917	27470	3471	Homozygous for SK1	Interstitial	Normal (2)
JAY3412-1	JS54R1	13	449412 - END	457907	2542	Homozygous for S288c	Terminal	Normal (2)
JAY3412-1	JS55R1	4	367564 - 369971	2407	6	Homozygous for SK1	Interstitial	Normal (2)
JAY3412-1	JS55R1	12	259471 - 264066	4595	22	Homozygous for S288c	Interstitial	Normal (2)
JAY3412-1	JS55R1	16	232435 - 244463	12028	40	Homozygous for S288c	Interstitial	Normal (2)
JAY3412-1	JS55R1	15	400447 - 427917	27470	3470	Homozygous for SK1	Interstitial	Normal (2)
JAY3412-1	JS55R1	13	271672 - END	635647	3507	Homozygous for S288c	Terminal	Normal (2)
JAY3412-1	JS55R2	4	367564 - 369971	2407	6	Homozygous for SK1	Interstitial	Normal (2)
JAY3412-1	JS55R2	15	400447 - 618889	218442	3472	Homozygous for SK1	Interstitial	Normal (2)
JAY3412-1	JS55R2	13	271672 - END	635647	3508	Homozygous for S288c	Terminal	Normal (2)
JAY3412-1	JS55R3	4	367564 - 369971	2407	5	Homozygous for S288c	Interstitial	Normal (2)
JAY3412-1	JS55R3	15	400447 - 409273	8826	3358	Homozygous for SK1	Interstitial	Normal (2)
JAY3412-1	JS55R3	13	271672 - END	635647	3470	Homozygous for S288c	Terminal	Normal (2)
JAY3412-1	JS55R4	4	367564 - 369971	2407	6	Homozygous for SK1	Interstitial	Normal (2)
JAY3412-1	JS55R4	15	400447 - 439194	38747	3475	Homozygous for SK1	Interstitial	Normal (2)
JAY3412-1	JS55R4	13	271672 - END	635647	3508	Homozygous for S288c	Terminal	Normal (2)
JAY3412-1	JS55R5	4	367564 - 369971	2407	6	Homozygous for SK1	Interstitial	Normal (2)
JAY3412-1	JS55R5	15	400447 - 940002	539555	3475	Homozygous for SK1	Interstitial	Normal (2)
JAY3412-1	JS55R5	13	271672 - END	635647	3508	Homozygous for S288c	Terminal	Normal (2)
JAY3412-1	JS55R6	4	367564 - 369971	2407	6	Homozygous for SK1	Interstitial	Normal (2)
JAY3412-1	JS55R6	15	400447 - 417628	17181	3474	Homozygous for SK1	Interstitial	Normal (2)
JAY3412-1	JS55R6	13	271672 - END	635647	3508	Homozygous for S288c	Terminal	Normal (2)
JAY3412-1	JS55R7	15	400447 - 427959	27512	35	Homozygous for SK1	Interstitial	Normal (2)
JAY3412-1	JS55R7	13	271672 - END	635647	3502	Homozygous for S288c	Terminal	Normal (2)
JAY3412-1	JS55R7	15	400447 - 1068527	668080	3408	Homozygous for SK1	Interstitial	Normal (2)
JAY3412-1	JS55R8	4	367564 - 369971	2407	4	Homozygous for SK1	Interstitial	Normal (2)
JAY3412-1	JS55R8	15	400447 - 416506	16059	31	Homozygous for SK1	Interstitial	Normal (2)
JAY3412-1	JS55R8	13	271672 - END	635647	3474	Homozygous for S288c	Terminal	Normal (2)
JAY3412-1	JS55R9	4	367564 - 369971	2407	6	Homozygous for SK1	Interstitial	Normal (2)
JAY3412-1	JS55R9	15	400447 - 427926	27479	3469	Homozygous for SK1	Interstitial	Normal (2)
JAY3412-1	JS55R9	13	271672 - END	635647	3508	Homozygous for S288c	Terminal	Normal (2)
JAY3412-2	JS56R1	13	833534 - END	73785	282	Homozygous for S288c	Terminal	Normal (2)
JAY3412-2	JS56R1	2	576818 - END	216324	1010	Homozygous for S288c	Terminal	Normal (2)
JAY3412-2	JS56R1	11	19020 - 338559	319539	1340	Homozygous for S288c	Terminal	Normal (2)
JAY3412-2	JS57R1	13	701606 - END	205713	1224	Homozygous for S288c	Terminal	Normal (2)
JAY3412-2	JS58R1	4	1423134 - 1425361	2227	18	Homozygous for SK1	Interstitial	Normal (2)
JAY3412-2	JS58R1	7	719651 - 725467	5816	34	Homozygous for SK1	Interstitial	Normal (2)
JAY3412-2	JS58R1	15	405487 - END	663040	3459	Homozygous for S288c	Terminal	Normal (2)
JAY3412-2	JS59R1	13	583157 - END	324162	1857	Homozygous for S288c	Terminal	Normal (2)
JAY3412-2	JS59R2	13	549635 - END	357684	2034	Homozygous for S288c	Terminal	Normal (2)
JAY3412-2	JS60R1	13	651277 - END	256042	1483	Homozygous for S288c	Terminal	Normal (2)
JAY3412-2	JS60R2	11	68298 - 82666	14368	32	Homozygous for S288c	Interstitial	Normal (2)
JAY3412-2	JS60R2	13	651277 - END	256042	1484	Homozygous for S288c	Terminal	Normal (2)
JAY3412-2	JS60R3	13	651277 - END	256042	1483	Homozygous for S288c	Terminal	Normal (2)
JAY3412-2	JS60R4	13	651277 - END	256042	1484	Homozygous for S288c	Terminal	Normal (2)
JAY3412-2	JS60R5	13	651277 - END	256042	1484	Homozygous for S288c	Terminal	Normal (2)
JAY3412-2	JS60R6	13	651277 - END	256042	1483	Homozygous for S288c	Terminal	Normal (2)
JAY3412-2	JS60R7	13	651277 - END	256042	1483	Homozygous for S288c	Terminal	Normal (2)

JAY3412-2	JS61R1	11	19020 - 79688	60668	194	Homozygous for S288c	Terminal	Duplication (3)
JAY3412-2	JS61R1	1	28352 - END	163936	743	Homozygous for S288c	Whole	Deletion (1)
JAY3412-2	JS61R1	5	237481 - END	328975	1746	Homozygous for S288c	Terminal	Normal (2)
JAY3412-2	JS61R1	13	8537 - END	898782	4786	Homozygous for S288c	Whole	Normal (2)
JAY3412-2	JS62R1	13	287411 - END	619908	3443	Homozygous for S288c	Terminal	Normal (2)

Supplementary Table 3. JSP phylogenies (*pol2-M644G*) sequencing notes. This table shows all LOH events detected through our analysis of WGS.

Parent Strain	Family Name	LOH Chromosome	LOH Range	LOH Tract Length	# of SNPS in Tract	S288c or SK1?	Type (Interstitial, Terminal, Whole)	Copy Number
JAY3441	JSP1R1	13	624603 - END	282716	125	Homozygous for S288c	Interstitial	Normal (2)
JAY3441	JSP2R1	13	682377 - END	287942	278	Homozygous for S288c	Interstitial	Normal (2)
JAY3441	JSP11R1	14	147466 - 153164	2272	7	Homozygous for S288c	Interstitial	Normal (2)
JAY3441	JSP11R1	15	718599 - END	2532	420	Homozygous for S288c	Terminal	Normal (2)
JAY3441	JSP12R1	13	449412 - END	2913	856	Homozygous for S288c	Terminal	Normal (2)
JAY3441	JSP13R1	15	748029 - END	2913	358	Homozygous for S288c	Interstitial	Normal (2)
JAY3441	JSP15R1	14	147716 - 152355	2913	7	Homozygous for S288c	Interstitial	Normal (2)
JAY3441	JSP15R1	15	409147 - END	2913	2142	Homozygous for S288c	Interstitial	Normal (2)
JAY3441	JSP16R1	12	823217 - END	2913	5	Homozygous for SK1	Interstitial	Normal (2)
JAY3441	JSP16R1	15	717433 - END	2913	18	Homozygous for S288c	Interstitial	Normal (2)
JAY3441	JSP17R1	13	389031 - 518403	2913	5	Homozygous for S288c	Interstitial	Normal (2)
JAY3441	JSP17R1	13	518469 - 695300	2964	4	Homozygous for S288c	Interstitial	Normal (2)
JAY3441	JSP17R1	13	827659 - END	3263	4	Homozygous for S288c	Terminal	Normal (2)
JAY3441	JSP18R1	9	31904 - 429417	3292	190	Homozygous for SK1	Interstitial	Duplication (3)
JAY3441	JSP18R2	9	26915 - END	3620	230	Homozygous for SK1	Interstitial	Normal (2)
JAY3441	JSP18R2	13	542389 - END	3755	53	Homozygous for S288c	Interstitial	Normal (2)
JAY3441	JSP18R3	9	26728 - 286125	4019	129	Homozygous for SK1	Interstitial	Normal (2)
JAY3441	JSP18R3	9	315075 - 424571	4058	61	Homozygous for SK1	Interstitial	Normal (2)
JAY3441	JSP18R3	13	546766 - END	4263	72	Homozygous for S288c	Terminal	Normal (2)
JAY3441	JSP20R1	4	656349 - END	4506	1285	Homozygous for SK1	Terminal	Normal (2)
JAY3441	JSP20R1	13	447488 - END	5033	872	Homozygous for S288c	Terminal	Normal (2)
JAY3441	JSP20R1	16	19818 - 292215	5179	623	Homozygous for S288c	Terminal	Normal (2)
JAY3441	JSP20R2	4	651672 - 493522	5236	2017	Homozygous for SK1	Interstitial	Normal (2)
JAY3441	JSP20R2	13	449175 - END	5698	1305	Homozygous for S288c	Terminal	Normal (2)
JAY3441	JSP20R2	14	147716 - 153810	5818	8	Homozygous for S288c	Interstitial	Normal (2)
JAY3441	JSP20R2	16	20127 - 293369	6094	871	Homozygous for S288c	Interstitial	Normal (2)
JAY3441	JSP21R1	7	514698 - END	7473	1555	Homozygous for SK1	Terminal	Normal (2)
JAY3441	JSP21R1	11	76124 - 81244	7680	16	Homozygous for S288c	Interstitial	Normal (2)
JAY3441	JSP21R1	14	147866 - 150779	8022	10	Homozygous for S288c	Interstitial	Normal (2)
JAY3441	JSP21R1	15	492629 - 590710	8145	21	Homozygous for SK1	Interstitial	Normal (2)
JAY3441	JSP21R1	15	617162 - 963149	8228	62	Homozygous for SK1	Interstitial	Normal (2)
JAY3441	JSP21R1	15	994833 - 491476	9042	15	Homozygous for SK1	Interstitial	Normal (2)
JAY3441	JSP22R1	14	147866 - 150779	9860	10	Homozygous for S288c	Interstitial	Normal (2)
JAY3441	JSP22R1	15	910701 - END	11163	968	Homozygous for S288c	Terminal	Normal (2)
JAY3441	JSP23R1	7	528828 - END	13720	3186	Homozygous for SK1	Terminal	Normal (2)
JAY3441	JSP23R1	13	264034 - END	16440	3366	Homozygous for S288c	Terminal	Normal (2)
JAY3441	JSP23R1	14	147866 - 150779	16948	10	Homozygous for S288c	Interstitial	Normal (2)
JAY3441	JSP24R1	14	147866 - 150779	16987	10	Homozygous for S288c	Interstitial	Normal (2)
JAY3441	JSP24R1	15	332378 - END	21154	3890	Homozygous for S288c	Terminal	Normal (2)
JAY3441	JSP25R1	14	147866 - 150779	24408	10	Homozygous for S288c	Interstitial	Normal (2)
JAY3441	JSP25R1	15	389653 - END	24408	3536	Homozygous for S288c	Terminal	Normal (2)
JAY3441	JSP25R2	14	147866 - 150779	24408	9	Homozygous for S288c	Interstitial	Normal (2)
JAY3441	JSP25R2	15	389653 - END	24408	3536	Homozygous for S288c	Terminal	Normal (2)
JAY3441	JSP25R3	14	147866 - 150779	32653	10	Homozygous for S288c	Interstitial	Normal (2)
JAY3441	JSP25R3	15	389653 - END	56669	3532	Homozygous for S288c	Terminal	Normal (2)
JAY3441	JSP25R4	14	147716 - 150779	69127	9	Homozygous for S288c	Interstitial	Normal (2)
JAY3441	JSP25R4	15	389653 - END	79660	3283	Homozygous for S288c	Interstitial	Normal (2)
JAY3441	JSP26R1	13	370776 - END	114243	2980	Homozygous for S288c	Terminal	Normal (2)
JAY3441	JSP26R1	14	147866 - 150779	125037	9	Homozygous for S288c	Interstitial	Normal (2)
JAY3441	JSP27R1	13	397898 - END	129372	2821	Homozygous for S288c	Terminal	Normal (2)
JAY3441	JSP27R1	14	147866 - 150779	156188	10	Homozygous for S288c	Interstitial	Normal (2)
JAY3441	JSP28R1	13	340906 - END	157826	3167	Homozygous for S288c	Terminal	Normal (2)
JAY3441	JSP28R1	14	147866 - 150779	172149	10	Homozygous for S288c	Interstitial	Normal (2)
JAY3441	JSP29R1	13	517277 - END	176831	2188	Homozygous for S288c	Terminal	Normal (2)
JAY3441	JSP29R1	14	147866 - 150779	176831	10	Homozygous for S288c	Interstitial	Normal (2)
JAY3441	JSP29R2	8	287899 - 290985	176831	17	Homozygous for SK1	Interstitial	Normal (2)
JAY3441	JSP29R2	13	517277 - END	178539	2186	Homozygous for S288c	Terminal	Normal (2)
JAY3441	JSP29R2	14	147866 - 150779	185585	10	Homozygous for S288c	Interstitial	Normal (2)
JAY3441	JSP30R1	5	380871 - END	230893	1029	Homozygous for SK1	Terminal	Normal (2)
JAY3441	JSP30R1	14	147866 - 150779	235407	10	Homozygous for S288c	Interstitial	Normal (2)
JAY3441	JSP30R1	15	617892 - END	235407	2536	Homozygous for S288c	Terminal	Normal (2)
JAY3441	JSP31R1	12	451522 - 995272	259397	1801	Homozygous for SK1	Interstitial	Normal (2)
JAY3441	JSP31R1	12	723182 - END	272397	561	Homozygous for SK1	Terminal	Normal (2)
JAY3441	JSP31R1	14	147866 - 150779	273242	10	Homozygous for S288c	Interstitial	Normal (2)
JAY3441	JSP31R1	15	511101 - END	282716	2918	Homozygous for S288c	Terminal	Normal (2)
JAY3441	JSP32R1	2	395656 - END	320498	1986	Homozygous for SK1	Terminal	Duplication (3)
JAY3441	JSP32R1	14	147866 - 150779	335442	10	Homozygous for S288c	Interstitial	Normal (2)
JAY3441	JSP32R1	15	594290 - END	345987	2072	Homozygous for SK1	Interstitial	Deletion (1)
JAY3441	JSP33R1	13	310813 - END	349802	3271	Homozygous for S288c	Terminal	Normal (2)
JAY3441	JSP33R1	14	147866 - 150779	349928	10	Homozygous for S288c	Interstitial	Normal (2)
JAY3441	JSP34R1	13	310813 - END	351094	3273	Homozygous for S288c	Terminal	Normal (2)
JAY3441	JSP34R1	14	147866 - 150779	351094	10	Homozygous for S288c	Interstitial	Normal (2)
JAY3441	JSP35R1	14	147866 - 150779	351094	10	Homozygous for S288c	Interstitial	Normal (2)
JAY3441	JSP35R1	15	383538 - END	351094	3584	Homozygous for S288c	Terminal	Normal (2)
JAY3441	JSP36R1	13	557517 - END	364930	1985	Homozygous for S288c	Terminal	Normal (2)
JAY3441	JSP36R1	14	147866 - 150779	364930	9	Homozygous for S288c	Interstitial	Normal (2)
JAY3441	JSP37R1	13	462388 - END	367559	2485	Homozygous for S288c	Terminal	Normal (2)
JAY3441	JSP37R1	14	147866 - 150779	367559	10	Homozygous for S288c	Interstitial	Normal (2)
JAY3441	JSP37R2	13	462388 - END	379808	2486	Homozygous for S288c	Terminal	Normal (2)
JAY3441	JSP37R2	14	147866 - 150779	390042	10	Homozygous for S288c	Interstitial	Normal (2)
JAY3441	JSP37R3	13	462388 - END	397486	2479	Homozygous for S288c	Terminal	Normal (2)
JAY3441	JSP37R3	14	147866 - 150779	397513	10	Homozygous for S288c	Interstitial	Normal (2)
JAY3441	JSP37R4	13	462388 - END	412520	2485	Homozygous for S288c	Terminal	Normal (2)
JAY3441	JSP37R4	14	147866 - 150779	412520	10	Homozygous for S288c	Interstitial	Normal (2)
JAY3441	JSP37R5	13	462388 - END	412520	2487	Homozygous for S288c	Terminal	Normal (2)
JAY3441	JSP37R5	14	147866 - 150779	412520	10	Homozygous for S288c	Interstitial	Normal (2)
JAY3441	JSP37R6	13	462388 - END	412520	2485	Homozygous for S288c	Terminal	Normal (2)
JAY3441	JSP37R6	14	147866 - 150779	444931	9	Homozygous for S288c	Interstitial	Normal (2)
JAY3441	JSP37R7	13	462388 - END	444931	2488	Homozygous for S288c	Terminal	Normal (2)
JAY3441	JSP37R7	14	147866 - 150779	444931	9	Homozygous for S288c	Interstitial	Normal (2)
JAY3441	JSP38R1	14	147866 - 150779	450635	10	Homozygous for S288c	Interstitial	Normal (2)
JAY3441	JSP38R1	15	511738 - 257252	453574	5	Homozygous for S288c	Interstitial	Normal (2)

JAY3441	JSP38R1	15	518151 - END	457907	2819	Homozygous for S288c	Interstitial	Normal (2)
JAY3441	JSP39R1	7	12020 - 78426	458144	381	Homozygous for S288c	Terminal	Normal (2)
JAY3441	JSP39R1	11	489952 - END	459831	833	Homozygous for SK1	Terminal	Normal (2)
JAY3441	JSP39R1	14	147866 - 150779	474237	10	Homozygous for S288c	Interstitial	Normal (2)
JAY3441	JSP39R1	15	688719 - END	482422	2129	Homozygous for S288c	Terminal	Normal (2)
JAY3441	JSP40R1	12	193932 - 195525	509421	12	Homozygous for SK1	Interstitial	Normal (2)
JAY3441	JSP40R1	13	313329 - END	535302	3315	Homozygous for S288c	Terminal	Normal (2)
JAY3441	JSP40R1	14	147866 - 150779	536543	10	Homozygous for S288c	Interstitial	Normal (2)
JAY3441	JSP40R2	14	147866 - 150779	543750	10	Homozygous for S288c	Interstitial	Normal (2)
JAY3441	JSP40R2	15	889988 - END	546800	1083	Homozygous for S288c	Terminal	Normal (2)
JAY3441	JSP41R1	13	733024 - END	550376	1023	Homozygous for S288c	Terminal	Normal (2)
JAY3441	JSP41R1	14	147866 - 150779	557426	10	Homozygous for S288c	Interstitial	Normal (2)
JAY3441	JSP42R1	13	277164 - END	566413	3494	Homozygous for S288c	Terminal	Normal (2)
JAY3441	JSP42R1	14	147866 - 150779	593990	10	Homozygous for S288c	Interstitial	Normal (2)
JAY3441	JSP43R1	11	74603 - 79688	596506	10	Homozygous for S288c	Interstitial	Normal (2)
JAY3441	JSP43R1	13	735170 - END	596506	1009	Homozygous for S288c	Terminal	Normal (2)
JAY3441	JSP43R1	14	147866 - 150779	625118	10	Homozygous for S288c	Interstitial	Normal (2)
JAY3441	JSP43R1	16	393808 - 405804	625118	47	Homozygous for S288c	Interstitial	Normal (2)
JAY3441	JSP44R1	11	55280 - 79688	625118	35	Homozygous for S288c	Interstitial	Normal (2)
JAY3441	JSP44R1	14	147866 - 150779	625118	10	Homozygous for S288c	Interstitial	Normal (2)
JAY3441	JSP44R1	15	700968 - END	630155	2066	Homozygous for S288c	Terminal	Normal (2)
JAY3441	JSP44R2	11	55280 - 79688	643285	35	Homozygous for S288c	Interstitial	Normal (2)
JAY3441	JSP44R2	14	147866 - 150779	659380	10	Homozygous for S288c	Interstitial	Normal (2)
JAY3441	JSP44R2	15	700948 - END	678874	2050	Homozygous for S288c	Terminal	Normal (2)
JAY3441	JSP44R3	11	55280 - 79688	678874	35	Homozygous for S288c	Interstitial	Normal (2)
JAY3441	JSP44R3	14	147866 - 150779	678874	10	Homozygous for S288c	Interstitial	Normal (2)
JAY3441	JSP44R3	15	700968 - END	678874	2067	Homozygous for S288c	Terminal	Normal (2)
JAY3441	JSP44R4	11	55280 - 79688	684989	35	Homozygous for S288c	Interstitial	Normal (2)
JAY3441	JSP44R4	14	147866 - 150779	736149	10	Homozygous for S288c	Interstitial	Normal (2)
JAY3441	JSP44R4	15	700968 - END	746761	2066	Homozygous for S288c	Terminal	Normal (2)
JAY3441	JSP45R1	7	1031011 - 1036371	795066	26	Homozygous for SK1	Interstitial	Normal (2)
JAY3441	JSP45R1	11	19020 - 83549	795066	214	Homozygous for S288c	Terminal	Normal (2)
JAY3441	JSP45R1	13	850650 - END	795066	202	Homozygous for S288c	Terminal	Normal (2)
JAY3441	JSP45R1	14	147866 - 150779	866481	10	Homozygous for S288c	Interstitial	Normal (2)